Dynamics and Control of Transportation Systems: Highway Traffic Jam Mitigation and Vehicle Automation

by

Fang-Chieh Chou

A dissertation submitted in partial satisfaction of the

requirements for the degree of

Doctor of Philosophy

in

Engineering - Mechanical Engineering

in the

Graduate Division

of the

University of California, Berkeley

Committee in charge:

Professor Alexandre M. Bayen, Co-chair
Professor Francesco Borrelli, Co-chair
Professor Roberto Horowitz
Dr. Steven Shladover

Spring 2021

Dynamics and Control of Transportation Systems: Highway Traffic Jam Mitigation and Vehicle Automation

Abstract

Dynamics and Control of Transportation Systems: Highway Traffic Jam Mitigation and Vehicle Automation

by

Fang-Chieh Chou

Doctor of Philosophy in Engineering - Mechanical Engineering

University of California, Berkeley

Professor Alexandre M. Bayen, Co-chair

Professor Francesco Borrelli, Co-chair

Highway traffic jams can be caused by external factors, such as physical bottlenecks and severe weather conditions, as well as internal disturbances induced by underlying driving behaviors of vehicles participating in the traffic. For example, conflicts of uncoordinated traffic can cause disturbances and thus impede the traffic throughput. As development of vehicle automation advanced in recent years, introducing vehicle automation technology in traffic became a potential solution to improve traffic flow. Vehicle automation technology can enable vehicles to coordinate with other vehicles and to respond faster and smoother to traffic situations, and thus reduce traffic jams. In this dissertation, we consider vehicle automation in three different traffic scenarios. Firstly, we study traffic jams at highway merging sections. The bottleneck at the intersection is because of accumulated conflicts of mainline traffic and on-ramp traffic. We propose methods based on vehicle-to-infrastructure and vehicle-to-vehicle communication to coordinate mainline traffic and on-ramp traffic. The effectiveness of proposed methods is evaluated in micro-simulation under different penetration rates of automated vehicles. Secondly, we study the phantom traffic jams, which are stop-and-go waves that spontaneously emerge without apparent external factors. Experiments on closed ring roads have demonstrated that the stop-and-go waves can be induced purely by underlying dynamics of driving behaviors in the traffic. The emergence of stop-and-go waves on normal highways can be modeled with string unstable car-following models and the emergence of stop-and-go waves on closed-ring roads can be seen as an unstable dynamical system. We prove that for traffic of non-identical car-following models, the ring road stability is necessary for string stable car-following models; the ring road stability is also sufficient for string stability if traffic is formed of identical car following models. Because the ring road stability is essential for string stability, the ring road can be used to verify whether an automated vehicle control has potential to dissipate stop-and-go waves on

normal highways. Because the ring road is a closed field, it is easier to control and easier to observe than an open-ended highway. Therefore, it would be an ideal field to benchmark performance of automated vehicle control. Ten automated vehicle controllers are benchmarked under different penetration rates and different distributions. Lastly, a car-following control system for trucks is developed. The controller is composed of an upper controller and a lower controller. An adaptive parameter estimation is integrated with the lower controller to deal with unknown parameters. The design of the upper controller considers actuator uncertainties and the string stability condition. To achieve better car following performance in practice, we use vehicle-to-vehicle communication to enhance the car following control system. Experimental results showed that the enhanced system enables the truck to follow the leading vehicle well while the leading vehicle speed is varying.

To my beloved family

Contents

List of Figures

List of Tables

Acknowledgments

Firstly, I want to acknowledge my research advisor, Professor Alexandre Bayen. When I was most helpless and anxious in the middle of my third year, he extended his hand to me and let me join his lab and guided me through the rest of the journey. I am sincerely grateful for his invaluable advice to my research problems and his tireless support to make this possible.

I would like to express my gratitude to Dr. Steven Shladover for providing research opportunities in PATH and mentoring me in the research projects. Conversations with him always inspires and enlightens me. I feel so grateful to have him serving on my dissertation committee.

I would like to thank Professor Karl Hedrick, who inspired me to study for a PhD. He was my advisor in the ME department before he passed away in 2017. His enthusiasm for the academy will last forever in my mind. Sincere thanks to Professor Francesco Borrelli for being an advisor in the ME department after that and serving as a co-chair on my dissertation committee. Thanks to Roberto Professor Horowitz for serving on my dissertation committee and being a chair on my qualifying exam committee. Thanks to Professor Alper Atamturk, Professor Anil Aswani, and Professor Mark Mueller for serving on my qualifying exam committee.

Thanks to Dr. Xiao-Yun Lu for offering me an opportunity to work on the exciting project of truck automation. The project is supported in part by King Abdulaziz City for Science and Technology (KACST). In the meantime, I want to thank my amazing collaborators in PATH and KACST: Dali Wei, Hao Liu, Hani Ramezani, Carlos Flores, David Nelson, John Spring, Fadwa Alaskar, Khalid Alshareef, Radwan Noor, and Hatim Bukhari. Thanks to them for valuable conversations and technical support to make all these possible.

I also want to acknowledge financial support from the California PATH program and Ministry of Education in Taiwan.

I could not imagine how depressed PhD life would be without many friends around me. I would like to thank to people in Bayen's lab, including Alexander Keimer, Yashar Zeiynali Farid, Alben Rome Bagabaldo, Thophiles Cabannes, Marsalis Gibson, Jessica Lazarus, Eugene Vinitsky, Aboudy Kreidieh, Joy Carpio, Fangyu Wu, Kathy Jang, Sulaiman Almatrudi, Shuxia Tang, Saleh Albeaik, Cathy Wu, Ashkan Yousefpour, and Helen. Thanks to them for helping my work and making this lab nice and warm. Thanks to my friends and collaborators in ME: Ugo Rosolia, Yi-Wen Liao, Monimoy Bujarbaruah, Chang Liu, Yujia Wu, Andreas Hansen, Yongkeun Choi, Yeojun Kim, Chen-Ju Wu, Hsien-Chung Lin, Chung-Yen Lin, Chan-Yu Chen, and Shang-Li Wu. Thanks to them for inspiring conversations and all the fun we had. Thanks to my friends in BATS, including Yen-Kai Lin, Yu-Hung Liao, Ching-Fu Chang, Zephy Leung, Chung-Kuan Lin, Li-Wei Chen, Wendy Lin, Albert, and Li-Hao Yeh. Thank them for all the help in life and making the process less stressful.

Finally, I want to thank my family, especially my parents, my grandparents, and my brothers, for their endless love and support for the past years, without whom, it was almost impossible to finish this.

Chapter 1

Introduction

1.1 Background and Motivation

Transportation is essential in everyone's life and it plays an important role for ever growing economies. As demand for transportation increases, congestion would become worse if the transportation system were not built to support excessive demand. Although many possible solutions have been deployed to accommodate increasing demands, deterioration of congestion has not be been restrained. Apparently, as traffic condition gets worse, not only the travel delay would continue to increase, *reliability* and *variability* of the transportation system would also get effected [37]. "Over the past 10 years, the total cost of delay in top urban areas in the US has grown by nearly 48%" [77]. Figure 1.1 shows the changes of annual hours of delay of the auto commuters in ten US cities for the past 30 years. Congestion does not only cause delays, but also cause extra consumption of fuels, which will thus contribute extra emission of greenhouse gas. "In 2017, the average auto commuter in the US spends 54 hours in congestion and wastes 21 gallons of fuel due to congestion" [77]. Totally, an extra 8.8 billion hours and an extra 3.3 billion gallons of fuels have been wasted in that year, which is about 2% of total fuel consumption for motor vehicles in the US[1].

Traffic congestion is a traffic condition where traffic flow speed is much slower than free flow speed. Roughly speaking, traffic congestion is a consequence of mismatched demand and capacity. When traffic flow exceeds the capacity of a portion of the roadway, traffic flow speed would be slower than normal free flow speed. Traffic demand and capacity may vary under different circumstances. For example, traffic demand is higher during rush hours or before and after an event; physical bottlenecks reduces the number of vehicles that can pass at the same time; road curvature (or severe weather condition) forces vehicles to slow down, and thus limited the through put. A few typical factors that causes increased demand or decreased capacity are summarized below [37]:

- Physical bottlenecks;

[1] In 2017, total fuel consumption for motor vehicles in the US is about 144 billion gallons [94].

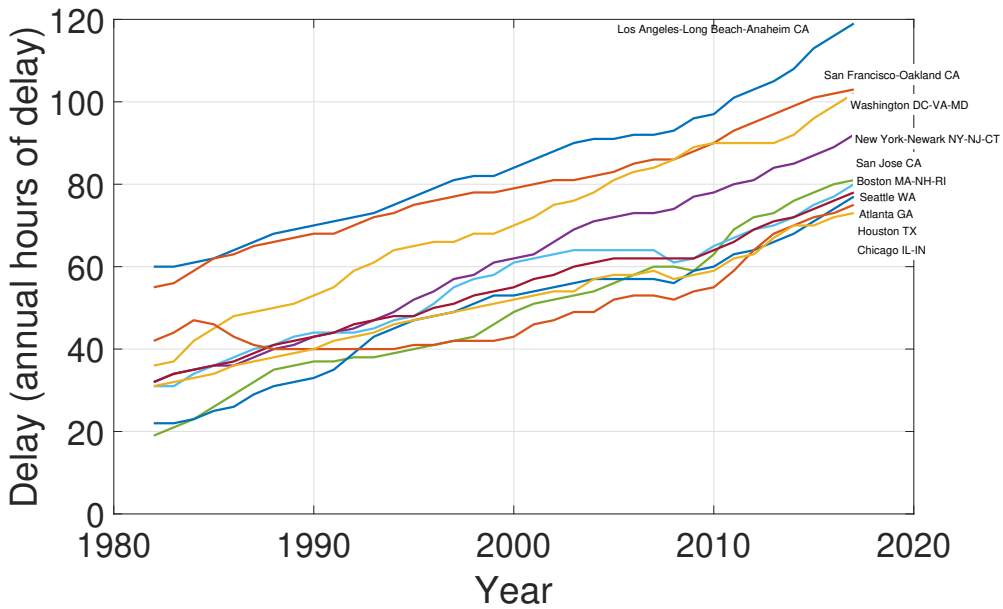

Figure 1.1: Annual hours of delays per commuter of 10 US cities from 1982 to 2017. Source: Urban Mobility Report(https://mobility.tamu.edu/umr/).

- Traffic incidents;
- Work zones;
- Weather;
- Traffic control devices;
- Special events;
- Fluctuations in traffic.

These factors can also interplay with each other to make the traffic condition even worse. We can further classify these factors into external factors and internal factors, where internal factors are factors with respect to interactions among participants in the traffic, while external factors are not. The first five factors are external factors that cause the reduction of capacity at a certain road section, and the following factor is an external factor that induces an excessive demand of a road section at a time. The last factor is an internal factor depending on driving behaviors of participants in the traffic. Human driving behaviors are not perfect. Human driving behaviors could trigger 'turbulence' to traffic flow, which makes the traffic throughput even worse. For example, at highway merging sections, accumulation of disturbances caused by conflicts of uncoordinated traffic may interrupt the traffic flow or make the already congested traffic even worse. Another example is the so-called phantom traffic jam, a sop-and-go wave emerging without an apparent bottleneck, which is caused by

limited human driving competence. We may reduce the disturbances to the traffic caused by limited behaviors of human drivers if we could manipulate all the vehicles in the traffic properly. Conventionally, human driving behavior can be manipulated by traffic management systems like ramp metering or variable speed limit are kinds of strategies [55] [32]. Effectiveness of this kind of strategy is limited because the control inputs are indirect and sparse, and the overall performance would be depending on compliance rates. As automated vehicles have advanced in recent years, vehicle automation provides us new opportunities to directly control vehicles, so that we can expect better traffic efficiency with proper controls.

Development of vehicle automation in recent decades gives us a lot of imaginations of a bright future of the transportation system. Since the concept of automated vehicle was introduced by Norman Bel Geddes in the General Motors Futurama exhibit at the New York World's Fair (1939-1940), automated vehicle technology have been advanced by many research projects in the US and around the world [21][25][81][82][92]. The emergence of modern vehicle automation was pushed forward when Defense Advanced Research Projects Agency (DARPA), the research arm of the United States Department of Defense, organized a series of challenges in 2004-2007. While it is believed that automated vehicles have potential to improve traffic efficiency, energy economy, and safety, efforts will be needed to advance the capability of automated vehicles. In this dissertation, particularly, we focus on the perspective of traffic efficiency.

In this thesis, we focus on traffic jams which are relevant to disturbances caused by driving behaviors and proposed solutions for improving traffic jams with vehicle automation. Firstly, we consider bottlenecks at the highway merging section. Recurrent bottlenecks at the highway merging section is a consequence of accumulated conflicts between mainline vehicles and on-ramp vehicles. By coordinating traffic coming from two directions, conflicts could be reduced and thus capacity drop can be mitigated or delayed. We want to study how much impact merging vehicles can cause to the highway traffic and also want to evaluate how much improvements with automated highway merging systems can possibly bring. Another focus of this dissertation is phantom traffic jams. Sometimes, even without apparent bottlenecks, mysterious phantom traffic jams could emerge spontaneously. Phantom traffic jams are related to human driving behaviors that tend to propagate and even amplify disturbance from downstream. We will analyze this phenomenon with analytical studies of car following models and numerically evaluate possible solutions for dissipating stop-and-go waves with control algorithms of automated vehicles. Lastly, we switch our focus to the automated truck control. Since truck is a major contribution of traffic congestion[2], and the growth of VMT traveled by truck is predicted to be faster than light vehicles[3], it is critical to consider how to reduce the negative impacts of trucks on the transportation system with vehicle automation.

[2] "Trucks account for 20 billion (11 percent) of the cost, a bigger share than their 7 percent of traffic" [77].

[3] FHWA Forecasts of Vehicle Miles Traveled (VMT): Spring 2019 (`https://www.fhwa.dot.gov/policyinformation/tables/vmt/vmt_forecast_sum.pdf`)

1.2 Overview and Contributions

In this dissertation, we study longitudinal control of automated vehicles and analyze their potential impacts on highway traffic, particularly in the sense of efficiency of the traffic flow. Overview and main contributions of each chapter is given below.

In chapter 2, V2I and V2V based automated highway merging control systems are studied. The impacts of both systems under different penetration rates of automated systems are evaluated. We propose both V2I and V2V enabled automated highway merging systems and validated their performances in microsimulation. We show that the both systems have potentials to accommodate higher traffic flows, V2I system being able to accommodating 200 more vehicles per hour and V2V system being able to accommodating 500 more vehicles per hour. Besides, we show that travel delays can be reduced significantly with V2V communication, and mildly improved with V2I system.

In chapter 3 and chapter 4, we focus on the phantom traffic jams, which is relevant to stability of the traffic dynamics. Stop-and-go waves can emerge spontaneously without an apparent bottleneck. Small fluctuations always exist in vehicles' motion, human driving behavior tends to amplify fluctuations. When traffic density is high, fluctuations would accumulate, and eventually stop-and-go waves would emerge. Experiments on closed-ring roads have proved that this phenomenon can be induced purely by human driving behavior [85]. Experiments on a closed-ring road have also demonstrated that the stop-and-go waves can be potentially dissipated with automated vehicles [84]. While traffic on the closed-ring road can be considered as an autonomous system composed of multiple car following models and appearance of stop-and-go waves on it can be considered as a stability problem, traffic on open highway can be modeled as an input-output system composed of multiple car following models and appearance of stop-and-go waves can be modeled with string unstable car following models. We study the connection between the two analytically and prove stability of the ring road traffic based on string stability of car following models. We extend previous analysis and show results for a general class of car following models. For traffic composed of heterogeneous car following models, we can show that ring road stability is essential to prevent stop-and-go waves on normal highways. For traffic of identical car following models, we show that ring road stability is if and only if condition for preventing stop-and-go waves on highways. Since ring road stability is essential for preventing phantom traffic on highways, ring roads can then be used to verify capability of automated vehicles to dissipate stop-and-go waves. In chapter 4, we numerically study performance of automated vehicle algorithms under different penetration rates in simulations.

In chapter 5, we focus on the controller design and implementation of longitudinal motion control for trucks. A hierarchical controller with an upper controller and a lower controller is developed, where the upper controller computes the desired acceleration for a given task and then the lower controller executes actuators for the given acceleration. The lower controller is developed based on a physical model of vehicle longitudinal dynamics. A parameter estimator is integrated with the lower controller to estimate unknown parameters. Two main functions are developed for the upper controller: speed following and car following.

For the speed following, a smooth speed profile considers acceleration constraint and jerk constraint is generated to avoid overshoot. For the car following controller, a robust string stability controller is designed considering the uncertainty of the actuator dynamics and the requirement of a sufficient condition for traffic stability. To enhance the car following performance, a vehicle-to-vehicle communication is used to access the leading vehicle speed directly. Simulations and experiments are carried out to validate the proposed controller. In chapter 6, final remarks of the dissertation and an outlook of future research are given.

Chapter 2

Automated Highway Merging System

2.1 Overview

Highway merging is one of the most challenging driving situations. During the merging process, a driver need to monitor the speeds and positions of other vehicles coming from another direction and predict theirs intentions, while adjusting its speed in order to merge smoothly and safely. Observations and predictions of other vehicles is critical for safe and smooth merging. However, observing other vehicles coming from the other directions may be difficult because the on-ramp road is usually curvilinear and physically separated from the highway lanes, making it hard to estimate speeds and distances of vehicles from both ends, and what is even worse is that the visibility of other vehicles may be fully blocked by the highway structure. The vehicles coming from both directions may only see vehicles from the other direction clearly when the on-ramp vehicles are in the acceleration lane on the highway, which means the time to response for the vehicles involved in the merging procedure is short. In addition to the limited response time, generally lacking of coordination among vehicles makes the highway merging even more stressful. Unlike driving through a traffic light controlled intersection, drivers are generally instructed whether they should go or not, during highway merging, drivers need to constantly judge other motions and intentions of other vehicles based on driving experience and common sense. This procedure could be not only physically challenging but also mentally intensive when multiple vehicles are trying to merge at the same time. From the perspective of transportation system, because the traffic from two directions are not coordinated, conflicts are likely to arise at the merging section, which makes the traffic at merging section less efficient and even less safe.

Therefore, frameworks leveraging wireless communications to coordinate traffic at the highway merging section are proposed to relieve the bottleneck at the highway merging section and assist human drivers at the merging section. We propose two frameworks based on *Vehicle-to-Infrastructure* (V2I) communication enabled automated highway merging system and *Vehicle-to-vehicle* (V2V) communication enabled automated highway merging system. In the first scenario, V2I communication is used to extend the abilities of on-ramp vehicles

to detect the vehicles on the mainline, so that on-ramp vehicles with wireless communication capability would be able to detect the mainline vehicles earlier and could adjust their speeds with sufficient time so that they could merge into highway more smoothly. In the scenario of V2V communication, vehicles with communication capability could not only 'see' each other, but also could coordinate with each other actively, which would further reduce the conflicts due to uncertainties of driving behaviors of others. To evaluate the performances of the proposed automated highway merging systems, the systems are modeled in the microsimulation. Performances under different penetration rates are evaluated in terms of travel time. Simulation results shows the potential of using V2I/V2V to improve the traffic flow at the highway merging section. Main contributions of this chapter are:

- we propose a framework of V2I communication based automated highway merging system to enhance traffic flow at the merging section;
- we propose a framework using V2V communication based automated highway merging system to enhance traffic flow at the merging section;
- we evaluate both systems with well-calibrated microsimulation models and demonstrate the potentials of proposed systems. The evaluation is done in several different scenarios under different penetrate rates;
- we show that both systems are able to accommodate higher traffic flows, V2I system being able to accommodating 200 more vehicles per hour and V2V system being able to accommodating 500 more vehicles per hour.
- we show that travel delays can be reduced significantly with V2V communication. When traffic flow is at 6800 veh/hr, mean travel delay has been reduced from more than 40 seconds to less than five seconds.

Vehicles entering the highway from the on-ramp would possibly conflict with vehicles on the mainline and interrupt highway traffic flow. These conflicts could slow down mainline traffic and cause a bottleneck [116][8]. To improve traffic at the merging section, many solutions have been proposed by coordinating on-ramp vehicles and mainline vehicles.

Coordination of vehicles can be done by means of V2V/V2I communication. WAVE / DSRC [45] is a technology that enables V2V communication and V2I communication and thus makes related applications possible. An overview of applications using V2V/V2I and also other communication frameworks are summarized in [10][23][76]. Lu *et al.* [51] established mathematical frameworks for automated highway merging problems and derived control algorithms for variety of situations. The derived controller have been implemented and tested [54][110] in real world experiments. Milanes *et al.* [61] proposed an automated highway merging system which generates reference target gaps for vehicles based on their distances to the merging point A fuzzy control is used to track the target gap. The system is validated in real world experiments. Davis [19] proposed an ACC based cooperative merging strategy to to reduce conflicts in a merging section, and simulation experiments were carried

out to validate the performance. Xu *et al.* [71] analyzed the effect cooperative merging under different penetration rates in terms of maximum braking effort and show that cooperative merging can generally reduce perturbations more with higher penetration rates. The need for cooperative merging is more critical in the future when more vehicles are automated and connected and are forming 'CACC platoons', where gaps between vehicles are shorter and thus harder for other vehicles to merge [95]. Pueboobpaphan *et al.* [70] proposed a highway merging control which mainline vehicles are maneuvered to open gaps for entering vehicles while on-ramp vehicles are driven manually. Their approach is similar to the V2I automated highway merging system we are showing here, only one side of the traffic is being controlled while the other side is driving manually; but in this work, we consider the controls of the on-ramp vehicles and let the mainline vehicles drive manually, which is more nature, because highway vehicles typically have higher priority in terms of right out of way. Besides longitudinal based maneuvers to match gap for on-ramp vehicles, advising mainline vehicles to make a lane change in advance to open spaces for on-ramp vehicles can also reduce conflicts. Park *et al.* [65] proposed a lane change advisory algorithm, which advising mainline vehicles to make lane changes in advance if there would be potential conflicts with the on-ramp vehicles.

Inspired by these works, two different frameworks using V2I and V2V communication are proposed and evaluated in the microsimulation under different penetration rates.

This study is based on a microsimulation at a highway merging section. A section of four-lane highway with a single one-lane on-ramp entering the highway is considered, where the on-ramp road is directly connected to an acceleration lane adjacent to four main lanes of the highway. The highway merging section used in the simulation is shown in the figure 2.1. The stretch of acceleration lane is not long and the entering vehicles must merge into the mainline highway before the acceleration lane ends. In this study, the baseline scenario is when all vehicles are driven manually, the vehicles entering the highway from the on-ramp could not see the vehicles on the mainline until the vehicles are in the acceleration lane of the highway, and vice versa. The on-ramp vehicles would only begin to match the speeds and gaps of the vehicles on the mainline when they are on the acceleration lane. In the meantime, the mainline vehicles may slowdown to allow gaps to let the on-ramp vehicles to enter the highway. A state of the art model human driving model [53][115] is used to simulate driving behavior at the merging section. The merging process generally does not go smoothly and introduces some disturbance to the highway traffic. When the traffic flows coming from both directions are high, the disturbance caused by merging vehicles would eventually cause traffic jams at the merging section. In the simulation, a fixed flow of the on-ramp vehicles is used, while the flow of highway mainline is varying so that we can observe how is the bottleneck getting worse with increased highway traffic flow. The on-ramp flow is picked with a high volume flow so that it can generate enough conflicts to induce traffic jams.

(Notations) Figure 2.2 is a snap shot of vehicles on the highway and the on-ramp, along with some notations indicating states of the vehicles. Let X_0 be a reference on the highway and $t \in [0, \infty)$ be the time variable. We define $x_i(t) \in \mathbb{R}$ as the distance of the vehicle $i \in \mathbb{N}$ to the reference point X_0 at time t. In other words, for vehicles on the mainline, $x_i(t)$ is

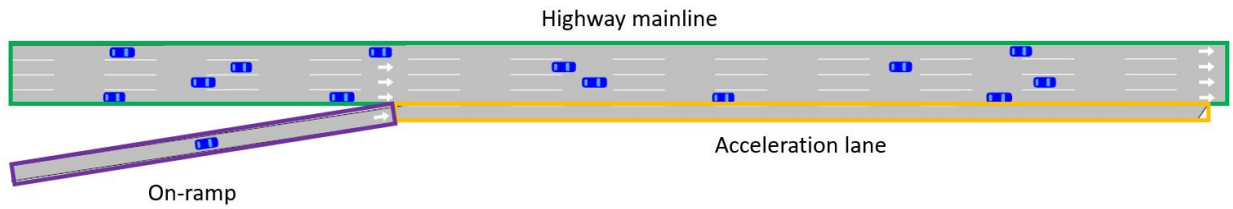

Figure 2.1: Four lane highway at the merging section. Green square indicates the area of highway mainline; yellow square indicates the area of the acceleration lane; and purple square indicates the on-ramp road.

the distance need to traverse on the highway before passing the X_0. We define $v_i(t) \in \mathbb{R}$ be the longitudinal speed of the vehicle i at time t. Because we mainly concern about the vehicles in the right most lane, only the vehicles in the right most lane are indexed. Mainline vehicles are indexed in increasing order based on the distance to the reference point X_0, i.e. $x_i(t) < x_j(t)$, $\forall i < j$, $i, j \in \mathbb{N}$. For example, in the figure 2.2, $x_1(t)$ of the vehicle 1 is shorter than $x_2(t)$ of the vehicle 2, which is shorter than $x_3(t)$ of the vehicle 3, and so one. Similarly, for on-ramp vehicles, we define the $x_{[i]}(t) \in \mathbb{R}$ as the sum of the distance it needs to take to enter the highway and the distance it needs to traverse along the highway to the reference point X_0; and $v_{[i]}(t) \in \mathbb{R}$ be the speed of the on-ramp vehicle vehicle $i \in \mathbb{N}$. For example, in figure 2.2, the position of the on-ramp vehicle is $x_{[1]}(t) = l_1 + l_2$ $(l_1, l_2 \in \mathbb{R})$ and its speed is $v_{[1]}(t)$.

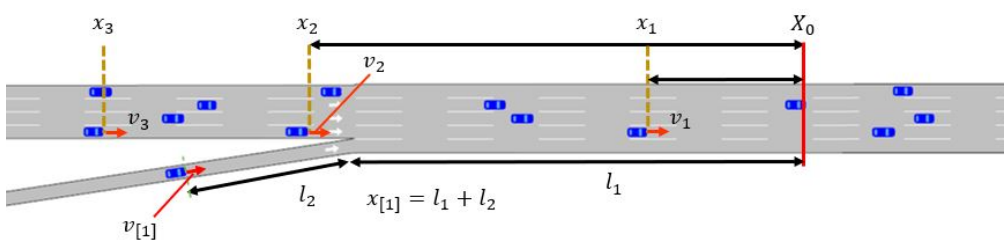

Figure 2.2: Illustration of vehicles around the highway merging section and their speeds and positions.

In the following sections, the V2I automated highway merging system and the V2V automated highway merging system will be introduced, followed by evaluations in the microsimulation.

2.2 V2I Automated Highway Merging System

(Overview of the V2I automated highway merging system) The basic concept of using V2I communication is to extend the line-of-sight of the on-ramp vehicles so that the

on-ramp vehicles can have more time to respond. The idea is using a *road-side-unit* (RSU) to sense the vehicle on the mainline and the on-ramp vehicles can access the data via use wireless communication to get the information of mainline vehicles earlier. Figure 2.3 illustrates the set up of the V2I automated highway merge system. Suppose the on-ramp intersects with the highway at Q_1. RSU is placed at the location Q_0. As mentioned, one of the main function of the RSU is detection the mainline vehicles, which can be done in practice with, for example, radar, lidar, vision sensor. Since the conflicts would likely to happen due to vehicles in the right most lane, the motions of the vehicles in the right most lane are particular interested. For simplicity, we assume the RSU only detects the right most lane. The red box indicates the region of the detection by RSU. We assume the range of RSU detection range is 200m, (i.e. $\overline{Q_0Q_2} = 200$). In addition, the RSU could also broadcast the information to on-ramp vehicles in the green region, so that on-ramps vehicles could 'see' vehicles on main line earlier. With the help of V2I, on ramp vehicles can observe mainline vehicles even before they are within the line-of-sight of the on-ramp vehicles and could use these information to control the on-ramp vehicle to match highway speed and a gap in mainline earlier. In the meanwhile, mainline vehicles are still controlled manually and their line-of-sight are still obscured by the highway structure and no extra information is available for them via V2I communication. This would also mean that mainline vehicles generally are not necessarily equipped with wireless communication equipment. Because mainline vehicles generally have right of way, it is mainly on-ramp vehicles' responsibility to match gaps. Provided that the mainline vehicles do not need to actively making gap to accommodate on-ramp vehicles, mainline vehicles may have little interests to having extra information of the on-ramp vehicles. Therefore, the V2I is designed mainly to benefit the on-ramp vehicles only.

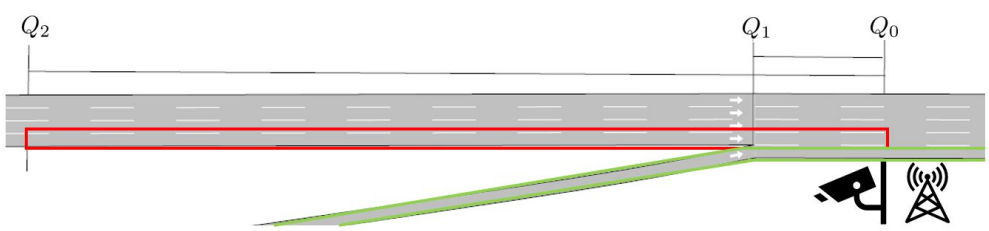

Figure 2.3: Illustration of the V2I automated highway merge system. Q_0 : location of the road side unit, which can detect positions and speeds of vehicles on the highway in the region indicated by the red box, and can also communicate with vehicles from the on-ramp (indicated by green lines). Q_1 is the intersection of the on-ramp and the highway. Q_2 is the farthest point that can be detected by the road side unit.

Details of the V2I automated highway merging system The model of the V2I automated highway merging system composed of four main steps. Process of each step is described below. For simplicity, in the following description, we assume there is only one vehicle entering the highway from the on-ramp, but the system can be easily extend to the case with multiple on-ramp vehicles.

1. Data processing: In this step, the average speed of the vehicle on the mainline is computed. Suppose there are $n \in \mathbb{R}$ vehicles in the right most lanes of the highway in the sensing range of the RSU, each having a speed $v_i(t), \forall i \in \{1, \ldots, n\}$. Let $\bar{v}_{hwy}(t) \in \mathbb{R}$ be the average highway speed at time $t \in [0, \infty)$:

$$\bar{v}_{hwy}(t) = \frac{1}{n} \sum_{i=1}^{n} v_i(t).$$

2. Speed harmonizing: The on-ramp vehicle would adjust its speed to follow the highway speed $\bar{v}_{hwy}(t)$, which is computed using the speed measurements of the vehicles in mainline. The acceleration command for the on-ramp vehicle $a_{[1]}(t) \in \mathbb{R}$ is defined as follows:

$$a_{[1]}(t) = k(\bar{v}_{hwy}(t) - v_{[1]}(t)),$$

where $k \in \mathbb{R}$ is a control parameter.

3. Gap searching: As soon as the on-ramp vehicle speed is close to the mainline vehicle speed (say at time $t_1 \in [0, \infty)$), it picks the closest vacant gap as the target merging gap:

$$G = \{p, q \in \mathbb{Z} | x_n(t_1) \geq \ldots \geq x_q(t_1) \geq x_{[1]]}(t_1) \geq x_p(t_1) \geq \ldots \geq x_1(t_1)\},$$

the vehicle p is the index of the *virtual leading vehicle*. It is virtual, because the on-ramp vehicle technically can not see it directly and the on-ramp vehicle is following it assuming it is physically ahead of it. Let $v_p(t) \in \mathbb{R}$ be the speed of the *virtual leading vehicle*.

4. Gap tracking: The on-ramp vehicle would follow the *virtual leading vehicle* closely with a new acceleration command based on relative speed and relative distance with following formulation:

$$a_{[1]}(t) = k_1(v_p(t) - v_{[1]}(t)) + k_2(x_{[1]}(t) - x_p(t) - d_{\text{des}} - k_3 v_{[1]}(t)),$$

where $d_{\text{des}} \in \mathbb{R}$ is a desired following distance; $k_1 \in \mathbb{R}$, $k_2 \in \mathbb{R}$, and $k_3 \in \mathbb{R}$ are design parameters. Ideally, the on-ramp vehicle would follow the *virtual leading vehicle* closely and the on-ramp vehicle should have already matched a gap and speed of the highway flow when it is in the acceleration lane. Matching a gap and speed of the highway flow is essential to merge into highway successfully.

5. Merging: When the on-ramp vehicle is in the acceleration lane and the gap to the leading vehicle and the following vehicle meet the requirement, the on-ramp vehicle would merge in.

There are some advantages of the V2I automated highway merging system:

- It does not require every vehicles have communication capability. Therefore, it is suitable even when penetration rates of the wireless communication on the vehicle is low;

- It can improve the traffic flow at the merging section by matching the speed of the on-ramp vehicle to highway speed and matching the position of the on-ramp vehicle to a gap earlier.

However, there are some limitations of the system. The system simply utilize one-way communication to help the on-ramp vehicle. It still relies implicit coordination between on-ramp vehicles and mainline vehicles at the end. Although the intention of the on-ramp vehicle may be more clear to mainline vehicles by matching the speed and align a gap earlier, ambiguity is not fully resolved because there is still no communication between vehicles directly. Therefore, an V2V based automated highway merging system is proposed.

2.3 V2V Automated Highway Merging System

Similar to the V2I automated highway merging system, the idea of V2V automated highway merging system is also using wireless communication to enhance the field of views of vehicles in the merging section. While increasing the field of view, V2V communication also enables vehicles from both directions to coordinate merging directly, so that the conflicts between two flows can be further reduced. In this V2V scenario, vehicles are still generally governed by the human driving model. Only a portion of vehicles that is equipped with vehicle to vehicle communication instruments would be controlled by the V2V automated highway merging system. The V2V automated highway system only controls vehicles near the merging section. The region of the control zone of the V2V automated highway merging system is depicted in figure 2.4, where V2V vehicles would participate in the V2V automated highway merging once they are inside the region and would resume manual driving as soon as they leave the region. The control range of the system is from 200 meters upstream (i.e. $\overline{Q_1Q_2} = 200$) to the end of the merging section (Q_0).

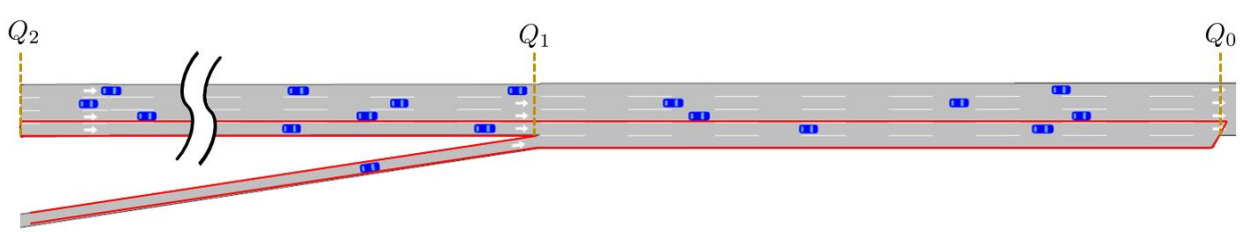

Figure 2.4: Illustration of the V2V automated highway merging system. V2V Vehicles inside the V2V automated highway merging control region (indicated by red lines) would be controlled by the automated vehicle highway merging and would resume manual driving once they leave the region.

Details of the V2V automated highway merging system The model of the V2V automated highway merging system is described below. Similarly, the V2V automated highway merging system also composed of a few steps. The process involves coordination between

mainline vehicles and on-ramp vehicles. Since the on-ramp vehicles are the ones required to find the gaps, the coordination is generally conducting by the on-ramp vehicles. That is, the on-ramp vehicles would be actively pairing with vehicles on the highway and requesting to form a 'virtual platoon'.

1. Data processing: Similar to the V2I automated highway merging system, the first step of the V2V automated highway merging system is also for the on-ramp vehicle to collect speeds and positions of mainline vehicles for later use. The information could be done with V2V communication to get the positions and speeds of mainline vehicles. Again, we use the average speed of vehicles on the mainline to compute a reference speed for on-ramp vehicle to follow:

$$\bar{v}_{hwy}(t) = \frac{1}{n}\sum_{i=1}^{n} v_i(t).$$

2. Speed coordination: The second step for the on-ramp vehicle-[1] is to match the speed of highway vehicles. The acceleration command $a_{[1]}(t)$ of the on-ramp vehicle could be computed as follows:

$$a_{[1]}(t) = k(\bar{v}_{hwy}(t) - v_{[1]}(t)),$$

where $k \in \mathbb{R}$ is a design parameter of the controller.

3. Gap alignment: The on-ramp vehicle needs to actively search for a gap on on the mainline. As soon as the on-ramp vehicle speed is close to the mainline vehicle speed (say at time $t_1 \in [0, \infty)$), the on-ramp vehicle needs to find a *virtual leader*(VL) and a *virtual follower*(VF). The *virtual leader* and the *virtual follower* are found by firstly projecting the position of the on-ramp vehicle on the mainline and the vehicle that is right ahead of the projection point is the *virtual leader* and the one that is behind the projection point is the *virtual follower*. Formally, the *virtual leader* and the *virtual follower* for the on-ramp vehicle could be defined as follows:

$$(VF, VL) = \{(p, q) \in \mathbb{Z}^2 | x_n(t_1) \ldots \geq x_p(t_1) \geq x_{[1]}(t_1) \geq x_q(t_1) \geq \ldots \geq x_1(t_1)\}.$$

Once the VF and VL are found, the on-ramp vehicle would need to connect with them with V2V communication and coordinate with them to form a *virtual platoon*. In the *virtual platoon*, the on-ramp vehicle would follow its *virtual leader*, at the same time it also plays the role as a *virtual leader* for its *virtual leader*. When there are multiple on-ramp vehicles entering the highway at the same time, each on-ramp vehicle would sequentially find their VL and VF on the mainline following the same logic shown above and form a long *virtual platoon*. For example, suppose there are two on-ramp vehicles-[1] and -[2] on the on-ramp and at the same time there are three mainline vehicles p, q, and r such that the their distance satisfy following conditions:

$$x_p(t_1) > x_{[2]}(t_1) > x_q(t_1) > x_{[1]}s(t_1) > x_r(t_1).$$

As a consequence, these five vehicle will form a *virtual platoon* : $r - [1] - q - [2] - p$, where vehicle-r is the VF of vehicle-[1], which is the VF of the vehicle q, and vehicle-q is also the VF of vehicle-[2], which is the VF of vehicle-q.

The idea of using V2V is to coordinate any two mainline vehicles to an entering on-ramp vehicle. Hence, the on-ramp vehicle need to communicate with both VF and VL at the same time. When the V2V penetration rate is low, finding both VF and VL may not always be possible. In the case that either VF and VL on the mainline could not be found, *virtual platoon* not being formed, the on-ramp vehicle should still be driven manually.

4. Virtual platoon: When the mainline vehicles and on-ramp vehicles form a virtual platoon, the longitudinal motions of the vehicles would be controlled by the V2V automated highway merging system. For the vehicles in the *virtual platoon*, their acceleration are governed by the relative distance and the relative speed to their virtual leader in the *virtual platoon.* We use $x_{VL,*}(t) \in \mathbb{R}$ and $v_{VL,*}(t) \in \mathbb{R}$ to denote position and speed of their corresponding virtual leader. Their acceleration command $a_*(t) \in \mathbb{R}$ is defined as follows:

$$a_*(t) = k_p(x_*(t) - x_{VL,*}(t) - h_d v_*(t)) + k_d(v_*(t) - v_{VL,*}(t) - a_*(t - \delta t)),$$

where $k_p \in \mathbb{R}$, $k_d \in \mathbb{R}$ and $h_d \in \mathbb{R}$ are control design parameters, $\delta t \in \mathbb{R}$ is a step size of the control system. The behavior of V2V automated highway merging system is similar to cooperative adaptive cruise control. Therefore, a model derived based on experimental data in real highway traffic [59] is used. In this work, h_d is set as the desired time gap headway of the manual driver model, 1.3 seconds.

5. Merging: When the on-ramp vehicle is in the acceleration lane and the gaps between VF and VF in consecutive positions in the adjacent mainline lane are safe to make a merge, the on-ramp vehicle will make a lane change and return the control to human driver. Otherwise, the members of the virtual platoon will apply the V2V merge control to adjust the gap until it is large enough to accommodate a safe merging.

The V2V automated highway merging exploits the advantages of direct communication between vehicles. The on-ramp vehicles and mainline vehicles can not only detect vehicles on the other side earlier but also directly coordinate with them to reduce conflicts. However, the coordination requires both vehicles on the mainline and vehicles on the on-ramp to have wireless communication capability. In principle, higher penetration rates of connected vehicles is needed to effectively deploy such system to improve traffic flow at the merging section. Evaluating the effectiveness of the system under different penetration rates is shown in the next section.

2.4 Simulation Studies

Evaluation of the automated highway merging systems is done in Aimsun, a microscopic traffic simulation software. A four-lane highway with a on-ramp road as described in section 2.1 is built in the simulation. The source of the highway is at 2000 meters away from the

merging section, so that the mainline traffic flow entering the merging section would be quite stable and perturbations to the traffic flow would be mainly from conflicts between on-ramp vehicles and mainline vehicles at the merging section. Traffic flow smoothness is assessed with regard to average travel time for vehicles to travel a 1500m long highway section stretching across the merging section. Several scenarios with different control systems are compared. For each scenario, the travel time is evaluated with varying highway traffic flow volume while keeping a high on-ramp flow volume fixed at 500 veh/hr. For a given highway flow, the travel time is computed over one hour of simulated operations.

We first evaluate the performances of the proposed two automated highway merging systems and compare them against baseline scenarios. The scenarios are:

- All manual: All vehicles are controlled by state-of-the-art human driving model described in [53][115]. This is a baseline scenarios, demonstrating the worst case without any control.
- V2I merge control: All on-ramp vehicles are controlled with V2I automated highway merging control (section 2.2), while other vehicles are controlled with human driving model.
- V2V merge control : All vehicles are assumed to have capability of wireless communication. Vehicles in the control zone of the system are controlled by the system, while all other vehicles are maneuvered by the human driving model (section 2.3).
- All V2V control: All vehicles are assumed to have capability of wireless communication. Similar to the previous scenario, but vehicles not involved in the automated highway merging would be controlled with cooperative adaptive cruise control (CACC). The CACC model is as described in [59]. This scenario demonstrated the ideal case when all vehicles are connected and cooperatively controlled.
- All manual w/o on-ramp: Similar to the first scenario, but without on-ramp traffic flow entering the highway. By comparing this scenario to the first scenario, one can observe the impact of the on-ramp traffic to the highway traffic flow.

Figure 2.5 shows the average travel time for mainline vehicles. Figure 2.6 shows only the average travel time for the on-ramp vehicles. As mentioned, the last scenarios has no on-ramp vehicles entering the highway. Thus, no travel time is being reported for this scenario in figure 2.6. Figure 2.7 shows the average travel time for all vehicles. Average travel time for on-ramp vehicles are generally longer than the mainline vehicle is due to the fact that initial speeds of on-ramp vehicles are lower than highway traveling speed. For each scenario, simulation results are done with mainline flows up to the point when no higher mainline traffic flow can be generated; for example, for *All manual w/o on-ramp* case, the maximum flow that can generate is 8300 veh/hr.

By comparing *All manual* and *All manual w/o on-ramp*, we can see that the on-ramp flow drastically disturbs the traffic flow near the merging section. Eventually, the on-ramp flow

causes a bottleneck at the merging section and reduce the capacity of the highway from more than 8000 veh/hr to around 7000 veh/hr. The improvement of the V2I system is limited at lower traffic flows and is more significant at higher flow volume, but it can effectively improve the throughput by around 300 veh/hr. As expected, the V2V system improves the travel time even more and can sustain maximum about 500 veh/hr more than the all manual driving scenario. The *all V2V control* scenario demonstrated ideal scenario and show that the traffic flow volume may be increase by 4000 veh/hr when all vehicles are connected and cooperatively controlled.

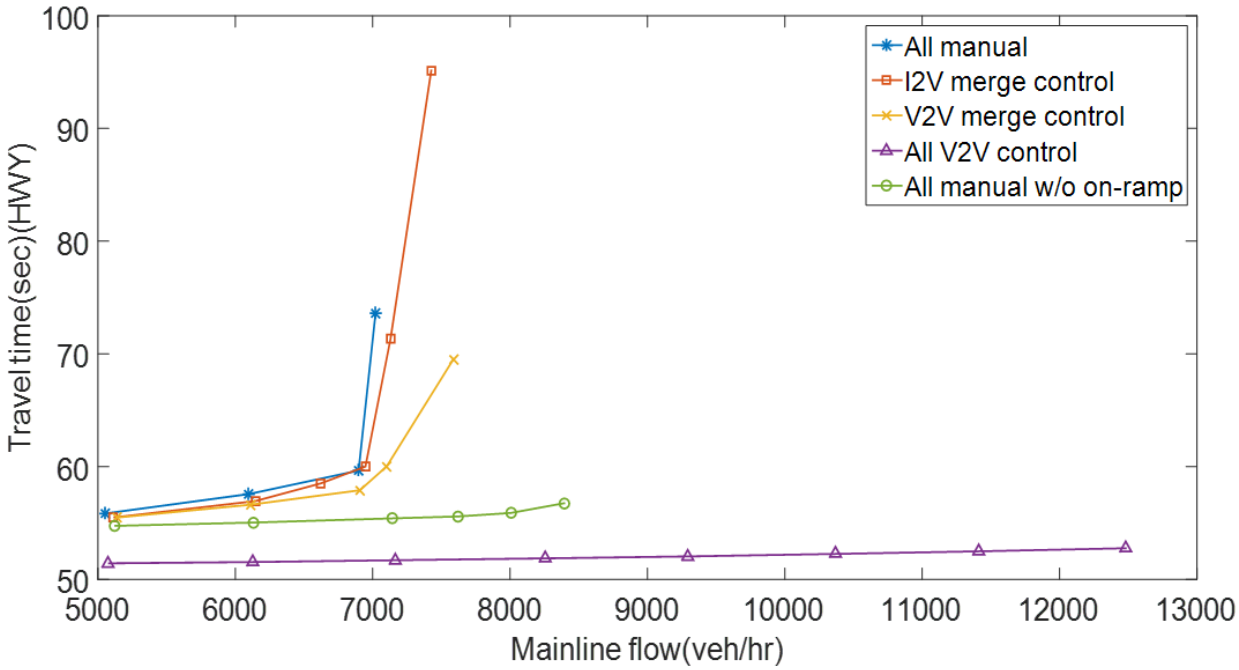

Figure 2.5: Average travel time of the mainline highway vehicles approaching from upstream.

According to the above results, we have seen the potential of the V2V system at 100% penetration rate of V2V communication. The V2V automated highway merging system in principle requires a higher penetration rates. We are interested to evaluate how sensitive the performance of the V2V with respect to the penetration rates of the connectivity. Thus, we evaluate the performance of the V2V automated highway merging system under different penetration rates, and combinations of V2V and V2I.

Penetration rate of 0% is shown as a baseline along with penetration rates of 25%, 50%, 75%, and 100%. Figure 2.8 shows the average travel time for mainline vehicles. Figure 2.9 shows only the average travel time for the on-ramp vehicles. Figure 2.10 shows the average travel time for all vehicles. Again, average travel time for on-ramp vehicles are generally longer than the mainline vehicle because of the fact that initial speeds of on-ramp vehicles are lower than highway traveling speed. The plotted results stop at the point where the merge junction is saturated and the traffic congestion propagates beyond the end of the

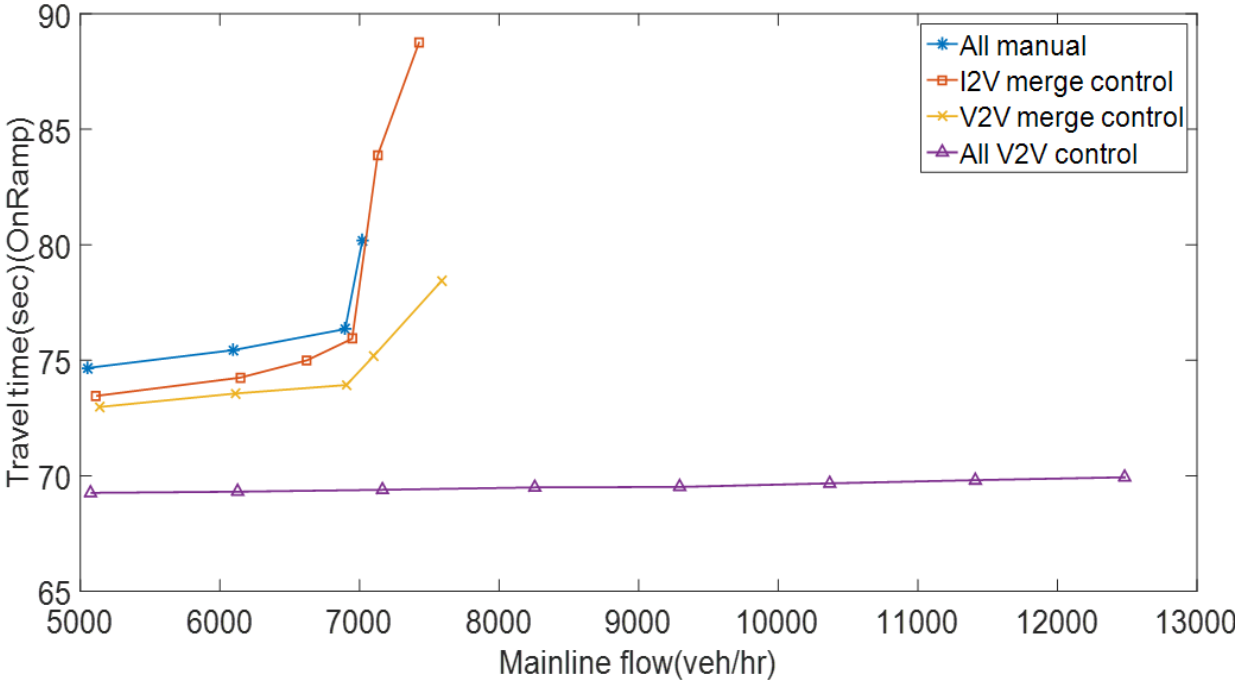

Figure 2.6: Average travel time of the vehicles entering the highway from the on-ramp. Because last scenario has no vehicles entering the highway, no data is being reported.

network. At travel flow 6800 veh/hr, the travel time for free-flow traffic is about 55 seconds. By comparing the travel time of 0% to 100% V2V at 6800 veh/hr, we can observe that the travel delay has been improved significantly with V2V (from more than 40 seconds of delay to less than five seconds). Besides, the V2V can improve the maximum flow by more than 500 veh/hr (from 6800 veh/hr to 7500 veh/hr).

As average travel time increase with traffic flow volume because more conflicts happen at higher flow, the benefit of the V2V system is more significant at higher flow volume. The results show that the performance of the V2V merge control improves with increases in the V2V penetration rate. Note that the results do not scale linearly with the market penetration, with the 50% case showing a relatively small improvement compared to the 100% case. This is because when the penetration rate is low, the probability of forming a virtual platoon is smaller, which means most vehicles would driven manually and the improvement would be less significant. When the penetration rate is low, the V2I system may still help on-ramp vehicles even. To maximize the benefit of vehicles with wireless communication device, We can consider to combine the V2V and V2I at medium penetration rates.

The results of V2V system combining with V2I system at medium penetration rates are shown. Figure 2.11 shows average travel time of vehicles with different combination of V2V system and V2V system when 50% of vehicles are equipped with wireless communication devices. Figure 2.12 shows the results when the penetration rate of communication device is 60%. With the help of V2I system, we can see that the travel time can be greatly improved

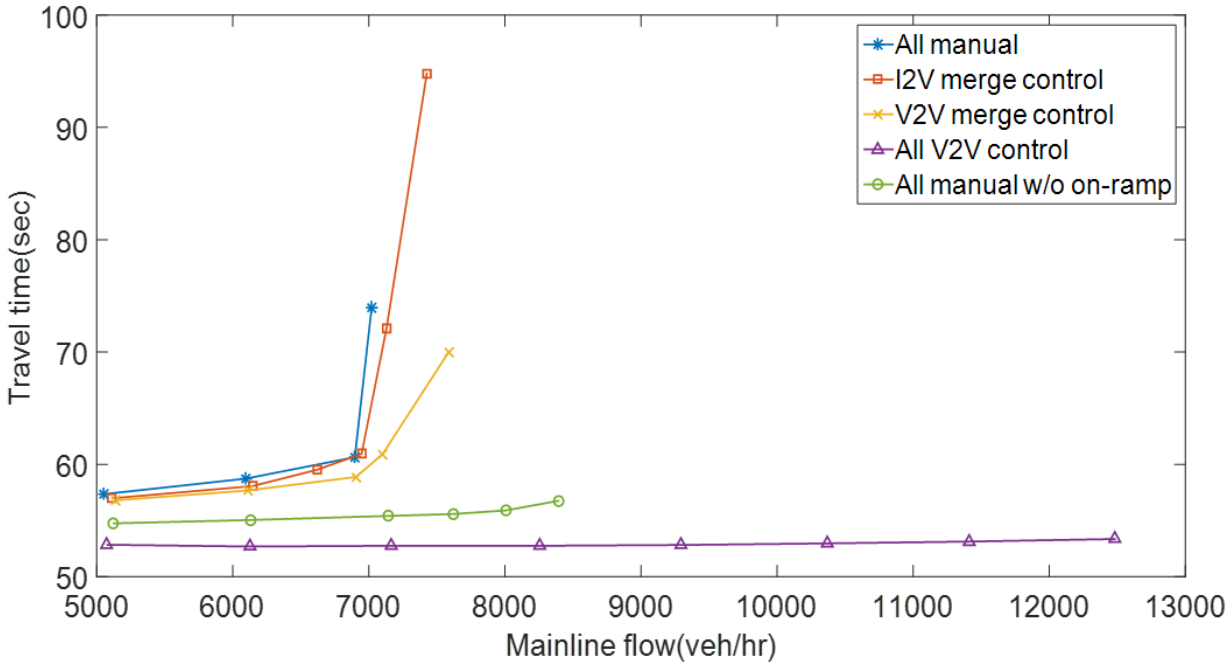

Figure 2.7: Average travel time of all vehicles(on-ramp+mainline vehicles)

comparing to V2V only system.

2.5 Summary

In this chapter, frameworks using wireless communication to relieve bottlenecks at highway merging section are proposed: the V2I automated highway merging system and the V2V automated highway merging system. These two systems are evaluated in microsimulation in terms of travel time. Comparisons with respect to baseline scenarios show that both systems have been successfully improved the traffic flow at the merging section, with the V2V system showing more significant improvement than the V2I system. Penetration rates study shows that the V2V system is sensitive to penetration rates of communication devices. Although improvement of the V2I system is not significant, technically, the required penetration rates for the V2I system is relative low. It can benefit every on-ramp vehicles with communication devices. Therefore, the benefit of the V2I system could be used as an incentive for adopting wireless communication devices at early phase when wireless communication device is firstly introduced to the market.

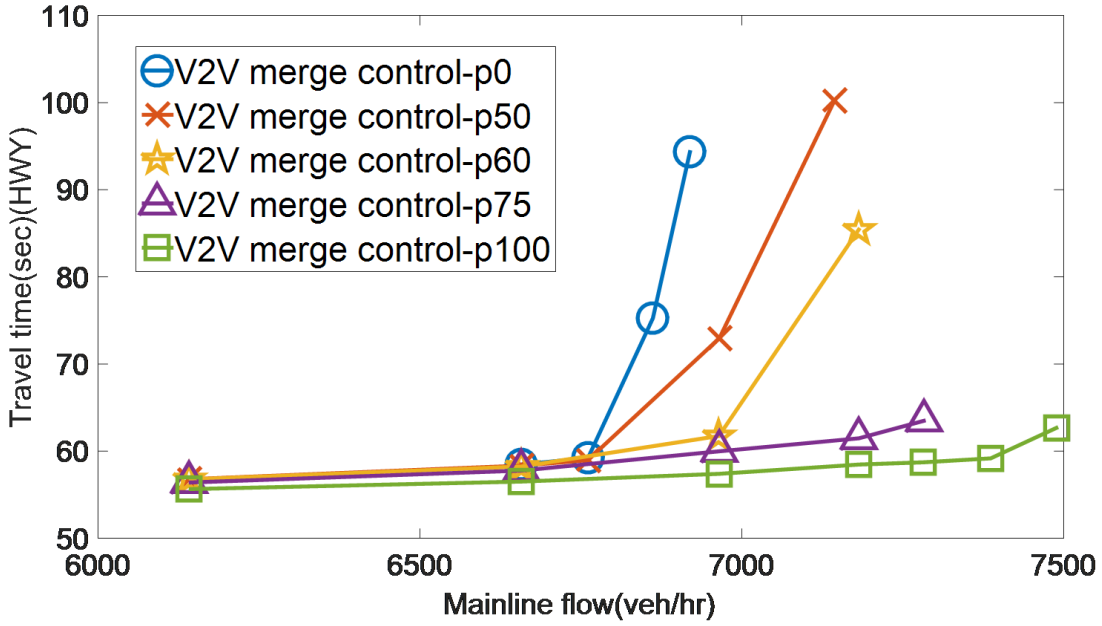

Figure 2.8: Average travel time of the mainline highway vehicles approaching from upstream.

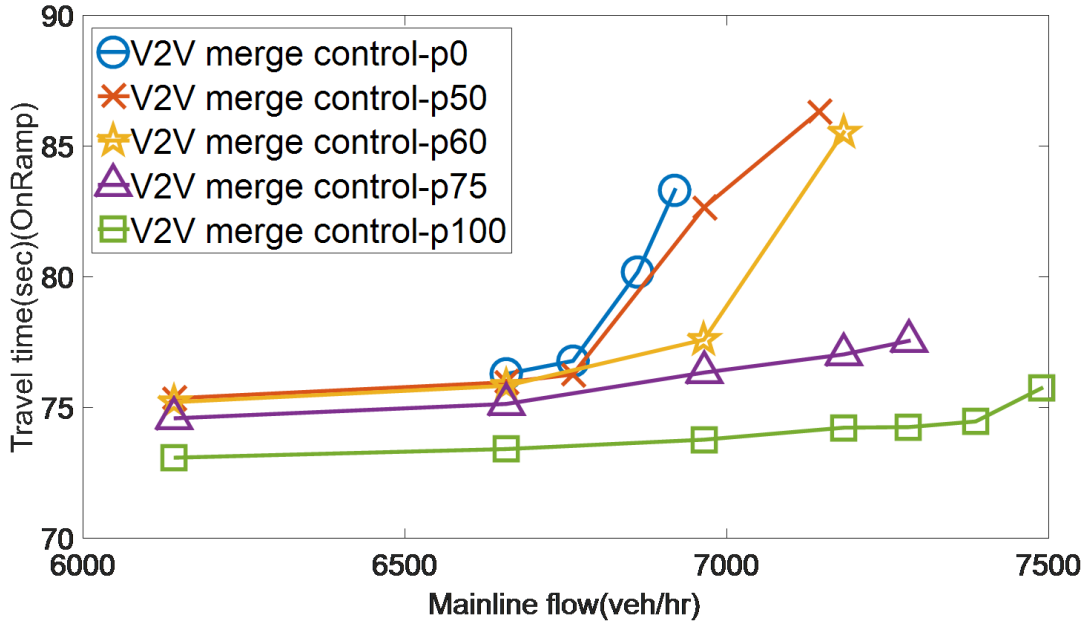

Figure 2.9: Average travel time of the on-ramp vehicles entering the highway.

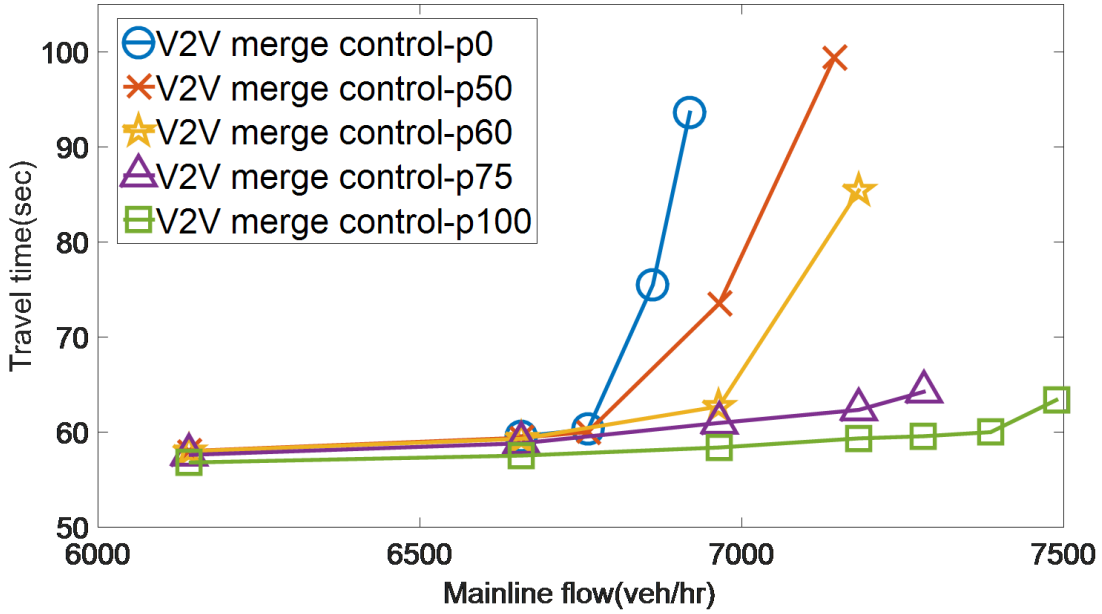

Figure 2.10: Average travel time of all vehicles(on-ramp vehicles+ mainline vehicles).

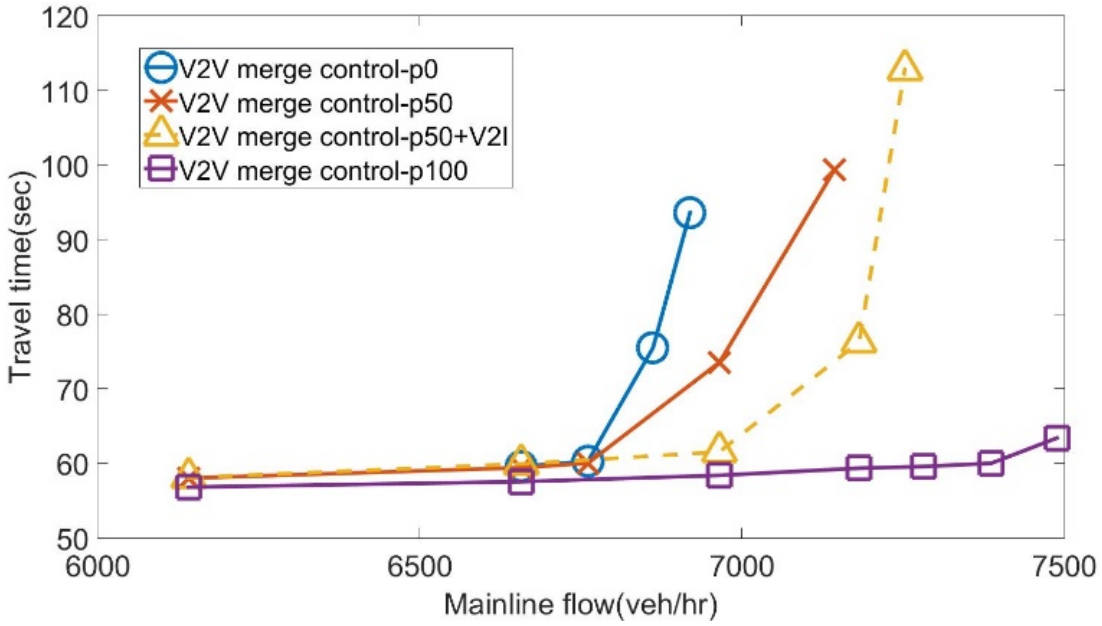

Figure 2.11: Average travel time of all vehicles with and without V2I merging control system when 50% of vehicles are equipped with communication devices.

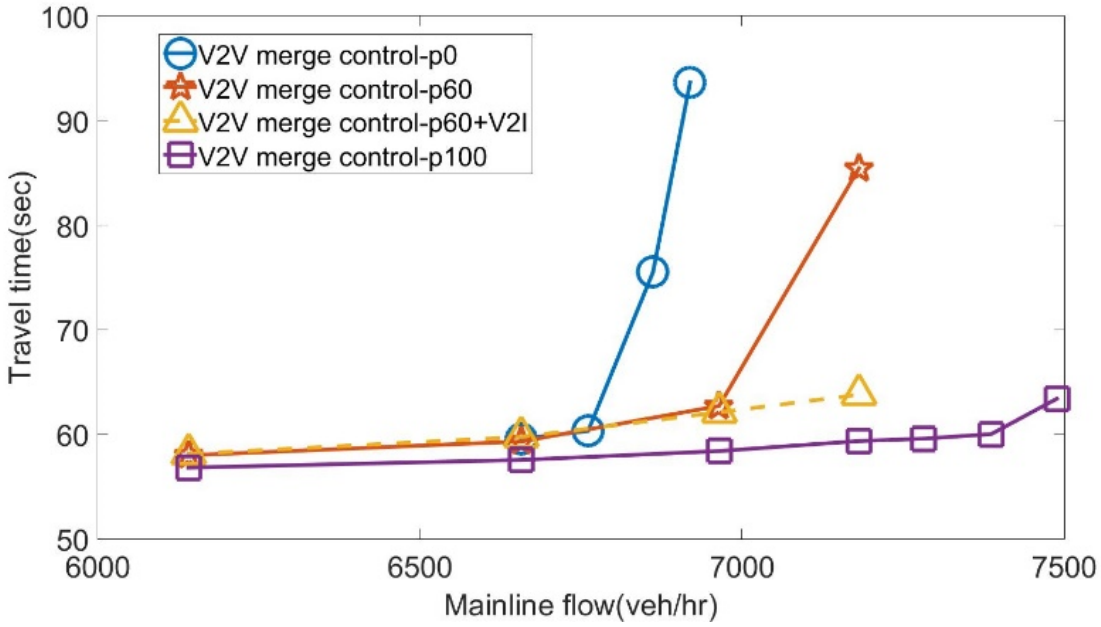

Figure 2.12: Average travel time of all vehicles with and without V2I merging control system when 60% of vehicles are equipped with communication devices.

Chapter 3

Traffic Stability Analysis on Ring Road

In this chapter and the next chapter, we will switch our focus to the phantom traffic jams, which is traffic jams not because of bottlenecks but because of underlying behaviors of vehicles in the traffic. Analytical studies are done in this chapter, while the next chapter is focused on numerical studies.

A string of vehicles on an open highway can be modeled as an input-output system composed of multiple car-following models, where the leading vehicle is 'seeing' its preceding vehicle and the preceding vehicle's state would act as input to the vehicle string. For the string of vehicles on highways, propagation of stop-and-go waves can be characterized with string stability. For a string of heterogeneous car following models, collective string stability is saying that the disturbance to the last vehicle in the string is smaller than the first vehicle in the string. For a string of identical car following models, the car following model is string stable if disturbance attenuates from downstream to upstream between any two consecutive vehicles. On the other hand, a string of vehicles on the closed-ring road can be seen as an autonomous system without exogenous input to the string. Input of every vehicle is the state of other vehicles in the string. In this case, emergence of stop-and-go waves can be considered as a stability problem. In this chapter, we analytically study the connection between string stability and ring road stability. We show that for a traffic composed of heterogeneous car following models, we showed that ring road stability is necessary for collective string stability. For traffic composed of identical car following models, ring road stability is necessary and sufficient for string stability the car following model. The results shown here can be used for stability analysis of traffic and for controller design. Simulation results are shown to test our analytical results.

3.1 Overview

In 2008, Sugiyama *et al.* [85] implemented the first ring road experiment to verify the supposition that traffic jams can emerge spontaneously without a bottleneck. In the experiment, a few vehicles were initially spaced equally on the ring road and drivers were asked to follow the traffic steadily. At the beginning of the experiment, vehicles were driving smoothly, but a few moments later, their speeds began to fluctuate, and eventually, stop-and-go waves appeared. Tadaki *et al.* [89] extended the ring road experiment in different settings and demonstrated that higher density would more likely trigger the emergence of stop-and-go waves. The emergence of stop-and-go waves can have adversarial impact to traffic efficiency and fuel economy and many previous works have demonstrated the potentials of improving traffic efficiency and fuel economy by smoothing traffic with control of automated vehicles (Alam *et al.* [3]; Malikopoulos *et al.* [57]; Wu *et al.* [103]; Xu *et al.* [112]; Zhao *et al.* [117]). In 2018, seminal experiments displaying implementations of stabilizing algorithms by Stern *et al.* [84] demonstrated the concept for the first time in real world experiments. In their experiments, capability of dissipating stop-and-go waves via an automated vehicle have been exhibited on a ring road, where both a Lyapunov based controller [20] and a hand designed controller [11],[12] are tested. Besides being used for validations, by modelling the ring road with car following models, the ring road can potentially be exploited for further usage, e.g. automated vehicle controller design (Kreidieh *et al.* [42]; Wu *et al.* [105]). While ring road models of car-following models can potentially bring new opportunities for transportation technology, comprehensive studies of the models are essential to leverage full utility of the models for extensive studies.

By modelling the ring road as a dynamical system composed of car-following models, the emergence of stop-and-go waves can be attributed to instability of the dynamical system. Bando *et al.* [5] pioneered the study and derived conditions of a car-following model for stable ring road based on analysis of eigenoscillation modes. Linear stability of the ring road can be studied based on eigenvalues of the ring road model. Orosz *et al.* [63][64] analyzed stability by Hopf bifurcations. Cui *et al.* [17] analyzed linear stability of the ring road based on eigenvalues of the linearized ring road model and derive a controller to stabilize the ring road. They both derived similar stability conditions on transfer functions of car-following models for a ring road of identical car-following models. A ring road model which consists of identical linear (or linearized) car-following models can be represented by a block circulant matrix. Eigenvalues of block circulant matrices can be determined by exploiting the special stricture [75][58][66]. Zheng *et al.* [118] analyzed stability of the ring road model by exploiting the structure of block circulant matrices and designed an optimal control to stabilize the ring road. These previous works were focused on identical car-following models or no more than two models. In this chapter, we provide a more general discussion of the ring road stability, not only for identical car-following models but also for heterogeneous car-following models. Particularly, string stability, which characterizes how disturbance is propagating between vehicles, is used to prove the stability of the ring road.

Different definitions of string stability can be found in the literature [24]. Swaroop *et al.*

introduced one of the earliest formal definition of string stability for a class on interconnected systems [87, 88]. Follow their definition, for linear systems, it is well-known that $\mathcal{H}_\infty$ norm of a transfer function being smaller or equal than one is considered as an equivalent condition for string stability [87, 72, 80]. A study of string stability for a platoon of heterogeneous linear vehicle models can be found in [79]. We follow the definition of string stability in the sense of the $\mathcal{H}_\infty$ norm to prove the stability of the ring road.

Main contributions of this chapter are summarized as follows:

- We formally model the ring road and study the ring road stability based on eigenvalues of the linearized model around an equilibrium point.
- We generally study the stability of a broader class of linear interconnected systems which has a structure similar to that of a ring road model. The stability can be determined based on string stability of subsystems. For the ring road of heterogeneous car following models, we prove that collective string stability is sufficient for a linear interconnected system having at most one pole at the origin and no poles in the right half complex plane.
- We show that the pole at the origin does not destroy asymptotic stability of the system, given that the system states satisfy the linear state constraint due to the structure of the ring road.
- For the linear interconnected systems which consist of identical subsystems, we show that the string stability of each subsystem is not only a sufficient condition but also a necessary condition for asymptotic stability of the interconnected systems when the number of the subsystems in the interconnected systems is large enough.
- We test our analytical results with linear and nonlinear car following models in simulations. Simulation results show that the ring road is not stable with string unstable models; and the ring road is stable with string stable models.
- Furthermore, we use the string stability condition for heterogeneous vehicles to synthesize a controller for an automated vehicle to stabilize a ring road which was not stable. A simulation result verified the design of the controller.

This chapter is organized as follows: Notations and preliminaries are introduced in section 3.2. In section 3.3, we briefly review a type of car following models and discuss the stability. In section 3.4, a ring road model is introduced with a discussions about the existence and the uniqueness of the equilibrium point for the ring road, followed by main results showing that the ring road stability can be characterized by the string stability of the car following models. To test our results, simulations of linear car following models are carried out in section 3.5. In section 3.6, we further validate our results with simulations of nonlinear car following models. Based on a string stability condition, a controller is synthesized. We show that this controller is capable of stabilizing the ring road which was originally unstable. Finally, section 3.7 summarizes this chapter.

3.2 Notations and Preliminaries

In this chapter, a ring road with $N \in \mathbb{N}$ vehicles is considered. We labeled vehicles with numbers from 1 to N sequentially, with $i-1$-th vehicle (called vehicle-$i-1$) generally being the preceding vehicle of the i-th vehicle $\forall i \in \{2, \ldots, N\}$; except for the first vehicle, vehicle-1, the preceding vehicle is vehicle-N. We use subscriptions to indicate the variables for each vehicle. For example, figure 3.1 is an illustration of three vehicles on the ring road with their variables indicated with subscriptions.

A few frequently used variables in this chapter are defined as follows:

$r_i(t) \in \mathbb{R}$: traversed distance of the vehicle-i at time $t \in [0, \infty)$;

$v_i(t) \in \mathbb{R}$: speed of the vehicle-i at time t;

$a_i(t) \in \mathbb{R}$: acceleration of the vehicle-i at time t;

$L_i \in \mathbb{R}$: length of the vehicle-i;

$d_i(t) \in \mathbb{R}$: inter-vehicle space between vehicle-i and the preceding vehicle at time t, where $d_i(t) = r_{i-1}(t) - r_i(t) - L_i$, $\forall i \in \{2, \ldots, N\}$, and $d_1(t) = r_N(t) - r_1(t) - L_1$.

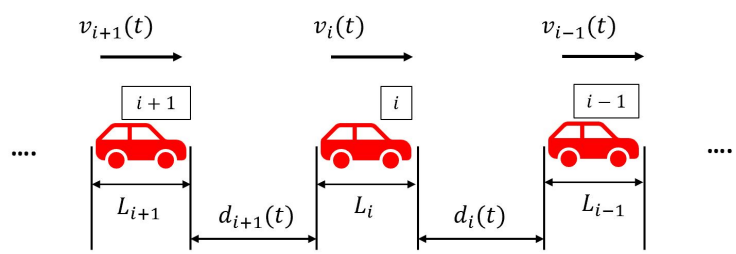

Figure 3.1: Illustration of three vehicles on the ring road. These vehicles are sequentially labeled as vehicle-$i-1$, vehicle-i, and vehicle-$i+1$. The speeds of these vehicles are $v_{i-1}(t)$, $v_i(t)$, and $v_{i+1}(t)$, respectively; and the lengths of the vehicles are L_{i-1}, L_i, and L_{i+1}, respectively. $d_{i+1}(t)$ and $d_i(t)$ are inter-vehicle spaces between vehicle-i and vehicle-$i+1$ and between vehicle-$i-1$ and vehicle-i, respectively.

3.3 Individual Car Following Model Stability

We consider car-following models that the acceleration of the model is formulated as a function of the subject vehicle speed ($v(t)$), the preceding vehicle speed ($v_{\mathrm{p}}(t)$), and the inter-vehicle distance between the subject vehicle and the preceding vehicle ($d(t)$), for example,

intelligent driver model (IDM)[90, 91] and *optimal velocity model* (OVM)[101, 6]. Generally, the model can be written as follows:

$$\begin{aligned} \dot{d}(t) &= v_{\mathrm{p}}(t) - v(t), && \forall t \geq 0 \\ \dot{v}(t) &= f(d(t), v(t), v_{\mathrm{p}}(t)), && \forall t \geq 0 \\ d(0) &= d_0, \\ v(0) &= v_0, \end{aligned} \tag{3.1}$$

where $d_0 \in \mathbb{R}$ is the initial distance between the subject vehicle and the preceding vehicle, $v_0 \in \mathbb{R}$ is the initial speed of the subject vehicle, and $f : \mathbb{R} \times \mathbb{R} \times \mathbb{R} \to \mathbb{R}$. We assume that there exists an unique solution $d(\cdot)$ and $v(\cdot)$ for a given $v_{\mathrm{p}} : [0, \infty) \to \mathbb{R}$ which is continuous in time.

The stability of the individual car-following model is the property that characterizes whether the subject vehicle can follow the leading vehicle steadily when the leading vehicle is driving at a constant speed, which is referred to as *individual vehicle stability* [72, Chapter 6], *local stability* [91, Chapter 15], or *platoon stability* [101]. Suppose the leading vehicle is driving at a constant speed, $v_{\mathrm{p}}(t) = v_{\mathrm{p}}^* \in \mathbb{R}_{\geq 0}, \forall t \geq 0$, stability of the car following model is defined as whether the subject vehicle can follow the leading vehicle steadily.

Definition 3.3.1. The car following model (3.1) is stable if

$$\lim_{t \to \infty} v(t) = v_{\mathrm{p}}^*.$$

For a given leading vehicle speed v_{p}^*, we assume that there exists a unique equilibrium point $(d^*, v^*) \in \mathbb{R}^2$ for the car following model (3.1), which is generally true for typical car following models, for example, both IDM and OVM have a unique equilibrium point (d^*, v^*) for a given leading vehicle speed. The equilibrium point (d^*, v^*) satisfies

$$\begin{aligned} 0 &= v_p^* - v^*, \\ 0 &= f(d^*, v^*, v_{\mathrm{p}}^*). \end{aligned}$$

In fact, the equilibrium speed of the subject vehicle v^* is equivalent to the preceding vehicle's speed v_{p}^*. Therefore, the second equation can be reduced to $0 = f(d^*, v^*, v^*)$.

By investigating eigenvalues of the linearized model, local stability around the equilibrium point can be assessed. For a given equilibrium point d^*, v^*, we define $\Delta d(t) := d(t) - d^*$ and $\Delta v := v(t) - v^*$. Taking the Jacobian of (3.1), we obtain the following linear system:

$$\begin{aligned} \Delta \dot{d}(t) &= -\Delta v(t), \\ \Delta \dot{v}(t) &= \alpha_1 \Delta d(t) + \alpha_2 \Delta v(t), \end{aligned}$$

where $\alpha_1 = \frac{\partial f}{\partial d}(d, v, v_{\mathrm{p}})|_{d=d^*, v=v^*, v_{\mathrm{p}}=v^*}$, and $\alpha_2 = \frac{\partial f}{\partial v}(d, v, v_{\mathrm{p}})|_{d=d^*, v=v^*, v_{\mathrm{p}}=v^*}$. The corresponding characteristic equation then is the following second order polynomial in λ:

$$\lambda^2 - \alpha_2 \lambda + \alpha_1 = 0.$$

The Routh-Hurwitz stability criterion [27] can be used to determine whether the poles are in the left half plane. If $\alpha_1 > 0$ and $\alpha_2 < 0$, all the poles are in the left half plane, and, then, the system would be stable.

3.4 Ring Road Stability

3.4.1 Ring Road Model

We consider the ring road formed of $N \in \mathbb{N}$ vehicles following each other, where each car following model can be modelled as (3.1); hence, the ring road dynamics is described follows:

$$\begin{aligned}
&\dot{d}_1(t) = v_N(t) - v_1(t),\\
&\dot{v}_1(t) = f_1\Big(d_1(t), v_1(t), v_N(t)\Big),\\
&\dot{d}_i(t) = v_{i-1}(t) - v_i(t), \quad \forall i \in \{2, \dots, N\}\\
&\dot{v}_i(t) = f_i\Big(d_i(t), v_i(t), v_{i-1}(t)\Big), \quad \forall i \in \{2, \dots, N\}\\
&d_i(0) = d_{i,0}, \quad \forall i \in \{1, \dots, N\},\\
&v_i(0) = v_{i,0}, \quad \forall i \in \{1, \dots, N\},\\
&\forall t \geq 0,
\end{aligned} \tag{3.2}$$

where $f_i : \mathbb{R} \times \mathbb{R} \times \mathbb{R} \to \mathbb{R}$ is continuous and differentiable, representing the car following model of each vehicle as described in section 3.3; $d_{i,0} \in \mathbb{R}$ is the initial space between of the vehicle-i and its preceding vehicle; and $v_{i,0} \in \mathbb{R}$ is the initial speed of the vehicle-i. Let $R_{\text{ring}} \in \mathbb{R}_{>0}$ be the ring road radius and suppose the radius of the ring road is large enough to accommodate N vehicles on the ring road, i.e. $2\pi R_{\text{ring}} - \sum_{i=1}^{N} L_i > 0$. It can be noted that the total length of these vehicles (distance headways and vehicle lengths) on the ring road is constant for the all time. This can be shown by aggregating derivative of $d_i(t)$: $\sum_{i=1}^{N} \dot{d}_i(t) = 0$; therefore, $\sum_{i=1}^{N} d_i(t)$ is a constant for all the all time. In fact, the length is equivalent to the circumference of the ring road:

$$\sum_{i=1}^{N} d_i(t) + \sum_{i=1}^{N} L_i = 2\pi R_{\text{ring}}, \quad t \geq 0. \tag{3.3}$$

This inherent property of the ring road is critical for calculating equilibrium points and determining stability of the ring road.

3.4.2 Ring Road Equilibrium Point

Suppose there exists an equilibrium point $(v_1^*, d_1^*, \dots, v_N^*, d_N^*) \in \mathbb{R}^{2N}$ for the ring road model. The equilibrium point can be calculated by the ring road model (3.2) with $\dot{d}_i(t) = 0$ and

$\dot{v}_i(t) = 0$, and the linear constraint of the total length (3.3):

$$\begin{aligned} 0 &= v_N^* - v_1^*, \\ 0 &= f_1\Big(d_1^*, v_1^*, v_N^*\Big), \\ 0 &= v_{i-1}^* - v_i^*, && \forall i \in \{2, \dots, N\} \\ 0 &= f_i\Big(d_i^*, v_i^*, v_{i-1}^*\Big), && \forall i \in \{2, \dots, N\}, \\ \sum_{i=1}^{N} d_i^* &= 2\pi R_{\text{ring}} - \sum_{i=1}^{N} L_i. \end{aligned} \tag{3.4}$$

It can be observed that at the equilibrium point, speeds for all the vehicles on the ring road are the same: $v_1^* = v_2^* = \cdots = v_N^* = v^*$, where $v^* \in \mathbb{R}$ represents a equilibrium speed of the ring. We can simplify (3.4) and obtain following equations:

$$\begin{aligned} v_i^* &= v^*, && \forall i \in \{1, \dots, N\} \\ 0 &= f_i\Big(d_i^*, v^*, v^*\Big), && \forall i \in \{1, \dots, N\}, \\ \sum_{i=1}^{N} d_i^* &= 2\pi R_{\text{ring}} - \sum_{i=1}^{N} L_i. \end{aligned} \tag{3.5}$$

The solution of (3.5) exists and is unique if following assumptions hold.

Assumption 1. *We assume that for each car following model, there exists a unique equilibrium state $(d^*, v^*) \in \mathbb{R}^2$. given a constant preceding vehicle speed. In other words, $0 = f_i(d_i^*, v^*, v^*)$ has a unique solution d_i^* for any given v^*.*

Assumption 2. *We assume that the equilibrium space d_i^* is monotonically increasing with respect to the equilibrium speed v^*. That is, for any tuples (d_i^*, v^*) and $(\bar{d}_i^*, \bar{v}^*)$, where $0 = f_i(d_i^*, v^*, v^*)$ and $0 = f_i(\bar{d}_i^*, \bar{v}^*, \bar{v}^*)$, $\bar{d}_i^* < d_i^*$ if and only if $\bar{v}^* < v^*$.*

Assumption 3. *We assume the circumference of the ring road is larger than the total length of vehicles at zero speed, i.e. $2\pi R_{ring} \geq \sum_{i=1}^{N} \underline{d_i} + L_i$, where $\underline{d_i} \in \mathbb{R}$ satisfies $f_i(\underline{d_i}, 0, 0) = 0, \forall i = \{1, \dots, N\}$*

Assumption 3 holds automatically for a ring road large enough. Assumption 1 and assumption 2 are relevant to properties of the car following models and they are generally valid for commonly used car following models, for example, IDM and OVM. We can show these two assumptions hold for IDM and OVM.

We show assumption 1 and assumption 2 are true for IDM and OVM. Recall formulation of IDM [91]:

$$\dot{v}(t) = a\Big(1 - \Big(\frac{v(t)}{v_0}\Big)^{\delta} - \Big(\frac{s^*(v(t), v_p(t))}{d(t)}\Big)^2\Big),$$
$$s^*(v(t), v_p(t)) = s_0 + v(t)T + \frac{v(t)(v_p(t) - v(t))}{2\sqrt{ab}},$$

where $a \in \mathbb{R}_{>0}$, $b \in \mathbb{R}_{>0}$, $v_0 \in \mathbb{R}_{>0}$, $s_0 \in \mathbb{R}_{>0}$, and $T \in \mathbb{R}_{>0}$ are parameters; $v(t) \in \mathbb{R}$ is the subject vehicle speed, $v_p(t) \in \mathbb{R}$ is the leading vehicle speed, and $d(t) \in \mathbb{R}$ is the distance gap between the leading vehicle and the subject vehicle. At steady state, $\dot{v}(t) = 0$ and subject vehicle speed is equivalent to the preceding vehicle speed : $v^* = v_p^* \in \mathbb{R}$. Thus, steady state $(v^*, d^*) \in \mathbb{R}^2$ satisfies following equation:

$$0 = a\Big(1 - \Big(\frac{v^*}{v_0}\Big)^{\delta} - \Big(\frac{s_0 + v^*T}{d^*}\Big)^2\Big).$$

We can solve the above equation and attain d^* as a function of v^*:

$$d^* = \sqrt{\frac{(s_0 + v^*T)^2}{1 - (\frac{v^*}{v_0})^{\delta}}}.$$

It can be noted that for any v^*, there exists an unique d^* and for any two steady states (v^*,d^*) and $(v^\dagger,d^\dagger) \in \mathbb{R}^2$, $d^* \leq d^\dagger$ if and only inf $0 \leq v^* \leq v^\dagger \leq v_0$. Similarly, we can also show the same thing for *optimal velocity model* [101]:

$$\dot{v}(t) = \frac{1}{T_{\text{ovm}}}\Big(\bar{V}(d(t)) - v(t)\Big) + b_{\text{ovm}}\Big(v_p(t) - v(t)\Big),$$

where $\bar{V} : \mathbb{R} \to \mathbb{R}$ is a continuous and monotonically increasing function. $b_{\text{ovm}} \in \mathbb{R}_{>0}$ and $T_{\text{ovm}} \in \mathbb{R}_{>0}$ are parameters. At steady state, $\dot{v}(t) = 0$ and subject vehicle speed is equivalent to the preceding vehicle speed : $v^* = v_p^*$; $(v^*, d^*) \in \mathbb{R}^2$ satisfies following equation:

$$0 = \frac{1}{T_{\text{ovm}}}\Big(\bar{V}(d^*) - v^*\Big).$$

Because $\bar{V}$ is monotonically increasing function, d^* is unique for a v^* and for any two steady states (v^*,d^*) and $(v^\dagger,d^\dagger) \in \mathbb{R}^2$, $d^* \leq d^\dagger$ if and only inf $v^* \leq v^\dagger$.

Theorem 3.4.1. *Suppose assumption 1 and assumption 2 hold for all car following models on the ring road and the radius of the ring road is large enough (assumption 3). Then, the ring road model* (3.2) *has an unique equilibrium point satisfying* (3.5).

Proof. We first show that (3.5) has a solution. For a given speed v^*, with assumption 1, there exists a unique total length of the vehicles $\sum_{i=1}^{N} d_i^* + L_i$. Following assumption 2, we know that the total length of the vehicles is longer at higher speed. Since the circumference of the ring road is larger than the steady state length at zero speed (assumption 3), there exists a speed $v^* > 0$ such that the total length of the vehicles matches the circumference of the ring road.

We then show the solution is unique by contradiction. Suppose that $(\bar{v}^*, \bar{d}_1^*, \ldots, \bar{d}_N^*)$, and $(v^*, d_1^*, \ldots, d_N^*)$ are both solutions of (3.5) and $\bar{v}^* > v^*$. Because $\bar{v}^* > v^*$, $\bar{d}_i^* > d_i^*$, $\forall i \in \{1, \ldots, N\}$, following assumption 2. This implies that $\bar{d}_1^* + \bar{d}_2^* + \cdots + \bar{d}_N^* > d_1^* + d_2^* + \cdots + d_N^*$. This contradicts the last equation of (3.5). □

Given the equilibrium point, the stability of the ring road dynamics is studied in the sense of the Lyapunov [39].

3.4.3 Ring Road Stability

Suppose $(d_1^*, v_1^*, \ldots, d_N^*, v_N^*) \in \mathbb{R}^{2N}$ is the equilibrium point of the ring road model (3.2). For convenience, we first translate the coordinate so that the equilibrium point is at the origin. We define $\Delta d_i(t) = d_i(t) - d_i^*$, and $\Delta v_i(t) = v_i(t) - v_i^*$, $\forall i \in \{1, \ldots, N\}$ and attain the ring road model (3.2) in the new coordinate:

$$\begin{aligned}
\dot{\Delta d}_1(t) &= \Delta v_N(t) - \Delta v_1(t), \\
\dot{\Delta v}_1(t) &= \bar{f}_1\Big(\Delta d_1(t), \Delta v_1(t), \Delta v_N(t)\Big), \\
\dot{\Delta d}_i(t) &= \Delta v_{i-1}(t) - \Delta v_i(t), \forall i \in \{2, \ldots, N\} \\
\dot{\Delta v}_i(t) &= \bar{f}_i\Big(\Delta d_i(t), \Delta v_i(t), \Delta v_{i-1}(t)\Big), \forall i \in \{2, \ldots, N\} \\
\Delta d_i(0) &= d_{i,0} - d_i^*, \quad \forall i \in \{1, \ldots, N\} \\
\Delta v_i(0) &= v_{i,0} - v_i^*, \quad \forall i \in \{1, \ldots, N\} \\
&\forall t \geq 0,
\end{aligned} \tag{3.6}$$

where $\bar{f}_1(\cdot, *, \star) := f_1(\cdot + d_1^*, * + v_1^*, \star + v_N^*)$ and $\bar{f}_i(\cdot, *, \star) := f_i(\cdot + d_i^*, * + v_i^*, \star + v_{i-1}^*), \forall i \in \{2, \ldots, N\}$.

The local stability of the nonlinear system can be determined based on stability of the

linearized model at an equilibrium point. The linearization of the ring road model is:

$$\begin{aligned}
&\dot{\Delta d}_1(t) = \Delta v_N(t) - \Delta v_1(t),\\
&\dot{\Delta v}_1(t) = \alpha_1^{(1)}\Delta d_1(t) + \alpha_2^{(1)}\Delta v_1(t) + \beta^{(1)}\Delta v_N(t),\\
&\dot{\Delta d}_i(t) = \Delta v_{i-1}(t) - \Delta v_i(t), \quad \forall i \in \{2,\dots,N\}\\
&\dot{\Delta v}_i(t) = \alpha_1^{(i)}\Delta d_i(t) + \alpha_2^{(i)}\Delta v_i(t) + \beta^{(i)}\Delta v_{i-1}(t), \quad \forall i \in \{2,\dots,N\}\\
&\Delta d_i(0) = d_{i,0} - d_i^*, \quad \forall i \in \{1,\dots,N\}\\
&\Delta v_i(0) = v_{i,0} - v_i^*, \quad \forall i \in \{1,\dots,N\},\\
&\quad \forall t \geq 0,
\end{aligned} \tag{3.7}$$

where $\alpha_1^{(i)} = \frac{\partial \bar{f}_i}{\partial \Delta d_i}|_{(0,0,0)}$, $\alpha_2^{(i)} = \frac{\partial \bar{f}_i}{\partial \Delta v_i}|_{(0,0,0)}$, and $\beta^{(i)} = \frac{\partial \bar{f}_i}{\partial \Delta v_{i-1}}|_{(0,0,0)}$. To determine the stability, we need to know the eigenvalues of the characteristics equation, which can be attained by solving a high order polynomial. However, it might be difficult to solve it; even numerically, it might be difficult to find all the roots. The ring road is a interconnected system which is composed of subsystems. It would be ideal if the stability of the interconnected systems can be indicated by properties of the subsystems. In addition to avoid the difficulties of solving a high order polynomial, by doing this way, we may simplify the analysis if we need to change subsystems or adding subsystems. We can ensure that stability still holds as long as new subsystems having a certain property without the need to recompute eigenvalues of the whole system again. Therefore, we will show that the stability of the linearized ring road can be determined based on the string stability of the car following models. We will study a general form of interconnected linear systems which can describe the linearized ring road and then apply the result to the linearized ring road.

3.4.4 Stability of the Cyclic Interconnected Linear Systems

Consider the linear interconnected systems which consists of $N \in \mathbb{N}$ single-input-single-output linear systems. They are interconnected in a way that one's output is the input of another subsystem next to it, and the last subsystem's output is the input of the first subsystem:

$$\begin{aligned}
&\dot{x}_1(t) = A_1 x_1(t) + B_1 y_N(t),\\
&y_1(t) = C_1 x_1(t),\\
&\dot{x}_i(t) = A_i x_i(t) + B_i y_{i-1}(t), && \forall i \in \{2,\dots,N\},\\
&y_i(t) = C_i x_i(t), && \forall i \in \{2,\dots,N\},\\
&x_i(0) = x_{i,0}, && \forall i \in \{1,\dots,N\},\\
&\forall t \geq 0,
\end{aligned} \tag{3.8}$$

where $A_i \in \mathbb{R}^{n\times n}$, $B_i \in \mathbb{R}^{n\times 1}$, $C_i \in \mathbb{R}^{1\times n}$, $x_i(t) \in \mathbb{R}^n$ is the state of each subsystem and $y_i(t) \in \mathbb{R}$ is the output of each subsystem, $\forall i \in \{1,\dots,N\}$. $n \in \mathbb{N}$ is the dimension of each subsystem. The linear system (3.8) can be written compactly as $\dot{\bar{X}}(t) = \bar{A}\bar{X}(t)$,

where $\bar{X}(t) = [x_1^T(t), x_2^T(t), \ldots, x_N^T(t)]^T$ is the collection of all subsystem states and $\bar{A}$ is the corresponding matrix composed of A_i, B_i, and C_i:

$$\bar{A} = \begin{bmatrix} A_1 & 0_{n,n} & \cdots & \cdots & 0_{n,n} & B_1C_N \\ B_2C_1 & A_2 & 0_{n,n} & \cdots & \cdots & 0_{n,n} \\ 0_{n,n} & B_3C_2 & A_3 & 0_{n,n} & \cdots & 0_{n,n} \\ \vdots & & \ddots & \ddots & & \vdots \\ 0_{n,n} & \cdots & 0_{n,n} & B_{N-1}C_{N-2} & A_{N-1} & 0_{n,n} \\ 0_{n,n} & \cdots & 0_{n,n} & 0_{n,n} & B_NC_{N-1} & A_N \end{bmatrix}.$$

The stability of such system can be determined by locations of eigenvalues, which can be computed by solving roots of the characteristic equation. Instead of solving it directly, as stated earlier, since we can gain some benefits determining the stability of the whole system based on the property of the subsystems, we will analyse the stability of the system based on string stability of the subsystems.

String stability is a property of interconnected systems, characterizing interactions among subsystems. D. Swaroop et al. ([87]; [88]) formally introduced the string stability for a class of interconnected systems. String stability is a desirable property for control of a platoon of automated vehicles [9, 69]. For linear car following models, a condition on the $\mathcal{H}_\infty$ norm of the transfer function is necessary for string stability [87, 72]. This condition is commonly used for linear car following models string stability analysis and controller design [102, 46, 28]. We will also use this condition to characterize the location of poles of the whole linear interconnected systems. Let $G_i : \mathbb{C} \to \mathbb{C}$ be the transfer function of the subsystem-i: $G_i(s) := C_i(sI - A_i)^{-1}B_i$, $\forall i \in \{1, \ldots, N\}$ in (3.8). We define **string stable** and **collective string stable** as follows and use them to show stability of the ring road model.

Definition 3.4.1. $G_i(\cdot)$ is **string stable** if $\|G_i\|_{\mathcal{H}_\infty} \leq 1$.

Definition 3.4.2. $\Pi_{i=1}^N G_i(\cdot)$ is **collective string stable** if $\|\Pi_{i=1}^N G_i\|_{\mathcal{H}_\infty} \leq 1$.

For a transfer function G, $\|G\|_{\mathcal{H}_\infty} := \sup_\omega |G(j\omega)|$. The stability of the interconnected systems can be determined by locations of roots of the characteristic equation, which is (3.8) $1 - \Pi_{i=1}^N G_i(s) = 0$. We use the Nyquist stability criterion [see 27, Chapter 6] to determine the poles of the system. Propositions which are required to show the main theorem are introduced.

Proposition 3.4.1. *Let $G_i : \mathbb{C} \to \mathbb{C}, \forall i \in \{1, \ldots, N\}$ be transfer functions of single input single output linear systems. Suppose G_i have no poles and zeros in the closed right half plane and G_i are strictly proper (degree of numerator is less than the degree of denominator) for all $i \in \{1, \ldots, N\}$. The closed-loop characteristic equation $1 - \Pi_{i=1}^N G_i(\cdot) = 0$ has at least one root at the origin and the rest of the roots are located in the open left half plane if $\Pi_{i=1}^N G_i(\cdot)$ is collective string stable and $G_i(0) = 1$, $\forall i \in \{1, \ldots, N\}$.*

Proposition 3.4.1 can be shown based on the Nyquist stability criterion. Given that $\|\Pi_{i=1}^N G_i(\cdot)\|_{\mathcal{H}_\infty} \leq 1$, the Nyquist plot of $\Pi_{i=1}^N G_i(\cdot)$ has no encirclement around the point $1 + 0j$ on the complex plane. Therefore, there is no root in the open right half plane. Because $G_i(0) = 1$ for all i, then $1 - \Pi_{i=1}^N G_i = 0$ also has root(s) at $s = 1$.

Proposition 3.4.2. *Let $G_i : \mathbb{C} \to \mathbb{C}, \forall i \in \{1, \ldots, N\}$ be transfer functions of single input single output linear systems. Suppose G_i have no poles and zeros in the closed right half plane and G_i are strictly proper for all $i \in \{1, \ldots, N\}$. The closed-loop characteristic equation $1 - \Pi_{i=1}^N G_i = 0$ has only one root at the origin and the rest of the roots are in the open left half plane if $\Pi_{i=1}^N G_i$ is collective string stable, $G_i(0) = 1$, and $\sum_{i=1}^N \frac{dG_i(s)}{ds}|_{s=0} \neq 0$.*

Based on proposition 3.4.1, proposition 3.4.2 further shows that the closed-loop characteristic equation has only one root at the origin if $\sum_{i=1}^N \frac{dG_i(s)}{ds}|_{s=0} \neq 0$. We can show this by firstly taking derivative of the closed-loop characteristic equation:

$$\frac{d(1-\Pi_{i=1}^N G_i(s))}{ds}|_{s=0} = \sum_{i=1}^N -\frac{dG_i(s)}{ds} \Pi_{k\in\{1,\ldots,N\}\setminus i} G_i(s). \tag{3.9}$$

Since we have $G_i(0) = 1, \forall i = 1, \ldots, N$, right hand side of the (3.9) can be reduced to $\sum_{i=1}^N -\frac{dG_i(s)}{ds}|_{s=0}$. Because of $\sum_{i=1}^N -\frac{dG_i(s)}{ds}|_{s=0} \neq 0$, $s = 0$ is not a multiple roots of $1-\Pi_{i=1}^N G_i$. The closed-loop characteristic equation has only one root at $s = 0$.

Proposition 3.4.1 and proposition 3.4.2 show sufficient conditions for the linear interconnected systems (3.8) having no pole in the open right half plane when subsystems are not necessarily identical. The following propositions will show similar results for the interconnected system which consists of identical systems, where $G_i = G, \forall i \in \{1, \ldots, N\}$. In this case, we will not use the condition on $\|G^N\|_{\mathcal{H}_\infty}$. Instead, we use condition on $\|G\|_{\mathcal{H}_\infty}$ to characterize locations of poles of the interconnected system $1 - G^N = 0$.

Proposition 3.4.3. *Let $G : \mathbb{C} \to \mathbb{C}$ be a transfer function of a single input single output linear system. Suppose G has no poles and zeros in the closed right half plane and G is strictly proper. For all $N \in \mathbb{N}$, the closed-loop characteristic equation $1 - G^N = 0$ has at least one root at the origin and the rest of the roots are in the left half plane if G is string stable and $G(0) = 1$.*

Proposition 3.4.4. *Let $G : \mathbb{C} \to \mathbb{C}$ be a transfer function of a single input single output linear system. Suppose G has no poles and zeros in the closed right half plane and G is strictly proper. For all $N \in \mathbb{N}$, the closed-loop characteristic equation $1 - G^N = 0$ has only one root at the origin and the rest of the roots are all in the left half plane if G is string stable, $G(0) = 1$, and $\frac{dG(s)}{ds}|_{s=0} \neq 0$.*

Proposition 3.4.3 and proposition 3.4.4 show sufficient conditions of G for the interconnected systems having no poles in the open right half plane. The following proposition further gives necessary conditions for having poles in the open right half plane.

Proposition 3.4.5. *Let $G : \mathbb{C} \to \mathbb{C}$ be a transfer function of a single input single output linear system. Suppose G has no poles and zeros in the closed right half plane and G is strictly proper. Define $N_1 := -\pi/\angle G(j\hat{\omega})$, where $\hat{\omega} := \arg\max_\omega |G(j\omega)|$, and $\angle G(j\hat{\omega})$ is the phase of $G(j\hat{\omega})$. For all $N \geq N_1$, the closed-loop characteristic equation $1 - G^N = 0$ has root(s) in the open right half plane if and only if G is not string stable.*

The above propositions are used to determine locations of the eigenvalues of the interconnected system (3.8). It has been shown that there is always a pole at zero, which is not sufficient to show the linear system being asymptotically stable. It is desirable to have the system being asymptotically stable in order to apply the results locally to nonlinear systems. As we saw earlier, the total inter-vehicle spaces of vehicles on the ring road model is a constant. We can also assume a similar linear constraint holds here: $M\bar{X}(t) = 0$, where $\bar{X}(t)$ is the collection of subsystem states: $[x_1^T(t), x_2^T(t), \ldots, x_N^T(t)]^T$. $M \in \mathbb{R}^{1\times Nn}$ is a constant vector and M is picked such that $[\bar{A}^T, M^T]^T$ has full column rank. The following theorems will show that the linear system with such linear constraint is asymptotically stable even if there exists one eigenvalue zero.

Theorem 3.4.2. *Consider the linear time invariant system:*

$$\begin{aligned} \dot{x}(t) &= Ax(t), \\ x(0) &= x_0, \\ \forall t \geq& 0, \end{aligned}$$

where $x : [0, \infty) \to \mathbb{R}^n$ and $A \in \mathbb{R}^{n\times n}$. Suppose there exists a row vector $M \in \mathbb{R}^{1\times n}$ such that $Mx(t) = 0, \forall t \in [0, \infty)$ and rank of $[A^T, M^T]^T$ is n. If A has one eigenvalue zero and the remaining eigenvalues are located in the left half plane, then the above system is asymptotically stable with respect to the origin.

Proof. Let $\lambda_0 \in \mathbb{R}^n$ be an eigenvector of A to the eigenvalue zero. For all $q \in \mathbb{R}$, $x^* = q\lambda_0$ is a stable equilibrium point of the linear time invariant system. Because $[A^T, M^T]^T x^* = 0$ and $[A^T, M^T]^T$ has rank n by LaSalle's theorem, the system is asymptotically stable at $x^* = 0$ [39, Theorem 4.4]. □

Theorem 3.4.3. *Consider the linear interconnected system* (3.8) *with transfer function $G_i(s) := C_i(sI - A_i)^{-1}B_i$, $G_i : \mathbb{C} \to \mathbb{C}$ such that $G_i(s)$ is strictly proper and its poles and zeros are in the left half plane. Suppose there exists a linear matrix M, such that $M\bar{X}(t) = 0$ and $[\bar{A}^T, M^T]^T$ has full column rank. The linear interconnected system* (3.8) *is asymptotically stable if $\Pi_{i=1}^N G_i$ is collective string stable, $G_i(0) = 1$, and $\sum_{i=1}^N \frac{dG_i(s)}{ds}|_{s=0} \neq 0$.*

Proof. By **proposition 3.4.2**, we know that the system (3.8) has no eigenvalues in the open right half plane and has one eigenvalue at the origin. The system is then asymptotically stable by **theorem 3.4.2**. □

Theorem 3.4.4. *Consider the linear interconnected system* (3.8) *with* $A_i = A \in \mathbb{R}^{n\times n}$, $B_i = B \in \mathbb{R}^{N\times 1}$, *and* $C_i = C \in \mathbb{R}^{1\times n}$, $\forall i \in \{1, \ldots, N\}$, *where transfer function for each subsystem is* $G(s) := C(sI - A)^{-1}B$, $G : \mathbb{C} \to \mathbb{C}$ *and* $G(s)$ *is strictly proper and its poles and zeros are in the left half plane. Suppose there exists a linear matrix* M, *such that* $M\bar{X}(t) = 0, \forall t \in [0, \infty)$ *and* $[\bar{A}^T, M^T]^T$ *has full column rank. Let* $\angle G(j\omega)$ *be the phase of* $G(j\omega)$. *Define* $\hat{\omega} = \arg\max_\omega \|G(j\omega)\|$ *and* $N_1 = -\pi/\angle G(j\hat{\omega})$. *Assume* $N > N_1$. *The linear cyclic interconnected system is asymptotically stable if and only if* G *is string stable.*

Proof. We first prove necessity: the interconnected system is stable if $\|G\|_{\mathcal{H}_\infty} \leq 1$. According to **proposition 3.4.4**, we know that the eigenvalues are all in the LHP, except one at the origin, *if* $\|G\|_{\mathcal{H}_\infty} \leq 1$. By **theorem 3.4.2**, we conclude that the system is asymptotically stable. To prove sufficiency, according to **proposition 3.4.5**, we know that the connected system is not stable for all $N > N_1$ if $\|G\|_{\mathcal{H}_\infty} > 1$. □

It can be noted that (3.8) is equivalent to (3.7) with $x_i(t) = [d_i(t), v_i(t)]^T$, $y_i(t) = v_i(t)$, $\forall t \in [0, \infty)$, and

$$A_i = \begin{bmatrix} 0, & -1 \\ \alpha_1^{(i)}, & \alpha_2^{(i)} \end{bmatrix}, B_i = \begin{bmatrix} 1 \\ \beta^{(i)} \end{bmatrix}, C_i = \begin{bmatrix} 0, 1 \end{bmatrix},$$

$\forall i \in \{1, \ldots, N\}$. As mentioned, the ring road model inherently has a linear constraint. For the model (3.7), the linear constraint is $M\bar{X}(t) = 0$ with $M = [1, 0, 1, 0, \ldots, 1, 0]^T$. Therefore, **theorem 3.4.3** and **theorem 3.4.4** can be applied to determine the stability of the linearized ring road model (3.7).

Theorem 3.4.3 and **theorem 3.4.4** are main results for showing conditions for ring road stability. In the following sections, we apply them to analyse the stability of the ring road and also design a car following controller that stabilizes the ring road. Simulations are carried out to validate the stability analyses and the controller design.

3.5 Adaptive Cruise Control on Ring Road

Following the results from the previous section, for a given car following model, one can analyse the stability of the ring road based on string stability. We consider an *adaptive cruise control* (ACC) as a study case. String stability is a critical property of an ACC. By selecting design parameters carefully, string stability can be achieved. To validate **theorem 3.4.4**, we design a string stable and a string unstable ACC and carry out simulations for a ring roads of string stable ACC and a ring road of string unstable ACC.

3.5.1 Adaptive Cruise Control

An adaptive cruise control system is an automatic vehicle longitudinal control system that regulates the relative distance and the relative speed with respect to the preceding vehicle.

A desired acceleration $a_{i,\mathrm{des}}(t) \in \mathbb{R}$ is calculated based on gap error and speed error [72, 60, 16, 114, 113, 68]:

$$a_{i,\mathrm{des}}(t) = k_1(d_i(t) - t_\mathrm{h} v_i(t)) + k_2(v_{i-1}(t) - v_i(t)), \tag{3.10}$$

where $t_\mathrm{h} \in \mathbb{R}_{>0}$ is the desired time gap, and $k_1 \in \mathbb{R}$ and $k_2 \in \mathbb{R}$ are controller parameters to be designed. Tracking of the desired acceleration is ensured by a controller that actuates the throttle and the brake. We assume the actual acceleration is tracking the desired acceleration with a time constant $\tau \in \mathbb{R}_{>0}$:

$$\begin{aligned} \dot{v}_i(t) &= a_i(t), \\ \dot{a}_i(t) &= -\frac{a_i(t)}{\tau} + \frac{a_{i,\mathrm{des}}(t)}{\tau}. \end{aligned} \tag{3.11}$$

Combining (3.10) and (3.11), we can attain a third order car following model as follows:

$$\begin{bmatrix} \dot{d}_i(t) \\ \dot{v}_i(t) \\ \dot{a}_i(t) \end{bmatrix} = \begin{bmatrix} 0 & -1 & 0 \\ 0 & 0 & 1 \\ \frac{k_1}{\tau} & \frac{-k_2 - k_1 t_\mathrm{h}}{\tau} & -\frac{1}{\tau} \end{bmatrix} \begin{bmatrix} d_i(t) \\ v_i(t) \\ a_i(t) \end{bmatrix} + \begin{bmatrix} 1 \\ 0 \\ \frac{k_2}{\tau} \end{bmatrix} v_{i-1}(t).$$

The ring road of ACC can be modelled as (3.8) with

$$A_i = \begin{bmatrix} 0 & -1 & 0 \\ 0 & 0 & 1 \\ \frac{k_1}{\tau} & \frac{-k_2 - k_1 t_\mathrm{h}}{\tau} & -\frac{1}{\tau} \end{bmatrix}, B_i = \begin{bmatrix} 1 \\ 0 \\ \frac{k_2}{\tau} \end{bmatrix}, C_i = \begin{bmatrix} 0 & 1 & 0 \end{bmatrix}.$$

The transfer function of each subsystem is

$$G_\mathrm{acc}(s) = \frac{k_2 s + k_1}{\tau s^3 + s^2 + (k_1 t_\mathrm{h} + k_2)s + k_1}. \tag{3.12}$$

According to theorem 3.4.4, if we can find a pair of k_1 and k_2 such that individual stability and string stability are guaranteed, the corresponding ring road is stable. On the other hand, if the individual vehicle is string unstable, then the ring road for a sufficient number of vehicles ($N > N_1$) is unstable. Given τ and t_h, the range of the k_1 and k_2 satisfying individual stability and string stability can be attained analytically. Conditions for individual stability and string stability are described below:

Individual stability condition for k_1 and k_2 Stability of the transfer function (3.12) can be shown based on locations of the poles. By applying *Routh-Hurwitz criterion* [27], poles are all in the left half plane if:

$$\begin{aligned} &k_1 > 0, \\ &k_1(t_\mathrm{h} + \tau) + k_2 > 0. \end{aligned}$$

(String stability condition for k_1 and k_2 $G_{\text{acc}}(s)$ being string stable is equivalent to have

$$|G_{\text{acc}}(j\omega)| < 1, \quad \omega \in \mathbb{R}_{>0}.$$

Given that $|G_{\text{acc}}(j0)| = 1$ and $\lim_{\omega\to\infty} |G_{\text{acc}}(j\omega)| = 0$, $|G_{\text{acc}}(j\omega)| = 1$ having no real solution other than zero is equivalent to have $|G_{\text{acc}}(j\omega)| < 1$ for all $\omega > 0$. $|G_{\text{acc}}(j\omega)|$ is:

$$|G_{\text{acc}}(j\omega)| = \frac{k_1^2 + (k_2\omega)^2}{(k_1 - \omega^2)^2 + (-\tau\omega^3 + (k_1 h + k_2)\omega)^2}.$$

Let $|G_{\text{acc}}(j\omega)| = 1$, we obtain

$$k_1^2 + (k_2\omega)^2 = (k_1 - \omega^2)^2 + (-\tau\omega^3 + (k_1 h + k_2)\omega)^2,$$

which has no positive real value solutions if k_1 and k_2 satisfy one of the following conditions:
(i)

$$(1 - 2\tau(k_1 h + k_2))^2 - 4\tau^2(k_1^2 h^2 + 2k_1 k_2 h - 2k_1) < 0,$$

(ii):

$$\begin{aligned}&(1 - 2\tau(k_1 h + k_2))^2 - 4\tau^2(k_1^2 h^2 + 2k_1 k_2 h - 2k_1) \geq 0\\ &\wedge(1 - 2\tau(k_1 h + k_2)) \geq 0\\ &\wedge 4\tau^2(k_1^2 h^2 + 2k_1 k_2 h - 2k_1) \geq 0.\end{aligned}$$

3.5.2 Simulation Validation

An instance of k_1 and k_2 is picked for both string stable and string unstable adaptive cruise control. We assume all vehicles have the same desired time headway, $t_{\text{h}} = 1$ and the same tracking time constant, $\tau = 0.1$. We simulate the ring road of all string stable adaptive cruise control vehicles and the ring road of all string unstable adaptive cruise control vehicles. Simulations is carried in MATLAB with an ODE solver : ode45. The ring road with 22 vehicles is illustrated in Fig. 3.2. Detailed setup of the simulation is described below:

- Number of vehicles N: 22
- Vehicle length L: 4.5m
- Ring radius R_{ring}: 41.4m
- Initial speed $v_{i,0}$: $6.8\,\text{m}\,\text{s}^{-1}$
- Initial spacing between vehicle i and $i-1$, $d_{i,0}$ $\forall i \in \{3, \cdots, 22\}$: 7.3m
- Initial spacing between vehicle 22 and vehicle 1, $d_{1,0}$: 12.8m

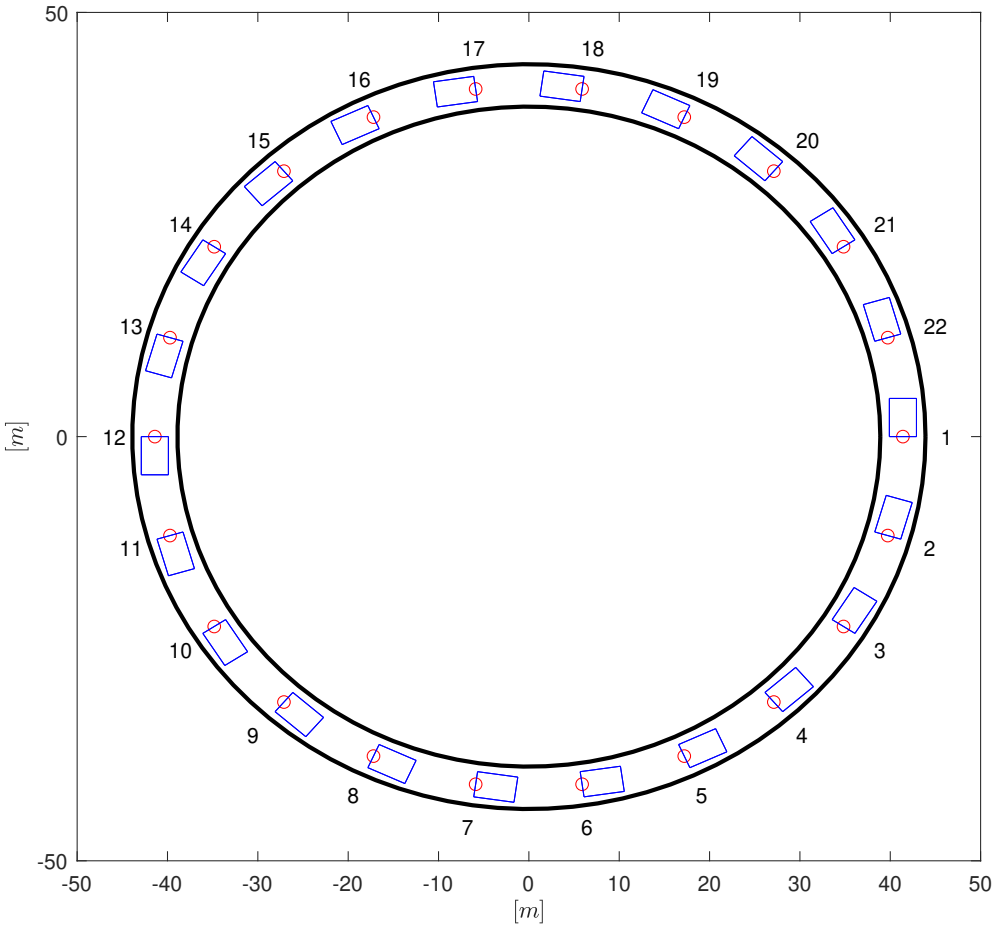

Figure 3.2: A schematic of the ring road with 22 vehicles. Each vehicle is illustrated as a blue box. The red circles represent rear ends of vehicles.

- Initial spacing between vehicle 1 and vehicle 2, $d_{2,0}$: 1.8m

Numerical example 1: ring not stable In this example, we present a scenario where the ring road is unstable, because of string unstable car following models. The parameters for ACC are $k_1 = 0.2, k_2 = 0.3$. We check string stability of the transfer function (3.12). $\|G_{\text{acc}}(s)\|_{\mathcal{H}_\infty} = 1.1955$, which is string unstable, so that following our derived equation we cannot expect ring stability. Speeds of vehicles are shown in figure 3.3. Speed variations among the traffic are increasing by time. The ring road is not stable.

Numerical example 2: ring stable In this example, we show the simulation of ACC with control parameters $k_1 = 0.7, k_2 = 0.8$. We check string stability of the transfer function (3.12). $\|G_{\text{acc}}(s)\|_{\mathcal{H}_\infty} = 1$, which is string stable. Therefore, the ring road should be stable. Speeds are shown in figure 3.4. The traffic speed converge to $7.3\text{m}\,\text{s}^{-1}$, which is the theoretical equilibrium speed. The ring road is stable.

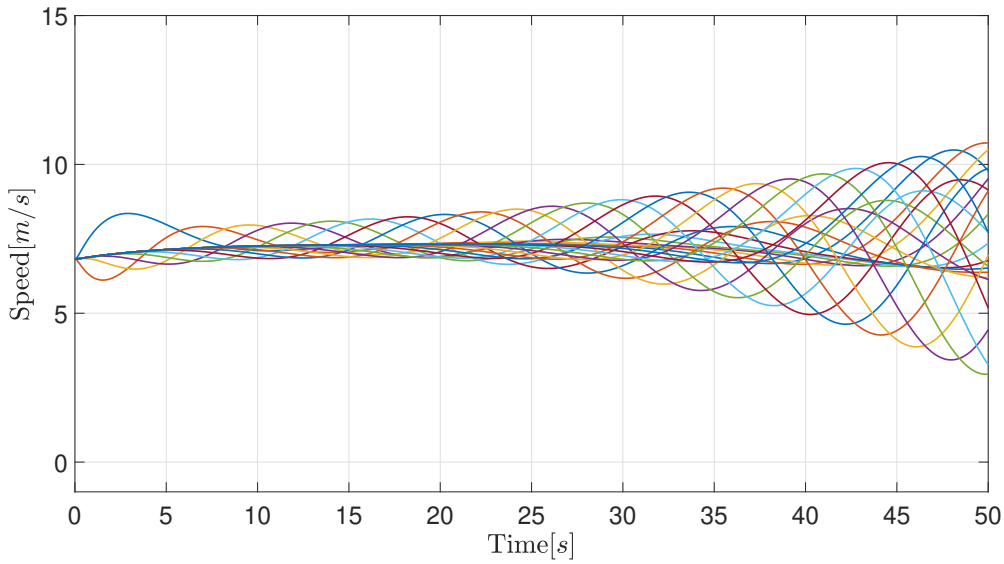

Figure 3.3: Speeds of the vehicles on the unstable ring road which consists of string unstable adaptive cruise control models. Each curve represents a speed of a vehicle changing by time. Oscillations of speeds increases by time, implying the ring road is unstable.

3.6 Optimal Velocity Model with Automated Vehicle Model on Ring Road

We also simulated ring road of a nonlinear car following model: OVM [7]. We first simulate the ring road of string unstable OVM, which results in a unstable ring road. We then design an automated vehicle model which makes the collective string stable. By replacing one OVM with the automated vehicle model, we stabilize the ring road which was not stable.

3.6.1 Optimal Velocity Model

We consider the ring road which consists of the optimal velocity models (Orosz et al., [64];Ward, [99](Chapter 1)):

$$\dot{d}_1(t) = v_N(t) - v_1(t), \tag{3.13}$$

$$\dot{v}_1(t) = \frac{1}{T}(V(d_1(t)) - v_1(t)) + b\dot{d}_1(t), \tag{3.14}$$

$$\dot{d}_i(t) = v_{i-1}(t) - v_i(t), \forall i \in \{2, \ldots, N\} \tag{3.15}$$

$$\dot{v}_i(t) = \frac{1}{T}(V(d_i(t)) - v_i(t)) + b\dot{d}_i(t), \forall i \in \{2, \ldots, N\}, \tag{3.16}$$

$$d_i(0) = d_{i,0}, \forall i \in \{1, \ldots, N\} \tag{3.17}$$

$$v_i(0) = v_{i,0}, \forall i \in \{1, \ldots, N\} \tag{3.18}$$

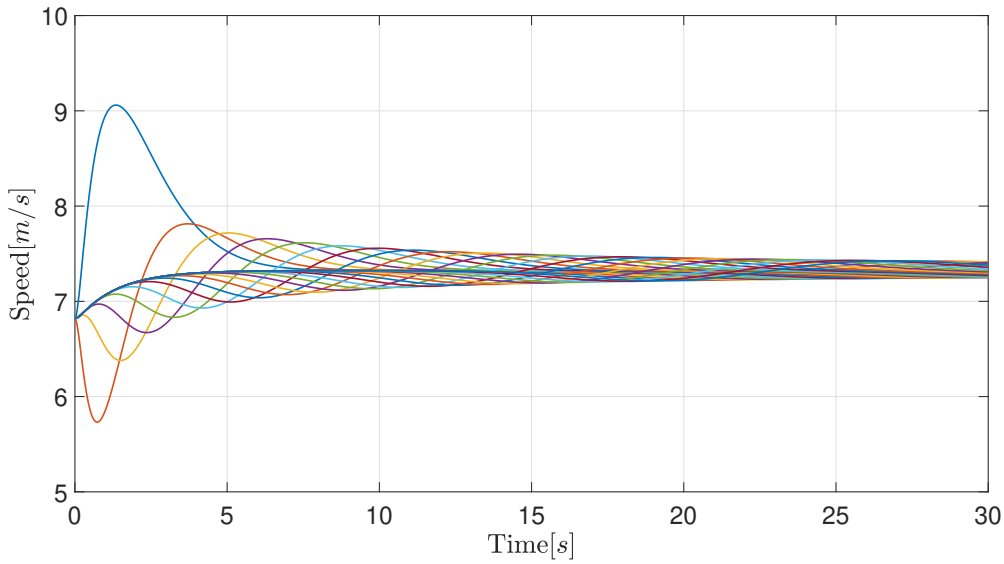

Figure 3.4: Speeds of the vehicles on the stable ring road which consists of string stable adaptive cruise control models. Each curve represents a speed of a vehicle changing by time. Speeds of the vehicles gradually converge to a constant speed, which implies the ring road is stable.

where

$$V(d) = \begin{cases} 0, & \text{if } d \leqslant s_{\text{st}}, \\ \frac{v_{\max}}{2}\left(1 - \cos\left(\pi \frac{d - s_{\text{st}}}{s_{\text{go}} - s_{\text{st}}}\right)\right), & \text{if } s_{\text{st}} < d < s_{\text{go}}, \\ v_{\max}, & \text{if } d \geqslant s_{\text{go}}, \end{cases} .$$

We pick $T = 5$, $b = 1$, $v_{\max} = 30, s_{\text{st}} = 2$, and $s_{\text{go}} = 15$ in the simulation. Parameters for the simulation and initial conditions for simulation are defined below: Detailed setup of the simulation is described below:

- Number of vehicles N: 22
- Vehicle length L: 4.5m
- Ring radius R_{ring}: 41.4m
- Initial speed $v_{i,0}$: $6.8\,\text{m}\,\text{s}^{-1}$
- Initial spacing between vehicle i and $i-1$, $d_{i,0}$ $\forall i \in \{3, \cdots, 22\}$: 7.3m
- Initial spacing between vehicle 22 and vehicle 1, $d_{1,0}$: 12.8m
- Initial spacing between vehicle 1 and vehicle 2, $d_{2,0}$: 1.8m

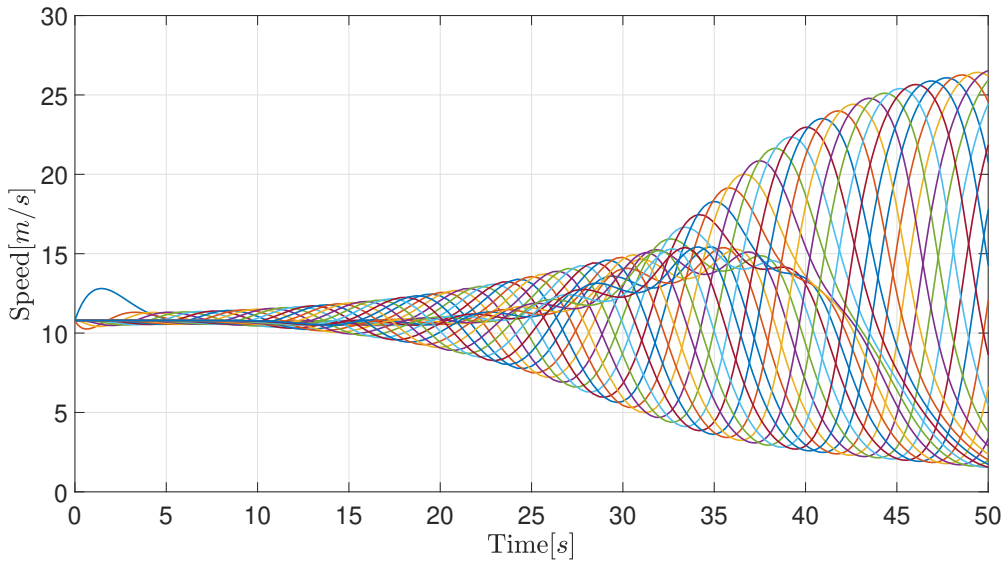

Figure 3.5: Speeds of vehicles on the ring road which consists of optimal velocity models. Each curve represents a speed of a vehicle changing by time. Oscillations of speeds increase by time, which implies the ring road is unstable.

Under the assumptions on the parameters given in the previous section, the equilibrium inter-vehicle space is $d^* = 7.3238$ and the equilibrium speed is $v^* = 10.7936$. We transform the coordinate such that equilibrium point is at the origin and take the linearization at the equilibrium point in order to determine the stability of the ring road model. The linerization of the optimal velocity model is:

$$\frac{d}{dt}\begin{bmatrix}\Delta d_i(t)\\ \Delta v_i(t)\end{bmatrix} = \begin{bmatrix}0, & -1\\ \alpha_1, & \alpha_2\end{bmatrix}\begin{bmatrix}\Delta d_i(t)\\ \Delta v_i(t)\end{bmatrix} + \begin{bmatrix}1\\ \beta\end{bmatrix}\Delta v_{i-1}(t).$$

The transfer function is

$$G_{\text{ovm}}(s) = \frac{\beta s + \alpha_1}{s^2 - \alpha_2 s + \alpha_1}, \tag{3.19}$$

with of $\alpha_1 = 0.6959$, $\alpha_2 = -1.2$, and $\beta = 1$. Since all car following models are identical, we can apply theorem 3.4.4 to determine the stability of the linearized ring road model by evaluating $\mathcal{H}_\infty$ norm of the transfer function. $\|G_{\text{ovm}}\|_{\mathcal{H}_\infty} = 1.1566$. Therefore, the ring road of optimal velocity models (3.13) - (3.18) is unstable. A simulation is carried out to validate this. Speeds of vehicles are shown in 3.5. Results show that speeds of vehicles are not converging. The ring road is not stable.

3.6.2 Ring Road stability of Optimal Velocity Model with Automated Vehicle Model

Inspired by previous works, an control for an automated vehicle is designed to stabilize the ring road. An automated vehicle model is synthesized such that platoon of OVM and automated vehicle is string stable. We replace OVM model of vehicle 1 by the automated vehicle model. The automated vehicle model is:

$$\dot{d}_1(t) = v_N(t) - v_1(t), \tag{3.20}$$

$$\begin{aligned}\dot{v}_1(t) &= k_{\mathrm{p}}(d_1(t) - d^*) + k_{\mathrm{d}}(v_1(t) - v_{\mathrm{av}}(t)) \\ &\quad - k_{\mathrm{v}}(v_1(t) - v^*).\end{aligned} \tag{3.21}$$

The transfer function of the automated vehicle model is:

$$G_{\mathrm{av}}(s) = \frac{k_{\mathrm{d}}s + k_{\mathrm{p}}}{s^2 + (k_{\mathrm{d}} + k_{\mathrm{v}})s + k_{\mathrm{p}}}. \tag{3.22}$$

We replace one of the optimal velocity models on the ring road with the automated vehicle model. In other words, we consider the ring road model of heterogeneous car following models described by (3.20), (3.21), and (3.15)-(3.18). The characteristic equation of the linearized ring road is $1 - G_{\mathrm{av}}(s)G_{\mathrm{ovm}}^{(N-1)}(s) = 0$. We pick parameters such that $\|G_{\mathrm{av}}G_{\mathrm{ovm}}^{(N-1)}\|_{\mathcal{H}_\infty} \leq 1$. $k_{\mathrm{p}} = 0.0018, k_{\mathrm{d}} = 0.0157, k_{\mathrm{v}} = 0.047$ meets the requirement. Speed profiles of vehicles are shown in figure 3.6. The speed profiles converge to the equilibrium speed because one optimal velocity model is replaced by the automated vehicle model.

3.7 Summary

In this chapter, we formulate a ring road model and study the stability of the ring road based on string stability conditions of vehicle models. Stability of the ring road models is locally determined based on eigenvalues of the linearized model around the equilibrium point. We use Nyquist criterion to determine locations of eigenvalues based on string stability and collective string stability of the car following models. We first show that string stability or collective string stability of the vehicles is sufficient for all the eigenvalues in the left half plane except one at zero. For the eigenvalue at the zero, we demonstrate that the system is asymptotically stable even with one eigenvalue at zero, thanks to the inherent linear state constraint of the ring road model. For the case that all vehicle models on the ring road are identical, we further show the string stability is also a necessary condition when there is a sufficient number of vehicles on the ring road. These results provide an analytical approach to analyse stability of the ring road or synthesize an automated vehicle to stabilize the ring road. We first validate our results in simulation with a linear adaptive cruise control vehicle model. We simulate cases for both string stable and string unstable vehicle models. Simulation results show that the ring road is unstable if the vehicle is not string stable, and

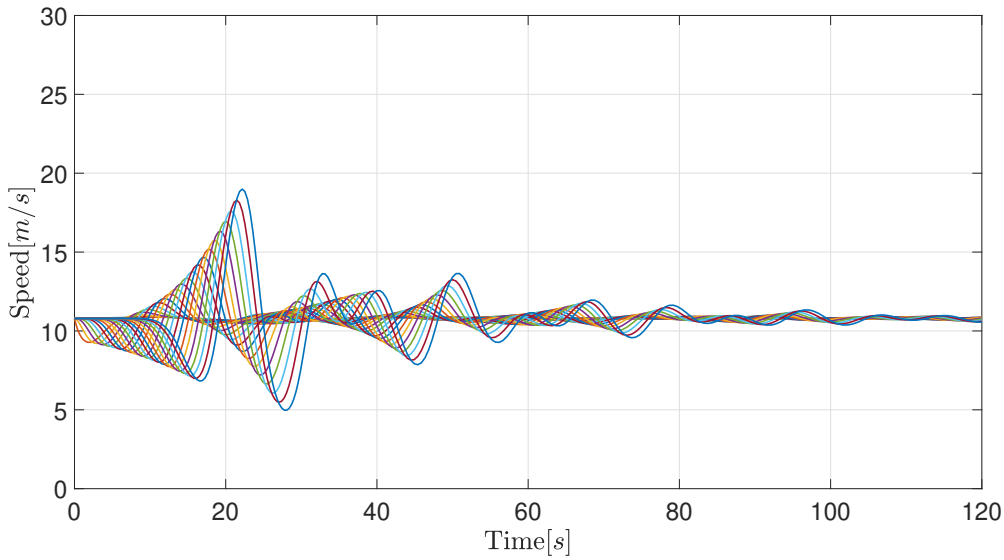

Figure 3.6: Speeds of vehicles on the ring road which consists of optimal velocity models and an automated vehicle model. Each curve represents a speed of a vehicle changing by time. Speeds of the vehicles converge to a constant speed, which means the ring road is stable.

the ring road is stable if the vehicle is string stable. Secondly, we simulate the ring road with optimal velocity models which are not string stable. Since the optimal velocity model is not string stable, the ring road of the optimal velocity model is unstable. To stabilize the ring road, we synthesized an automated vehicle model such that the platoon mixed of automated vehicle model and optimal velocity models is string stable. Simulation results demonstrated that the ring road is stabilized with the automated vehicle.

Although we have shown a theoretical approach to design a controller to stabilize the ring road, the condition is not necessary for a controller to dissipate stop-and-go waves. The controller could still dissipate stop-and-go waves even not satisfying collective string stability, for example, heuristic based controller [84] and learning based controller [104]. Since these models are generally too complex to analyze analytically, alternative approach to analyze stability of the traffic composed of such controller is by simulations. In chapter 4, we are going to use simulations to evaluate performances of a few different controllers under different penetration rates and different distributions.

Chapter 4

Evaluation of Automated Vehicle Controls for Traffic Smoothing on Ring Road

In the chapter 3, emergence of stop-and-go waves is viewed as stability of the traffic dynamics and theoretical conditions of vehicle models for traffic stability are discussed. Limitations of the theoretical approach is that it is not generally applicable to models that are too complex to analyze, for example, data driven models are not linearizable and thus can not apply theorems shown in the last chapter. Besides, for traffic mixed of different car following models, only sufficient condition is found, which means automated vehicle controllers do not necessarily need to satisfy theoretical conditions to be able to dissipate stop-and-go waves.

Many different controllers showing success of dissipating stop-and-go waves have been proposed in the literature. It is necessary to study the performances of controllers thoroughly under different scenarios in order to get a better understanding about the interactions of automated vehicles and stop-and-go waves. In this chapter, we evaluate these automated vehicle models found in the literature in the simulations with performance metrics. Considering that the penetration rates of automated vehicles would not be 100 percent over night. Performances are evaluated under different penetration rates and different distributions among human driving vehicles.

4.1 Overview

Car Following Models (CFMs) are used to describe driving behavioral patterns of Human-driving vehicles (HVs) and are considered to be the most important representatives of microscopic traffic flow models in studying traffic behavior to address congestion [91]. The early works in developing CFMs date back to the 1950s. The first two researchers who are known to introduce dynamical elements of a line of vehicles are Reuschel in 1950 [74] and Pipes in 1953 [67]. In their works, they were able to include an important element of modern mi-

croscopic modeling: the safety distance between vehicles (*i.e.* minimum bumper-to-bumper distance of a vehicle following a leading vehicle). Their models focus on the dynamical behavior of a stream of vehicles as they accelerate or decelerate and as each leader-follower pair follows each other, making it a foundation among the most recent advances in CFMs. There are many other researchers who extended the works of Reuschel and Pipes. Among them are Kometani and Sasaki in 1958 [40] and Herman and his associates at *General Motors*[33]. These early works were called *minimal models* because they are "not complete and can't describe either free traffic or approaches to standing obstacles[91, Chapter 10]."

It had been more challenging to solve for time-continuous models because they tend to be highly computationally expensive in the earlier years. To compensate for this, discrete-time models had been developed. One of the arguably simplest discrete-time models is the Newell's CFM [62]. It considers that a leading vehicle is following a preceding vehicle on a homogeneous highway, and the time-space trajectory of the leading vehicle is assumed to be the same as the preceding vehicle. Along the traffic wave speed, the leading vehicle changes its speed based on the preceding vehicle at any time-space point. However, the advancements in computing technologies has allowed the use of time-continuous models to be more feasible and flexible. Examples of popular continuous time models are Intelligent Driver Model [91, Chapter 11] and Optimal Velocity Model [6].

To replicate the emergence of stop-and-go waves in simulation as observed in the real world [85][89], simulation models of car following models need to be picked carefully. As shown in the chapter 3, car following model can trigger the instability of the traffic jam if string stability condition is violated. With models that can replicate the emergence of stop-and-go waves, performances of controllers for automated vehicles can be validated in simulations in terms of capabilities of dissipating stop-and-go waves.

The emergence of AVs was pushed forward when Defense Advanced Research Projects Agency, the research arm of the United States Department of Defense, organized a series of challenges in 2004-2007. This interest for AVs grew further when Tesla's Autopilot was launched in 2014. The transportation network companies like Uber and Lyft are also now invested in research for automated cars. It is expected that AVs has potential to improve safety [100][56][26], but also efficiency [2][93] and mobility [102] [18]. The idea of using AVs to stabilize a stop-and-go waves on a ring road had been studied. The emergence of stop-and-go waves on a ring road can be viewed as instability of a dynamical system. Theoretically, the ring road is not controllable, but it is stabilizable [97]. Therefore, the ring road can be stabilized with an automated vehicle as a state feedback controller, although full state feedback controller may not be necessarily needed for stabilizing the system. The dynamics of the ring road can be totally different by replacing a HV by an AV, and so does the stability. If the AV model is selected carefully, the ring road stability may be achieved even without a full state feedback controller. Cui *et al.* [17] carried out a stability analysis and showed the possibility of smoothing traffic flow with a single automated vehicle on ring road in the simulation. Stern *et al.* [84] verified the idea of smoothing traffic on a ring road. Horn *et al.* [34] proposed bilateral controller to stabilize the ring road traffic. Wu *et al.* [104] showed using the reinforcement learning controller to stabilize a ring road traffic. Delle

Monache et al. [20] proposed Lyapunov based controller for dissipating traffic waves and validated it on the ring road. Zheng *et al.* [118] considered a full state feedback controller and derived a AV controller based on optimal control to stabilize a ring road. Li *et al.* [44] further investigates the impact of the penetration rates and distributions of the optimal control method, in which optimal distributions based on $\mathcal{H}_2$ norm are shown dependent on penetration rates and the set up of car-following models. While many controllers have been successfully demonstrated the capabilities of improving traffic flows on the ring road in the literature, most of them are not generally benchmarked under different penetration rates and distributions. Since the penetration rates and distribution may have great impact to the traffic [111][44], it is essential to evaluate controllers thoroughly under different penetration rates and distributions. Given that the analysis may generally not be tractable for all controllers, analysis based on simulations is done in this work. This work aims to make a general comparisons of these controllers under different penetration rates and distributions, particularly focusing on controllers that have been validated against ring road traffic in simulations or real world experiments. Kreidieh *et al.* [43] found that controllers generated in closed network scenarios having otherwise similar densities and perturbing behaviors confirms that closed network policies are transferable to open network scenarios. While Wang *et al.* [96] was able to verify in their work in leading cruise control the potential to control traffic using connected AVs in an open road.

Ten AV models found in the literature will be evaluated in this chapter. In the remainder of this chapter, human driving model and automated vehicle models used are introduced, followed by descriptions for the simulation environment. We studied the performance of AVs by carrying out experiments on a ring road using state-of-the-art traffic simulation platform considering various penetration rates and distribution of AVs for each AV model. Time to stabilize, maximum distance-gap, vehicle miles traveled (VMT), and fuel economy are used to evaluate their performances. Simulation results are summarized in the end.

In this chapter, we assess improvement of traffic with AVs on a ring road under different penetration rates and distributions. The time to stabilize, the maximum distance-gap, vehicle miles traveled, and fuel economy are used to evaluate their performances. Using these metrics, we benchmarked their performances and found unusual behaviors of controllers under different penetration rates and distributions. Results also demonstrated that the learning based approach has a great potential under all traffic scenarios.

4.2 Notations and Abbreviations

Many of notations used for chapter 3 will continue to use in this chapter. Specifically, for variables relevant to car following models, such as vehicle position, speed, acceleration, and relative distance defined in section 3.2 will be used. Many controllers are discussed in this chapter. For readability, they are frequently being referred by abbreviations. For convenience, a list of frequently abbreviations are listed below:

AVs	Automated vehicles
HVs	Human-driven vehicles
CFM	Car following model
RL	Reinforcement learning
IDM	Intelligent driver model
VMT	Vehicle miles traveled
AUG	Augmented Optimal Velocity Follow-the-Leader
BCM	Bilateral control model
FS	FollowerStopper controller
PI	Proportional-integral with saturation controller
HBEFA	Handbook Emission for Road Transportation
ACC	Adaptive cruise control
LACC	Linear adaptive cruise control
MLYAU1	Modified Lyapunov 1 controller
MLYAU2	Modified Lyapunov 2 controller
LinOpt	Linear optimal controller
MLP	Multilayer perceptron
GRU	Gated recurrent unit
PPO	Proximal policy optimization
SUMO	Simulation of Urban Mobility
ICs	Initial conditions
FUZ	Fuzzy controller

4.3 Intelligent Driving Model (IDM) as Human Driver Car following Model

As mentioned in section 4.1, there are many extensive studies to model how people drive on the road. The conceptual bases of these models are supported by empirical data [13]. Despite the numerous models developed, this is still an active field of research given the modeling challenges caused by heterogeneity of traffic and varying characteristics of drivers. Other examples of CFMs include Optimal Velocity Model [7][5], second-order linear model [63] and IDM [90][91]. Among these models, IDM is recognized for being capable of accurately representing realistic driver behavior [90]. Hence, IDM is adopted in this work and used to represent human-driven cars. IDM is also among the time-continuous and dynamical models for longitudinal movement.

M. Treiber *et al.* [90][91] provided a comprehensive and instructive coverage of vehicular traffic flow dynamics and modeling in their work leading to the formulation of IDM, a continuous-time CFM for the simulation of freeway and urban traffic. It describes the dynamics of the positions and velocities of single vehicles. The acceleration in IDM which

we defined as time-derivative of speed, $\dot{v}_i(t)$, is shown below:

$$\dot{d}_i(t) = v_{i-1}(t) - v_i(t), \tag{4.1}$$

$$\dot{v}_i(t) = a_{max}\left[1 - \left(\frac{v_i(t)}{v_0}\right)^{\delta} - \left(\frac{s^*\left(v_i(t), \dot{d}_i(t)\right)}{d_i(t)}\right)^2\right], \tag{4.2}$$

where $v_0 \in \mathbb{R}$ is the desired velocity, $a_{max} \in \mathbb{R}$ is the maximum acceleration, $\delta \in \mathbb{R}$ is the acceleration exponent, $b \in \mathbb{R}$ is the desired deceleration, and $s^* : \mathbb{R} \times \mathbb{R} \to \mathbb{R}$ is the desired distance-gap of the vehicle for a given vehicle speed and a relative speed, denoted by:

$$s^*\left(v_i(t), \dot{d}_i(t)\right) = s_0 + \max\left(0, v_i(t)T - \frac{v_i(t)\dot{d}_i(t)}{2\sqrt{a_{max}b}}\right). \tag{4.3}$$

where $T \in \mathbb{R}$ is the safe time headway, and $s_0 \in \mathbb{R}$ is the jam distance or minimum gap. Values of the parameters are presented in section 4.5.2.

4.4 Automated Vehicle Car-Following Models

This section discusses the known models for car-following control. Note that as the level of automation increases, there are also increased capabilities with respect to what the vehicles on its own like the ones described for Level 1 and Level 2 here. Unlike human behavior CFMs, models introduced here are not meant to replicate human driving behavior. These AV-CFMs were designed to have some properties or meet some criteria.

4.4.1 Augmented OV-FTL model

Cui et al. [17] augmented the optimal-velocity-follow-the-leader (*OV-FTL*) model with a term penalizing the difference between the automated vehicle speed and the equilibrium speed $v_{eq} \in \mathbb{R}$:

$$\dot{d}_i(t) = v_{i-1}(t) - v_i(t), \tag{4.4}$$

$$\dot{v}_i(t) = k_a(V(d_i(t)) - v_i(t)) + k_b\frac{v_{i-1}(t) - v_i(t)}{d_i(t)^2} + k_c(v_{eq} - v_i(t)), \tag{4.5}$$

where $k_a \in \mathbb{R}$, $k_b \in \mathbb{R}$, and $k_c \in \mathbb{R}$ are positive parameters; $V(\cdot) : \mathbb{R} \to \mathbb{R}$ is a monotonically non-decreasing function:

$$V(d_n) = \begin{cases} 0, & \text{if} \quad d_n \leqslant s_{\text{st}}, \\ \frac{v_{\max}}{2}\left(1 - \cos\left(\pi\frac{d_n - s_{\text{st}}}{s_{go} - s_{\text{st}}}\right)\right), & \text{if} \quad s_{\text{st}} < d_n < s_{\text{go}}, \\ v_{\max}, & \text{if} \quad d_n \geqslant s_{\text{go}} \end{cases} \tag{4.6}$$

where $s_{st} \in \mathbb{R}$, $s_{go} \in \mathbb{R}$ are parameters.

4.4.2 Bilateral Control Model

This controller is almost similar to the linear ACC, except that instead of considering the relative speed and the spacing headway only with respect to the preceding vehicle as applied in the linear ACC, it is now considering relative speeds and the spacing headways with respect to its preceding vehicle and its following vehicle wherein it is assumed that these information can be obtained by the subject vehicle using sensors in the front and in the back. By that, the vehicle tries to be halfway between the leading and the following vehicle. Following this, the ith vehicle uses the following acceleration equation [34]:

$$\dot{d}_i(t) = v_{i-1}(t) - v_i(t), \tag{4.7}$$

$$\dot{v}_i(t) = k_d\left(d_i(t) - d_{i+1}(t)\right) + k_v\Big(\left(v_{i-1}(t) - v_i(t)\right) - \left(v_i(t) - v_{i+1}(t)\right)\Big) + k_p(v_{des} - v_i(t)), \tag{4.8}$$

where $k_d \in \mathbb{R}$, $k_v \in \mathbb{R}$, and $k_p \in \mathbb{R}$ are parameters where with any arbitrary positive constants will always lead to ring stability [35] [98]; $v_{des} \in \mathbb{R}$ is a design parameter representing the desired speed.

4.4.3 FollowerStopper

The FollowerStopper controller [84] generates the speed command $v^{cmd}(\cdot,\cdot) : \mathbb{R} \times \mathbb{R} \to \mathbb{R}$ based on the combinative conditions of the headway $d_i(t)$ and the relative speed $\dot{d}_i(t)$. The condition of the headway and the relative speed are divided into four regions. In each region, safety speed command is determined in order to prevent the automated vehicle from crashing into the vehicle in front of it. Speed command v^{cmd} in each region is shown below, followed be the definition of each region:

$$v^{cmd}(d_i(t), \dot{d}_i(t)) = \begin{cases} 0 & \text{if } d_i(t) \leq \Delta x_1 \text{ (Stopping region)} \\ \hat{v}(t)\frac{d_i(t)-\Delta x_1}{\Delta x_2 - \Delta x_1} & \text{if } \Delta x_1 < d_i(t) \leq \Delta x_2 \text{ (Adaptation region I)} \\ \hat{v}(t) + (U - \hat{v}(t))\frac{d_i(t)-\Delta x_2}{\Delta x_3 - \Delta x_2} & \text{if } \Delta x_2 < d_i(t) \leq \Delta x_3 \text{ (Adaptation region II)} \\ U & \text{if } \Delta x_3 < d_i(t) \text{ (Safe region)} \end{cases}, \tag{4.9}$$

where $\hat{v}(t) = \min\{\max\{v_{i-1}(t), 0\}, U\}$. A safe cruise speed $U \in \mathbb{R}$ is assigned as reference speed in the safe region. In the stopping region, zero velocity is commanded. In the adaptation region (two parts), some average of desired and lead vehicle velocity is commanded. Boundary of each region is defined as follows:

$$\Delta x_k = \Delta x_k^0 + \frac{1}{2d_k}\left(\Delta v_-(t)\right)^2, \quad \forall k = 1, 2, 3, \tag{4.10}$$

where $\Delta v_-(t) = \min(\dot{d}_i(t), 0)$. $\Delta x_1^0 \in \mathbb{R}$, $\Delta x_2^0 \in \mathbb{R}$, $\Delta x_3^0 \in \mathbb{R}$, $d_1 \in \mathbb{R}$, $d_2 \in \mathbb{R}$, and $d_3 \in \mathbb{R}$ are design parameters.

4.4.4 Proportional-Integral (PI) with Saturation

The *PI with Saturation* controller is a controller for speed control. It has been implemented on the real vehicle and used to dissipate stop and go waves in the circuit ring road [20][84]. The controller is modeled in the discrete manner and $v^{\text{cmd}}[k]$ denotes the speed command at time step $k \in \mathbb{Z}_{\geq 0}$:

$$v^{\text{cmd}}[k+1] = \beta[k]\left(\alpha[k]v^{\text{target}}[k] + (1-\alpha[k])\, v^{\text{lead}}[k]\right) + (1-\beta[k])\, v^{\text{cmd}}[k]. \tag{4.11}$$

The speed command $v^{\text{cmd}}[k] \in \mathbb{R}$ is basically the low-pass filtered output of the weighted average of the preceding vehicle speed $v^{\text{lead}}[k] \in \mathbb{R}$ and the subject vehicle's own target speed $v^{\text{target}}[k] \in \mathbb{R}$. The automated vehicle's target speed is defined as follows:

$$v^{\text{target}}[k] = \bar{U}[k] + v^{\text{ catch}} \times \min\left\{\max\left\{\frac{d_i[k]-g_l}{g_u-g_l}, 0\right\}, 1\right\}, \tag{4.12}$$

where $\bar{U}[k] \in \mathbb{R}$ is the temporal average of own speed over an historic interval, which is $\bar{U}[k] = \frac{1}{m}\sum_{j=k-1}^{k-m} v^{AV}[j]$; $v^{\text{catch}} \in \mathbb{R}$, $g_l \in \mathbb{R}$, and $g_u \in \mathbb{R}$ are design parameters. $v^{\text{catch}} \in \mathbb{R}$ is the catch-up speed that allow the target speed to be larger than average speed in the past, so that the automated vehicle can speed up when the headway is large. The parameters $\alpha[k] \in \mathbb{R}$ and $\beta[k] \in \mathbb{R}$ are formulated to be dependent on the headway $d_i[k] \in \mathbb{R}$ at time step k, which are shown as follows:

$$\alpha[k] = \min\left\{\max\left\{\frac{d_i[k]-\Delta x^{\text{s}}[k]}{\gamma}, 0\right\}, 1\right\}, \tag{4.13}$$

$$\beta[k] = 1 - \frac{1}{2}\alpha[k], \tag{4.14}$$

where $\gamma \in \mathbb{R}$ is a design parameter and $\Delta x^{\text{s}}[k] \in \mathbb{R}$ is defined as:

$$\Delta x^{\text{s}}[k] = \max\left\{2\left(v^{\text{lead}}[k] - v^{\text{AV}}[k]\right), 4\right\}. \tag{4.15}$$

This controller has also been called as the MLB controller in [20].

4.4.5 Linear Adaptive Cruise Control

Adaptive cruise control is a driver-assistance system which can keep vehicle speed at a set speed when there is no any vehicle ahead and automatically adjusts its speed to maintain a safety spacing if there is a preceding vehicle. Dynamics of the adaptive cruise control system controlled vehicle involved vehicle longitudinal dynamics, sensor response, sophisticated in-vehicle network and intricate control algorithms, which is usually not easy to model. The linear model can be used to approximate the dynamics with accuracy [59][15], and the model is sufficient for analysis in micro-simulations[48][73]. In this work, we also use the

linear model to approximate the vehicle dynamics and use the linear control to approximate the control system. The vehicle longitudinal dynamics can be approximated with a first order ordinary differential equation [114][46]. We postulate that there exists a response lag between the desired acceleration and the real acceleration. The linear vehicle longitudinal dynamics can be written as follows:

$$\dot{x}_i(t) = v_i(t), \tag{4.16}$$

$$\dot{v}_i(t) = a_i(t), \tag{4.17}$$

$$\dot{a}_i(t) = -\frac{a_i(t)}{\tau} + \frac{a_{i,des}(t)}{\tau}, \tag{4.18}$$

where $a_{i,des}(t) \in \mathbb{R}$ is the desired acceleration of the vehicle, which is a function of relative distance and relative speed, as described below; and $\tau \in \mathbb{R}$ is the lag time. For the adaptive cruise controller, the time gap spacing policy is usually used. The time gap spacing policy sets the desired spacing between vehicles as proportional to the vehicle speed. The time gap spacing policy mimics the human driving behavior and it is believed to be safer because it allowed longer reaction time to emergency brake ahead. Time gap spacing car-following controller is described below. The controller mainly consists of two parts: gap error $e_{x,i}(t) \in \mathbb{R}$ and speed error $e_{v,i}(t) \in \mathbb{R}$, which are defined as follows:

$$e_{x,i}(t) = d_i(t) - hv_i(t), \tag{4.19}$$

$$e_{v,i}(t) = v_{i-1}(t) - v_i(t), \tag{4.20}$$

where h is the desired time gap. The control consists of linear combination of gap error and speed error:

$$a_{i,des}(t) = k_1 e_{x,i}(t) + k_2 e_{v,i}(t). \tag{4.21}$$

$k_1 \in \mathbb{R}$ and $k_2 \in \mathbb{R}$ are positive design parameters. These parameter can be calibrated using the collected data from the field experiment.

4.4.6 Optimal Control Strategy

Zheng et al. [118] proposed a strategy of optimal control. The human driver CFM is firstly linearized. Suppose that vehicle-1 is the automated vehicle, linear optimal control is derived in the follows form:

$$\dot{v}_1(t) = -\left[k_{1,1}(d_1(t) - d_c^*) + k_{1,2}(v_1(t) - v^*) + \sum_{i=2}^{N} k_{i,1}(d_i(t) - d^*) + k_{i,2}(v_i(t) - v^*)\right]. \tag{4.22}$$

Parameters $k_{i,1} \in \mathbb{R}$, $k_{i,2} \in \mathbb{R}, \forall i \in \{1, \ldots, N\}$ are obtained by optimal control. To obtain these parameters, we define $K = [k_{1,1}, k_{1,2}, k_{2,1}, k_{2,2}, \cdots, k_{N,1}, k_{N,2}] \in \mathbb{R}^{1\times 2N}$ and let K equals

ZX^{-1}, where $Z \in \mathbb{R}^{1\times 2N}$ and $X \in \mathbb{R}^{2N\times 2N}$ are optimizer of the following optimization problem:

$$\begin{aligned} &\min_{X,Y,Z} Trace(QX) + Trace(RY) \\ \text{subject to} \quad &(AX - BZ) + (AX - BZ)^T + HH^T \preceq 0, \\ &\begin{bmatrix} Y & Z \\ Z^T & X \end{bmatrix} \succeq 0, \qquad X \succeq 0, \end{aligned}$$

where $A \in \mathbb{R}^{2N\times 2N}$, $B \in \mathbb{R}^{2N}$, $H \in \mathbb{R}^{2N}$ are matrices for the state space model of the linearized ring road dynamics. Q and R are design parameters, which are defined as $Q = diag(\gamma_s^2, \gamma_v^2, \ldots, \gamma_s^2, \gamma_v^2) \in \mathbb{R}^{2N\times 2N}$ and $R = \gamma_u^2 \in \mathbb{R}$. Although the optimal control can be redesigned to achieve an optimal performance under different penetration rates and different distributions [44], in this work, for our purpose, we do not redesign the controller for different penetration rates and distributions. The optimal controller is derived based traffic of 1 AV and 22 HVs and tested under all scenarios in the simulation studies.

4.4.7 Lyapunov Based Controller

Delle Monache et al. [20] proposed two types of Lyapunov based controller. The controllers are firstly derived using Lyapunov like function. Controllers are then discretized considering that the controllers are deployed on the digital system, where target speed at each time step is issued as the input to the lower system of the automated vehicle. The first Lyapunov based controller is as follows:

$$v_i^{target,1}[k+1] = (u[k] - \bar{v}[k])exp(-\Delta t) + \bar{v}[k]. \tag{4.23}$$

The second controller is as shown below:

$$v_i^{target,2}[k+1] = (u[k] - \frac{v_{i-1}[k] + \bar{v}[k]}{2})exp(-\Delta t) + \frac{v_{i-1}[k] + \bar{v}[k]}{2}. \tag{4.24}$$

$v_i^{target,1}[k+1] \in \mathbb{R}$, $v_i^{target,2}[k+1] \in \mathbb{R}$ are target speeds of the i-th vehicle of the first and the second controller at time step $k+1$. $u[k] \in \mathbb{R}$ and $\bar{v}[k] \in \mathbb{R}$ are defined as follows:

$$u[k+1] = \beta[k](\alpha[k]v_i^{target,j}[k] + (1-\alpha[k])v_{i-1}[k]) + (1-\beta[k])u[k], \qquad (j = 1, 2), \tag{4.25}$$

$$\bar{v}[k] = \min\left\{\frac{\sum_{m=1}^{k-1} v_{i-1}[m]}{k-1}, \frac{\sum_{m=1}^{k-1} u[m]}{k-1}\right\}. \tag{4.26}$$

Controller gains $\alpha[k] \in \mathbb{R}$ and $\beta[k] \in \mathbb{R}$ are defined as follows:

$$\alpha[k] = \min\left\{\max\left\{\frac{d_i[k] - \Delta x^s[k]}{\gamma}, 0\right\}, 1\right\}, \tag{4.27}$$

$$\beta[k] = 1 - \frac{1}{2}\alpha[k], \tag{4.28}$$

where

$$\Delta x^{\mathrm{s}}[k] = \max\left\{2\Big(v_{i-1}[k] - v_i[k]\Big), 4\right\}.$$

4.4.8 Fuzzy Controller

Haulcy et al. [30] proposed fuzzy controller for stabilizing a ring road. In the fuzzy logic, the space headway and the relative speed are processed to determine the desired speed change. Triangular shape membership functions are constructed to represent the levels of the different classes of the distances and the speed differences. The speed change command is determined following the inference process and the defuzzification process.

4.4.9 Reinforcement Learning Control

Reinforcement learning control is a data driven controller. In the scheme of reinforcement learning, control policy for an agent is being trained to maximize cumulative reward. The agent does random actions at first and maps out each of these actions to determine which among them maximizes the numerical rewards. Mathematically, an agent learns a policy $\pi(state) = action$, maps from states *state* to actions *action*, to achieve a goal in an environment under uncertainty. Through repeated environment interactions, a reinforcement learning agent strives to develop an optimal policy π^*, which maximizes the sum of the rewards. RL is often used in solving sequential decision-making problems [86]. To deal with the traffic control with the reinforcement learning, Wu *et al.* [106][107] proposed framework for traffic control using deep reinforcement learning . The framework integrates the traffic simulation environment SUMO and the reinforcement learning library such as rllab [22] and rllib [47] so that the policy cna be learnt to optimize the cumulative reward using sampled data from SUMO. The policy usually consists of neural networks, and may be of several forms. Two policies: the Multilayer Perceptron and Gated Recurrent Unit are proposed for a ring road problem in the [107]. MLP is a classical (feedforward) artificial neural network with multiple hidden layers and utilizes back propagation to optimize its parameters. GRUs are recurrent neural network capable of storing memory on the previous states of the system through the use of parameterized update and reset gates, which are also optimized by the policy gradient method. One of the advanced reinforcement learning algorithms is the Proximal Policy Optimization [78] which is said to perform comparably or better than state-of-the-art approaches. Other advanced reinforcement learning, such as soft-actor critic [29], not covered in this work, can also be investigated in the near future. The RL control tested in this work is trained on the ring road of 1 agent and 21 HVs. The *state* are the distance between the agent and its leading vehicle ($d_i(t)$), the leading vehicle speed ($v_{i-1}(t)$), and the agent speed ($v_i(t)$). The *action* is the agent acceleration ($a_i(t)$). Suppose, the RL agent is i-the vehicle in the ring road, the *reward* $r_i(t) \in \mathbb{R}$ is designed in a way that high average speed of all vehicles is rewarded, while high acceleration of the agent is penalized.

The reward is:

$$r_i(t) = \eta_1 \sum_{j=1}^{22} v_j(t) - \eta_2 \max\{0, a_i(t)\}.$$

Once the policy is trained on the ring road of 1 agent and 21 HVs, it is tested under different penetration rates and distributions with no modification.

4.4.10 Summary Table for AV Controllers

In the table 4.1, properties of the automated vehicle models considered in this chapter are summarized, including the needed input, the controller type, the design parameters, and the design method. In terms of input needed for the controllers, all the controllers need at least the speed measurements of the leading vehicle and the subject vehicle, and most of them also use the measurement of the spacing ahead of the subject vehicle, except MLYAU1 and MLYAU2. Without using the feedback of the spacing ahead, the following distance of MLYAU1 and MLYAU2 cannot be controlled. In addition to the spacing ahead and the speed of the leading vehicle, the BCM also uses the spacing behind and the speed of the following vehicle. The optimal control needs the most information, not only the spacing and the speeds of the vehicles near by, but also spacing and speeds of all the vehicles on the ring road. To access these information, wireless communication between vehicles is necessary. Third column shows the types of the controller. Four of the controllers are nonlinear controllers, and the rest of the controllers are linear. The design parameters of the controllers are listed in the forth column; except FUZ and RL, because the parameters these two controllers are too many to show here. The references for these two controllers are provided instead. Inspired by the classification in [97], the last column summarized the ways controllers are derived. Three controllers are designed based on observations in the real world. RL is the only controller that is based on learning. The rest of the controllers are based on analyses of the car following models.

4.5 Simulation

4.5.1 Simulation Platform

SUMO [49] is a microsimulation software. We used this simulation software since it is an open-source enabling interested parties to reproduce the results we have. SUMO has the capability to generate microscopic models of inter-modal traffic systems including road vehicles, public transport and pedestrians. It allows customized models and has various APIs to control the simulations remotely. It also allowed us to calculate the fuel economy which calculates it based on the Handbook Emission Factors for Road Transport 3 Euro 4 passenger car emission model.

AV models	Input	Controller type	Design parameters	Design Method
AUG	$d_i(t), v_i(t), v_{i-1}(t)$	Linear	k_a, k_b, k_c, v_{eq}	Model-based
BCM	$d_i(t), d_{i+1}(t)$ $v_i(t), v_{i-1}(t), v_{i+1}(t)$	Linear	k_d, k_v, k_p, v_{des}	Model-based
FS	$d_i(t), v_i(t), v_{i-1}(t)$	Nonlinear	$U, \Delta x_1^0, \Delta x_2^0, \Delta x_3^0,$ d_1, d_2, d_3	Heuristic
PI	$d_i(t), v_i(t), v_{i-1}(t)$	Nonlinear	$v^{\text{catch}}, g_u, g_l, \gamma$	Heuristic
LACC	$d_i(t), v_i(t), v_{i-1}(t)$	Linear	k_1, k_2, h	Model-based
LinOpt	$d_i(t), v_i(t),$ $\forall i \in \{1, 2, \ldots, N\}$	Linear	$\gamma_s, \gamma_v, \gamma_u$	Model-based
MLYAU1	$v_i(t), v_{i-1}(t)$	Linear	γ	Model-based
MLYAU2	$v_i(t), v_{i-1}(t)$	Linear	γ	Model-based
FUZ	$d_i(t), v_i(t), v_{i-1}(t)$	Nonlinear	see details in [30]	Heuristic
RL	$d_i(t), v_i(t), v_{i-1}(t)$	Nonlinear	see details in [104]	Learning-based

Table 4.1: Summary of the AV models on a ring road.

To run the simulations in SUMO, we also utilized existing libraries of code available in Flow [104][105] which is a computational framework mainly developed to enable the use of reinforcement learning methods such as policy gradient methods for traffic control and enables benchmarking of the performance of classical controllers which is then built to work the SUMO microsimulator. Flow is developed by the Mobile Sensing Lab at the University of California, Berkeley.

This study is the general investigation of behavior of vehicles driving on the closed circuit road. Since the ring itself is a closed loop, we used the continuous router which ensures the continuous rerouting of the vehicles in a closed loop. This class is useful if vehicles are expected to continuously follow the same route, and repeat said route once it reaches its end.

4.5.2 Simulation Setup and Simulation Parameters

We are interested in the dynamic behavior of the closed circuit ring road. The simulation environment is set up similar to the real experiment shown in [84]. There are 22 vehicles on the single lane circuit ring road, which the radius is 41.38m (circumference is 260m). At the beginning of the simulation, the vehicle are placed uniformly, i.e. each distance gap are being set equally; and the initial speeds are all zero. Depends on the scenarios (section 4.5.3) running, each vehicle is assigned as human-driving vehicle or as a different type of automated vehicle. In each simulation run, there is always 300 seconds warm-up, in which all vehicles are running with IDM to make the ring traffic in the status of having stop-and-go waves. After that, the assigned automated vehicles switch to the automated control. For each model, values of parameters used in the simulations in this work are summarized in this

section. Selection of parameters may have influence on the performances. For the purpose of bench-marking, values of the original articles are used if they are available. Otherwise, values based on design criteria shown in the origin articles are used. None of these values are fine-tuned, although performances may be improved after careful tuning.

- **Intelligent Driver Model (IDM)** The parameters chosen for the IDM are as follows: $\delta = 4$, safe time headway $T = 1$s, maximum acceleration $a_{\max} = 1\mathrm{m\,s^{-2}}$, desired deceleration $b = 1.5\mathrm{m\,s^{-2}}$, jam distance $s_0 = 2$m, and maximum speed $v_0 = 30\mathrm{m\,s^{-1}}$ [91, Chapter 11].

- **Augmented OV-FTL (AUG)** $k_a = 1$, $k_b = 1$, $k_c = 11.0$, $h_{st} = 2$m, $h_{go} = 15$m, $v_{\max} = 30\mathrm{m\,s^{-1}}$, and $v_{eq} = 4.8\mathrm{m\,s^{-1}}$, where k_a, k_b are arbitrary positive numbers and k_c is selected based on the criterion shown in [17]; h_{st}, h_{go}, and v_{max} are default value in the FLOW [104]; v_{eq} is the equilibrium speed of 22 IDMs on the ring road.

- **Bilateral Control Model (BCM)** The bilateral CFM (section 4.4.2) and the parameters of the controller used are: $k_d = 1$, $k_v = 1$, $k_p = 1$, $v_{des} = 4.8\mathrm{m\,s^{-1}}$.It has been proven in [98] that the system of BCM vehicles is chain stable for arbitrary values of k_d and k_v that are greater than 0. v_{des} is picked as the equilibrium speed of 22 IDMs on the ring road.

- **FollowerStopper (FS)** The parameters defining the four regions of the controller are as follows: $\Delta x_1^0 = 4.5$m, $\Delta x_2^0 = 5.0$m,and $\Delta x_3^0 = 6.0$m. Also, the deceleration rates are defined to be: $d_1 = 1.5$m, $d_2 = 1.0$m, $d_3 = 0.5$m, and $U = 4.8\mathrm{m\,s^{-1}}$. Parameters shown in [84] are used. U is the target speed of the FollowerStopper. It is picked as the equilibrium speed of 22 IDMs on the ring road.

- **PI with saturation (PI)** Parameters used in simulation are: $\gamma = 2$, $g_l = 7$m, $g_u = 30$m, and $v^{\text{catch}} = 1\mathrm{m\,s^{-1}}$. Parameters shown in [84] are used.

- **Linear Adaptive Cruise Control** All the ACC controlled vehicles have the same parameters for dynamics and control: $\tau = 0.1$, $h = 1.4$s, $k_1 = 0.4$, and $k_2 = 0.7$. These parameters are picked such that its equilibrium speed is close to IDM's; and string stability condition for a linear car following model can be satisfied.

- **Linear optimal control (LinOpt)** The controller gains are designed using the gains as follows: $\gamma_s = 1$, $\gamma_v = 1$, $\gamma_u = 1$. These values are arbitrary selected.

- **Lyapunov-based controllers (MLYAU1 and MLYAU2)** For both the type 1 and the type 2, they have the same parameter: $\gamma = 2$. The parameter value shown in [20] is used.

4.5.3 Scenario

Given the goal of this work, we designed our simulations to include cases of varying percentages of AVs in the system.

Baseline case (No automation) In this chapter, the baseline scenario we are considering is all human driving vehicles on the ring. We are using IDM to model the human driving behavior. In order to stimulate instability of ring road model to reproduce stop-and-go waves, acceleration noises are intentionally injected to all the car-following models. Another way of stimulating speed fluctuations is by inducing a sudden speed changes of vehicles in the traffic, e.g.[28][34][118]. In this works, persistent excitation of the traffic with acceleration noises are used, because we can produce stop-and-go waves more easily by doing this. Speed profiles of the 22 vehicles of IDM on the ring is shown in the figure 4.1. The plot shows how the speed profiles of the vehicles greatly vary with time especially after a certain time greater than 200s.

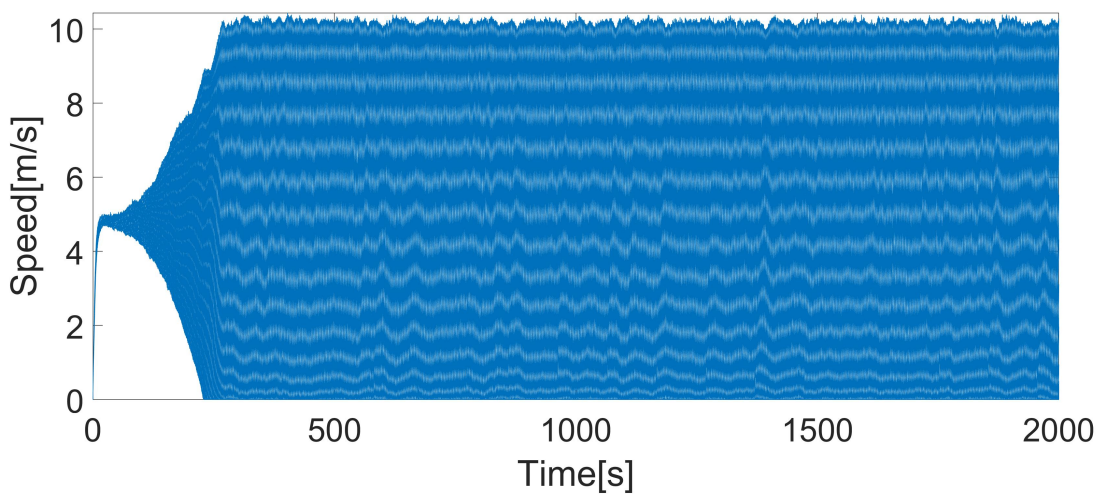

Figure 4.1: Speed profiles of all IDM vehicles on the ring. The stop-and-go waves are fully developed at around 300 seconds and persist for the rest of the time.

As an integral part of the simulations, we included a variation in the number of AVs in the system to test how the controllers perform under different penetration rates to see if there is also a significance in their performance depending on the percentage of penetration. Besides the penetration rate, we also investigate the impact of different distributions of AVs among HVs. Table 4.2 summarized the setups for scenarios we are studying in this chapter. In the *scenario I: platooned*, automated vehicles are placed in the clustered manner, which AVs are placed consecutively and HVs are also placed consecutively. Penetration of 1 AVs all the way to 22 AVs are studied. Then, in *scenario II: evenly distributed* is the case where the AVs are placed as evenly distributed as possible. That is the minimum number of HVs

between any two AVs is maximized. A maximum of 11 AVs are placed on the ring is studied in this scenario, because any number more than 11 will no longer keep AVs separated evenly by HVs. Simulation results of these scenarios are shown in the next section. To help reader visualize scenarios, table 4.3 and table 4.4 are provided, showing the types of each vehicle on the road under different penetration rate at different scenarios. In order to compare the performances of controllers in terms of capabilities of dissipating stop-and-go waves, the controllers would only be activated after 300s, a time at which the stop-and-go waves are fully formed.

	scenario I	*scenario II*
AV(s) activation time	300	300
ICs (positions)	$d_i(0) = d_{eq} + \tilde{d}_i$, $\forall i = \{1, \ldots, 22\}$	$d_i(0) = d_{eq} + \tilde{d}_i$, $\forall i = \{1, \ldots, 22\}$
ICs (speeds)	$v_i(0) = 0, \forall i = \{1, \ldots, 22\}$	$v_i(0) = 0, \forall i = \{1, \ldots, 22\}$
AV distribution	clustered	evenly distributed
Number of AVs (= n)	$n \in \{1, 2, \cdots, 22\}$	$n \in \{2, \cdots, 11\}$
IDM noise	0.1	0.1

Table 4.2: Scenarios of experiments in FLOW. $d_{eq} := (2\pi R_{ring} - \sum_{i=1}^{22} L_i)/22$, where $R_{ring} \in \mathbb{R}$ is radius of the ring road; and $\tilde{d}_i \in \mathbb{R}$ are random variables and are sampled such that $\sum_{i=1}^{22} \tilde{d}_i = 0$ to keep the sum of the headway matches the perimeter of the ring road. *AV(s) activation time* is the time at which AV controllers start to actively control the vehicles. *ICs(positions)* are the initial conditions of vehicle positions on the ring road. *ICs(speeds)* are the initial conditions of vehicle speeds on the ring road. *AV distribution* is the way AVs are distributed among other vehicles. *Number of AVs* is the number of AVs being placed on the ring road. *IDM noise* is the magnitude of the acceleration noise (in $\mathrm{m\,s^{-2}}$) added to vehicles. The distributions of AVs for *scenario I* are shown below in the table 4.3, and the distributions of AVs for *scenario II* are shown in below in the table 4.4.

4.5.4 Results

Some simulation results are shown in this section and performances of the AV algorithms are evaluated. The metrics we are using for evaluation including : *Time to stabilize*, *Maximum final gap*, *Vehicle Miles of Travel (VMT)*, and *fuel economy*.

Definition (Time to stabilize) The minimum time it takes for the standard deviation of the speeds across all vehicles to become smaller than 0.1, which is the noise we intentionally inject into the acceleration command. To be more precise, mathematical description is shown

(%)	Vehicle Type																					
4.55	AV	HV	HV	HV	HV	HV	HV	HV	HV	HV	HV	HV	HV	HV	HV	HV	HV	HV	HV	HV	HV	HV
9.09	AV	AV	HV	HV	HV	HV	HV	HV	HV	HV	HV	HV	HV	HV	HV	HV	HV	HV	HV	HV	HV	HV
13.64	AV	AV	AV	HV	HV	HV	HV	HV	HV	HV	HV	HV	HV	HV	HV	HV	HV	HV	HV	HV	HV	HV
18.18	AV	AV	AV	AV	HV	HV	HV	HV	HV	HV	HV	HV	HV	HV	HV	HV	HV	HV	HV	HV	HV	HV
22.73	AV	AV	AV	AV	AV	HV	HV	HV	HV	HV	HV	HV	HV	HV	HV	HV	HV	HV	HV	HV	HV	HV
27.27	AV	AV	AV	AV	AV	AV	HV	HV	HV	HV	HV	HV	HV	HV	HV	HV	HV	HV	HV	HV	HV	HV
31.82	AV	AV	AV	AV	AV	AV	AV	HV	HV	HV	HV	HV	HV	HV	HV	HV	HV	HV	HV	HV	HV	HV
36.36	AV	AV	AV	AV	AV	AV	AV	AV	HV	HV	HV	HV	HV	HV	HV	HV	HV	HV	HV	HV	HV	HV
40.91	AV	AV	AV	AV	AV	AV	AV	AV	AV	HV	HV	HV	HV	HV	HV	HV	HV	HV	HV	HV	HV	HV
45.45	AV	AV	AV	AV	AV	AV	AV	AV	AV	AV	HV	HV	HV	HV	HV	HV	HV	HV	HV	HV	HV	HV
50.00	AV	AV	AV	AV	AV	AV	AV	AV	AV	AV	AV	HV	HV	HV	HV	HV	HV	HV	HV	HV	HV	HV
54.55	AV	AV	AV	AV	AV	AV	AV	AV	AV	AV	AV	AV	HV	HV	HV	HV	HV	HV	HV	HV	HV	HV
59.09	AV	AV	AV	AV	AV	AV	AV	AV	AV	AV	AV	AV	AV	HV	HV	HV	HV	HV	HV	HV	HV	HV
63.64	AV	AV	AV	AV	AV	AV	AV	AV	AV	AV	AV	AV	AV	AV	HV	HV	HV	HV	HV	HV	HV	HV
68.38	AV	AV	AV	AV	AV	AV	AV	AV	AV	AV	AV	AV	AV	AV	AV	HV	HV	HV	HV	HV	HV	HV
72.73	AV	AV	AV	AV	AV	AV	AV	AV	AV	AV	AV	AV	AV	AV	AV	AV	HV	HV	HV	HV	HV	HV
77.27	AV	AV	AV	AV	AV	AV	AV	AV	AV	AV	AV	AV	AV	AV	AV	AV	AV	HV	HV	HV	HV	HV
81.82	AV	AV	AV	AV	AV	AV	AV	AV	AV	AV	AV	AV	AV	AV	AV	AV	AV	AV	HV	HV	HV	HV
86.36	AV	AV	AV	AV	AV	AV	AV	AV	AV	AV	AV	AV	AV	AV	AV	AV	AV	AV	AV	HV	HV	HV
90.91	AV	AV	AV	AV	AV	AV	AV	AV	AV	AV	AV	AV	AV	AV	AV	AV	AV	AV	AV	AV	HV	HV
95.45	AV	AV	AV	AV	AV	AV	AV	AV	AV	AV	AV	AV	AV	AV	AV	AV	AV	AV	AV	AV	AV	HV
100.00	AV	AV	AV	AV	AV	AV	AV	AV	AV	AV	AV	AV	AV	AV	AV	AV	AV	AV	AV	AV	AV	AV

Table 4.3: AV distribution for scenario I-platooned under different penetration rates.

%	Vehicle Type																					
9.09	AV	HV	HV	HV	HV	HV	HV	HV	HV	HV	HV	AV	HV	HV	HV	HV	HV	HV	HV	HV	HV	HV
13.64	AV	HV	HV	HV	HV	HV	HV	AV	HV	HV	HV	HV	HV	HV	HV	AV	HV	HV	HV	HV	HV	HV
18.18	AV	HV	HV	HV	HV	AV	HV	HV	HV	HV	HV	AV	HV	HV	HV	HV	AV	HV	HV	HV	HV	HV
22.73	AV	HV	HV	HV	AV	HV	HV	HV	HV	AV	HV	HV	HV	AV	HV	HV	HV	HV	AV	HV	HV	HV
27.27	AV	HV	HV	HV	AV	HV	HV	AV	HV	HV	HV	AV	HV	HV	HV	AV	HV	HV	AV	HV	HV	HV
31.82	AV	HV	HV	AV	HV	HV	AV	HV	HV	AV	HV	HV	HV	AV	HV	HV	AV	HV	HV	AV	HV	HV
36.36	AV	HV	HV	AV	HV	AV	HV	HV	AV	HV	HV	AV	HV	HV	AV	HV	AV	HV	HV	AV	HV	HV
40.91	AV	HV	AV	HV	HV	AV	HV	AV	HV	HV	AV	HV	AV	HV	HV	AV	HV	AV	HV	HV	AV	HV
45.45	AV	HV	HV	AV	HV	AV	HV	AV	HV	AV	HV	AV	HV	HV	AV	HV	AV	HV	AV	HV	AV	HV
50.00	AV	HV	AV	HV	AV	HV	AV	HV	AV	HV	AV	HV	AV	HV	AV	HV	AV	HV	AV	HV	AV	HV

Table 4.4: AV distribution for scenario II-evenly distributed under different penetration rates.

below:

$$T_{stable} = arg\min_{t}\left\{t : \sqrt{\frac{1}{21}\sum_{i=1}^{22}(v_i(t)-\mu(t))^2} \leq 0.1, \mu(t) = \sum_{i=1}^{22} v_i(t)\right\} - t_{activation}, \quad (4.29)$$

where $t_{activation}$ is the time when we switch on the automated vehicle, which is 300s in our simulation. The shorter time implies better wave dissipation capability.

Definition (Maximum final gap) The maximum gap between any of two consecutive vehicles on the ring if a ring road is stable. This can be used to evaluate the efficiency of

the use of spacing. The smaller is better. Formal mathematical definition is as follows:

$$\bar{S}_{final} = \max_{t \in [t_{activation}+T_{stable}, T_{final}]} \max_{\forall \in i=1,2,\ldots,22} d_i(t), \tag{4.30}$$

where T_{final} is the time step at the end of the simulation. To reduce the variations of these values because of randomness of the microsimulation, the values we are showing below are averages of 10 simulation runs. Because of the randomness, for a few of the controllers, some of the stable(unstable) results are not 100% reproducible. That is, for a few AV, under the same distribution and the same penetration rate, the simulations may not always stable(unstable). For those marginal cases, we can say they are stable if more than 50% of the simulation runs are stable. For reference, we keep the number of unstable runs for each scenario and show them in table 4.5 and 4.6. Because of the randomness, for a few of the controllers, some of the stable(unstable) results are not 100% reproducible. That is, for a few AVs, at the same distribution and the same penetration rate, the simulations may not always stable(unstable). For those marginal cases, we say they are not stable if more than 50% of the simulation runs are not stable.

Penetration Rate (%)	AUG	BCM	FS	FUZ	LACC	LinOpt	MLYAU1	MLYAU2	PI	RL
4.55	10	10	0	10	10	0	0	0	1	0
9.09	10	10	0	10	10	0	0	0	0	0
13.64	10	10	0	10	10	0	0	0	0	0
18.18	7	0	0	10	10	0	0	0	0	0
22.73	0	0	0	10	10	0	0	0	0	0
27.27	0	0	0	10	10	0	0	0	0	0
31.82	0	0	0	10	10	0	0	0	0	0
36.36	0	0	0	10	10	0	0	0	1	0
40.91	0	0	0	10	0	0	0	0	8	0
45.45	0	0	0	10	0	0	0	0	9	0
50.00	0	0	0	10	0	0	0	0	9	0
54.55	0	0	0	10	0	0	0	0	10	0
59.09	0	0	0	10	0	0	0	0	10	0
63.64	0	0	0	10	0	0	0	0	10	0
68.18	0	0	0	10	0	0	0	0	10	0
72.73	0	0	0	10	0	0	0	0	10	0
77.27	0	0	0	10	0	0	0	0	10	0
81.82	0	0	0	10	0	0	0	0	10	0
86.36	0	0	0	10	0	0	0	0	9	0
90.91	0	0	0	10	0	0	0	0	6	0
95.45	0	0	0	10	0	0	0	0	10	0
100.00	0	0	0	10	0	0	0	0	10	0

Table 4.5: Number of unstable runs (out of 10) - Clustered

4.5.4.1 Scenario I

Given the metrics defined, we can now evaluate the performance of different AV controllers. In the first scenario, AV penetration rate from 0 to 100 percent are studied, where AVs are

Penetration Rate (%)	AUG	BCM	FS	FUZ	LACC	LinOpt	MLYAU2	MLYAU2	PI	RL
9.09	10	10	0	10	10	0	0	0	0	0
13.64	10	10	0	10	10	0	0	0	0	0
18.18	10	10	0	10	10	0	0	0	0	0
22.73	10	5	0	10	10	0	0	0	0	0
27.27	0	0	0	10	10	0	0	0	0	0
31.82	0	0	0	10	10	0	0	0	10	0
36.36	0	0	0	10	10	0	0	0	10	0
40.91	0	0	0	10	0	0	0	0	10	0
45.45	0	0	0	10	0	0	0	0	10	0
50.00	0	0	0	10	0	0	0	0	10	0

Table 4.6: Number of unstable runs (out of 10) - Evenly distributed

placed in the platoon. Some AV controllers can successfully stabilize the ring at relative low penetration rate while some need higher penetration rate to stabilize the ring. Table 4.7 shows the minimum number of AVs needed to stabilize the ring and their corresponding *time to stabilize*, *max gap*, *VMT*, and *fuel economy*. To be noted, FUZ cannot stabilize the ring for any penetration rate. Therefore, no values are available. To illustrate the simulation, speed profiles of each vehicle of each case in the table are shown in the figure 4.2; and gaps of each case in the table are shown in figure 4.3, where red curves represent AVs and blue curves represent HVs. Results of Fuzzy controller are not shown here because the ring is not stabilized for any penetration rates. Table 4.7 also shows the VMT and the fuel economy for AVs that stabilized the traffic on the ring. The fuel economy is calculated using the built-in fuel consumption model of SUMO which uses the HBEFA 3 Euro 4 passenger car emission model.

Controller	Min no. of AVs to stabilize	Time to stabilize in *sec*	Max gap in *m*	VMT	Fuel economy in *mpg*
AUG	5	313.48	12.22	132.87	20.00
BCM	4	319.68	12.11	128.59	21.46
FS	1	270.85	12.96	126.54	20.51
FUZ	*Unstable*	*N/A*	*N/A*	*N/A*	*N/A*
LACC	9	1104.77	12.14	130.15	21.15
LinOpt	1	471.23	12.19	125.78	20.89
MLYAU1	1	62.64	116.49	21.83	7.39
MLYAU2	1	625.66	39.65	99.83	16.15
PI	1	263.74	12.03	125.67	20.71
RL	1	102.20	13.12	142.64	20.64

Table 4.7: Average performance comparison of scenario I

Based on table 4.7, we can tell that the following controllers are able to stabilize the traffic on the ring with a minimum of one (1) AV: FollowerStopper, PI with Saturation, Linear

Optimal Controller, Lyapunov-based Controllers Type 1 and Type 2, and Reinforcement Learning. While AUG needs fives AVs, BCM needs four AVs, and LACC needs 9 AVs to stabilize the ring, the rest of the controllers need only one AV to stabilize the ring. Among these controllers, the Lyapunov-based Controller Type 1 (4.4.7) yields the fastest time to stabilize. However, from figure 4.2, it is notable that after a few seconds that the vehicles are stable, all of them simply stops. This is a trivial solution to be stable. Because of this, we can consider that the RL controller performs the best in terms of *time to stabilize*.

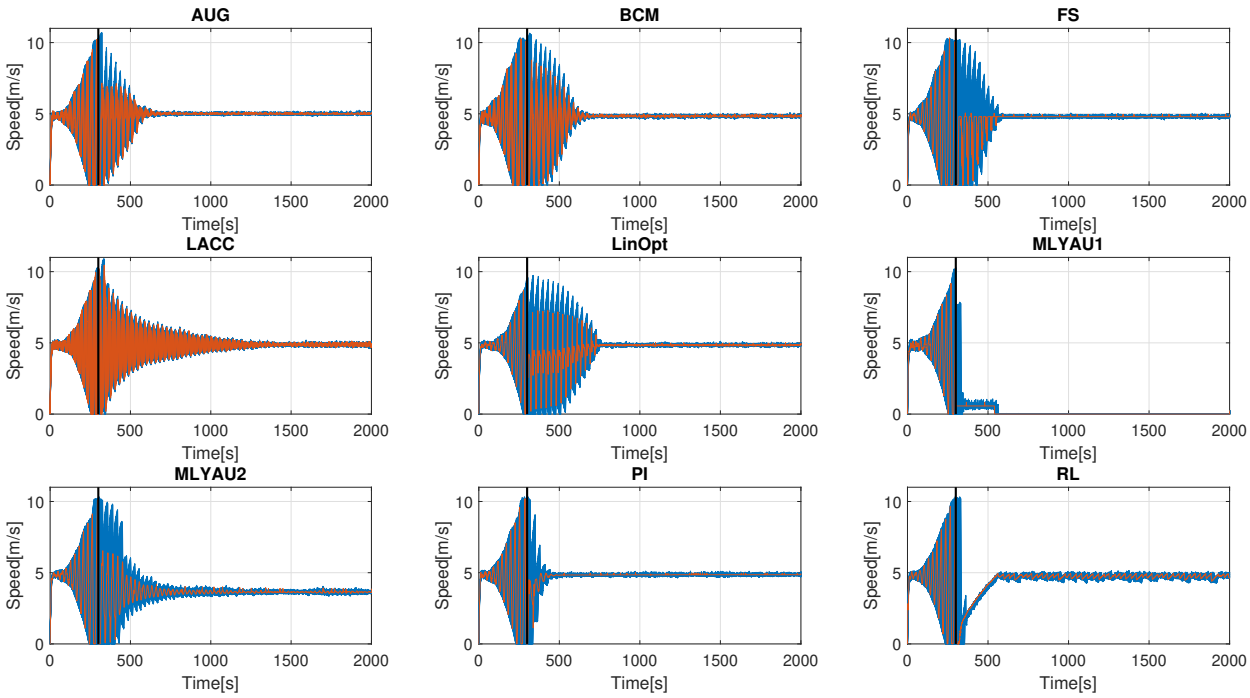

Figure 4.2: Speed profiles of the stabilized results; red: automated vehicle; blue: human driving vehicle; black: indication of beginning of AV control. For the results of AUG and BCM, four AVs are placed on the ring road. For the result of LACC, nine AVs are placed on the ring road. For the result of the rest of the AVs, only one AV is placed on the ring road.

By looking at the distance-gaps, we can observe that whether the traffic flow density on the ring road is uniform. We can observe that gaps between vehicles converge to a steady state when the traffic on the ring road is stable for all cases in figure 4.3. Most AV controllers have similar gap, except MLYAU1 and MLYAU2 where they have relative large distance-gaps. MLYAU1 gives the highest distance-gaps since the vehicles go to a complete stop a few seconds after being stable creating a huge gap between the AV and the HVs. The baseline values of VMT and fuel economy are 96.71[$miles$] and 13.43[mpg] when all the vehicles are HVs. In terms of VMT, all cases in the table perform better than the baseline, because the flow is smoother, except that MLYAU1 is basically blocking the traffic, as mentioned. Fuel economy for all cases are generally better than baseline as well, except MLYAU1.

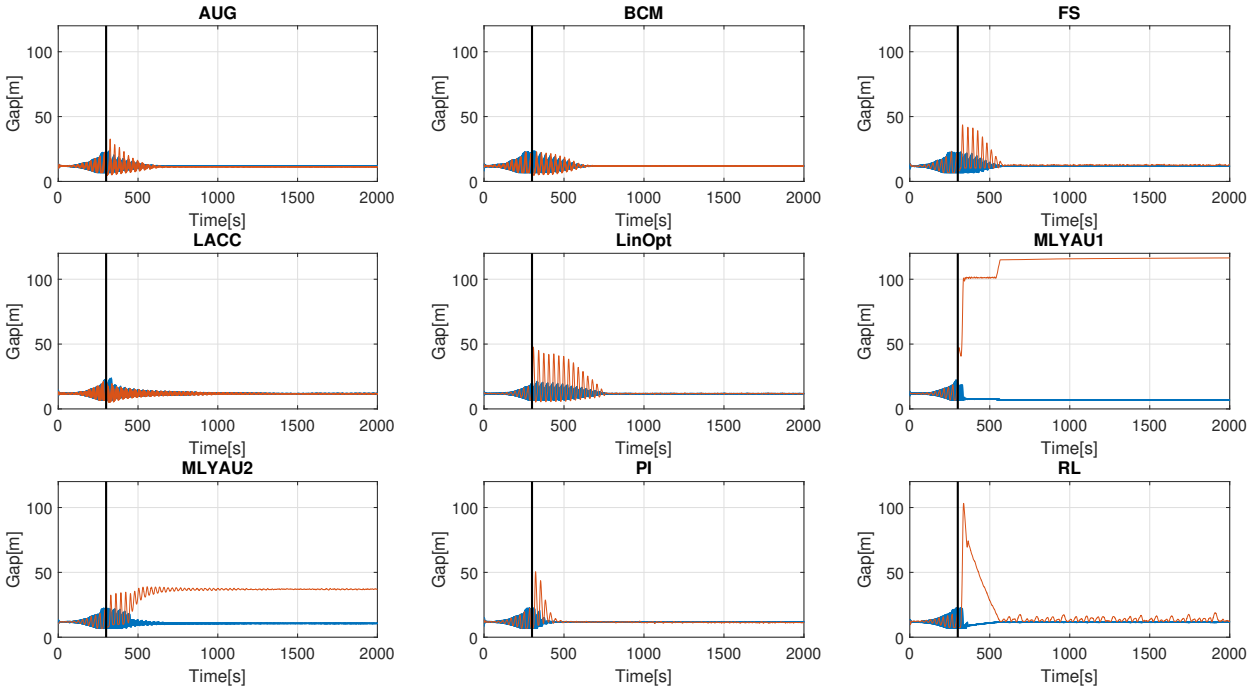

Figure 4.3: Gap profiles of the stabilized results;red: automated vehicle; blue: human driving vehicle; black: indication of beginning of AV control. For the results of AUG and BCM, four AVs are placed on the ring road. For the result of LACC, nine AVs are placed on the ring road. For the result of the rest of the AVs, only one AV is placed on the ring road.

Figure 4.4 further shows *time to stabilize*, *maximum final gap*, *VMT*, and *fuel economy* across different number of automated vehicle on the ring, respectively. Only the data point that the ring is being stabilized before the end of the simulation is shown. In the figure 4.4-(a), it can be observed that generally, the time need to be stable is shorter with more AVs on the ring, except PI. The PI eventually make the traffic into totally chaos when there are more than 8 AVs (˜36% penetration rate) on the ring. In figure 4.4-(b), we can also observe that the maximum distance-gap is also not much dependent on the number of AVs on the ring, but is relatively dependent on the AV types. To be noted, that the MLYAU1 has relatively large distance-gap because the controller basically stops all the traffic behind.

Figure 4.4-(c) shows the comparison of VMT and figure 4.4-(d) show the fuel economy, respectively. In terms of VMT, we can see that the AVs generally improves the VMT, except the FUZ, which is not stable, and the MLYAU1, which basically stops the traffic as we saw previously. The VMT are improved because the traffic flow are smoother than the baseline scenario. The VMT is generally positively related to the stability of ring road. The VMT are almost the same for AVs whose stabilizing time is almost the same for different penetration rates. For AVs that get more stable (shorter stabilizing time) with increasing penetration rate, the VMT is increasing with penetration rates, e.g. BCM, LACC, AUG. On the other hand, for the AV getting less stable at higher penetration rates, the VMT decreases, e.g.

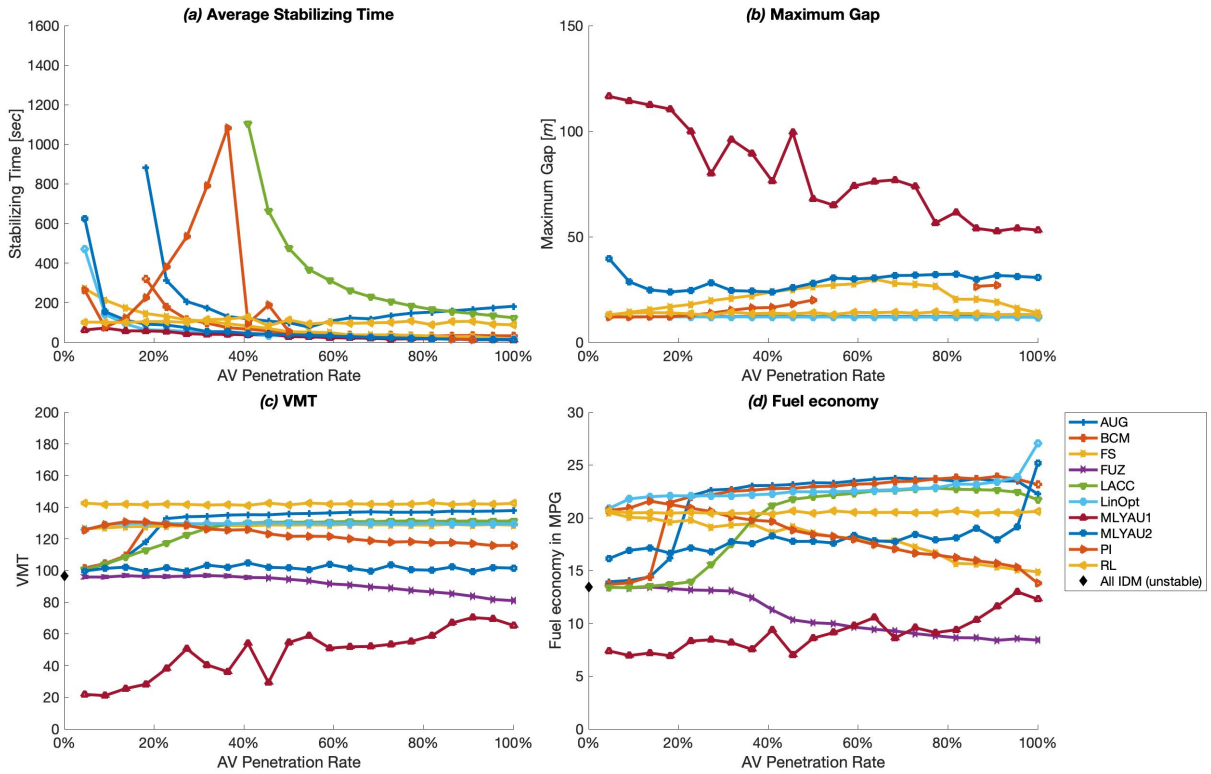

Figure 4.4: *(a)* Time to stabilize; *(b)* Maximum final gap; *(c)* VMT; *(d)* Fuel economy for the clustered case scenario. For (c) and (d), black dots are the baseline scenario values, where all vehicles are HVs.

PI. For fuel economy, we can observe that the fuel economy is improved for AVs with better stability. While most AVs have generally improved fuel economy than the baseline case, except some AVs, both FUZ and MLYAU1 have worse fuel economy, because they either make the traffic less stable or block the traffic. Fuel economy generally gets better with increase penetration rates. It is particularly significant for the AVs that are not stable at lower penetration rates, e.g. AUG, BCM, LACC. There are two exceptions that the fuel economy is getting worse at higher penetration rates: FS, and PI. For PI, as we have seen, the stability is getting worse at higher penetration rates; hence, the fuel economy is also getting worse at higher penetration rates. It is interesting to notice that the fuel economy of FS also gets worse even though the traffic flow is getting smoother. The possible reason is that FS is actually doing a lot of subtle acceleration and deceleration. This is because FS is essentially a speed controller, the process of converting speed command to acceleration introduces 'noise' into acceleration command, which causes higher fuel consumption.

4.5.4.2 Scenario II

Results of scenario II are presented in this section. Similar to the previous section, for scenario II, the corresponding values when the traffic on the ring is stable are presented in table 4.8. In this scenario, the penetration rate is only limited to about 9% to 50% of AV penetration in the system given that the placement of the AVs has to follow an even distribution (as shown in table 4.4).

Controller	Min no. of AVs to stabilize	Time to stabilize in *sec*	Max gap in *m*	VMT	Fuel economy in *mpg*
AUG	6	272.04	12.19	133.83	22.28
BCM	5	1516.9	12.29	127.06	19.32
FS	1	196.23	12.70	127.17	20.18
FUZ	*Unstable*	*N/A*	*N/A*	*N/A*	*N/A*
LACC	9	1213.55	12.13	129.98	21.05
LinOpt	1	120.50	12.12	128.99	21.82
MLYAU1	1	61.41	114.97	24.27	7.70
MLYAU2	1	151.23	36.87	101.13	16.82
PI	1	86.98	12.01	128.69	21.13
RL	1	241.03	14.52	138.69	19.70

Table 4.8: Average performance comparison of scenario II - Evenly Distributed

From table 4.8, we can easily see that the overall results appear to be similar in Scenario I with minimal changes in the values. Again, it failed to stabilize when the FUZ is used. It takes the most number of AVs for LACC to work while the number of AUG needs to be increased to six (6) from three (3) and the number of BCM needs to be increased to five (5) from three (3) in Scenario I for the system to be stable.

To further differentiate the controllers based on their performance at different penetration rates, results across different penetration rates also presented here is figure 4.5. Again, we can see the same trend as in the previous scenario if we look at figure 4.5-(a) where the time to stabilize for the ring generally decreases as AV penetration rate increases, except for PI where it is also could get unstable at high penetration rates. In figures 4.5-(b), we can restate our prior observations that the maximum gap is invariant with respect to the penetration rate except for the two Lyapunov-based controllers for the same reasons that are previously mentioned. In figure 4.5-(c) and 4.5-(d), the trends of VMT and fuel economy are also similar to the previous scenario.

4.5.4.3 Comparison across two scenarios

To further compare the influences of distributions of AVs, figure 4.6-figure 4.9 arrange the results in a different way. We overlay the results of different scenarios on top of each other scenario for different types of automated vehicles. Figure 4.6 shows the time to stabilize for

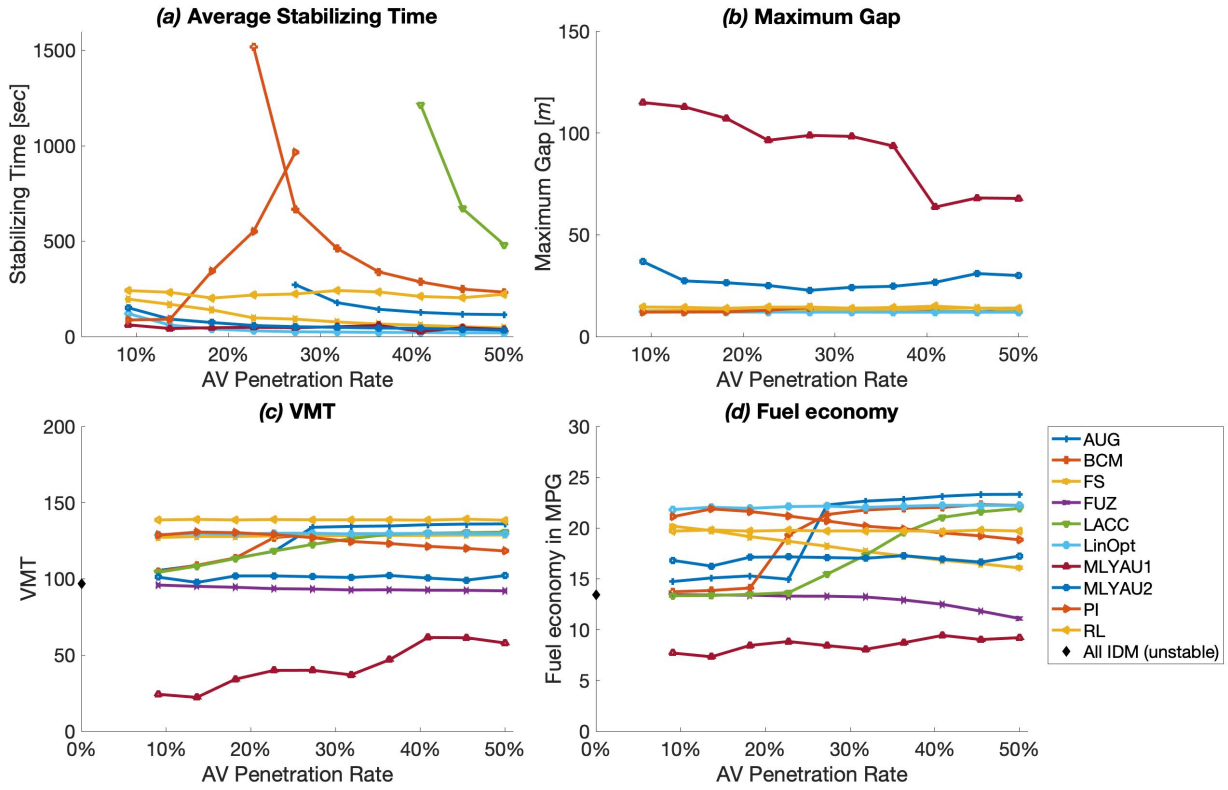

Figure 4.5: *(a)* Time to stabilize; *(b)* Maximum final gap; *(c)* VMT; *(d)* Fuel economy for the evenly distributed scenario. For (c) and (d), black dots are the baseline scenario values, where all vehicles are HVs.

each AV. For most of the AVs, time to stabilize is decreasing with increasing penetration rate, or kept the same. However, PI shows that as penetration rate increases, traffic becomes less stable. This may imply that the PI is more appropriate when AV penetration rate is low. For most of the AVs, It can be noted that variation of the stabilizing time is not significant across different AV distributions while it is more relevant to AV types and penetration rate. The BCM shows significant difference between two distributions. The performance of BCM is much better when they are clustered together than being separated.

Figure 4.7 shows maximum gap for each AV. Only the results of FS show that the maximum gap is a little shorter in the case of the evenly distributed scenario. There is no significant discrepancy for other type of AVs.

Figure 4.8 shows the VMT for each AV. VMT is also not sensitive to the variation of AV distributions. With the help of AVs smoothing traffic flow, the VMTs are significantly increased compared to the baseline case, except for FUZ and MLYAU1. FUZ results in slightly lower VMT because it was not able to stabilize the traffic flow under any penetration

rate. MLYAU1 stops the traffic so that the VMT is much smaller than the baseline. Figure 4.9 shows the fuel economy for each AV. For AVs, fuel economy does not show much change with the change in penetration rates and AV distributions.

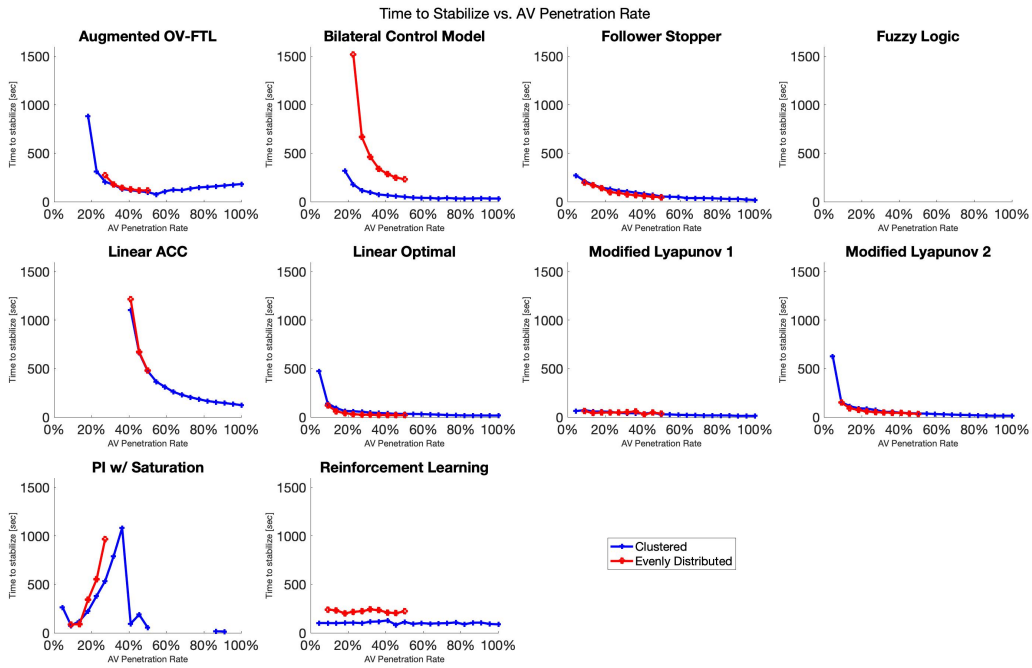

Figure 4.6: Time to stabilize the ring road for AV controllers under different penetration rates and different distributions.

4.6 Summary

In this chapter, automated vehicles dissipating stop and go waves on a ring road are studied under different distributions and penetration rates. To evaluate their performances, experiments are carried out in the state of the art simulation framework. Our findings are summarized as follows:

- Out of 10 automated vehicles, 6 automated vehicles models are able to stabilize the ring road traffic at penetration rate as low as 5 percent. They are FS, LinOpt, MLYAU1, MLYAU2, PI, and RL.
- Generally, *stabilizing time* is shorter if more AVs are placed in the traffic. However, for PI, the performance is degraded when more AVs are placed.

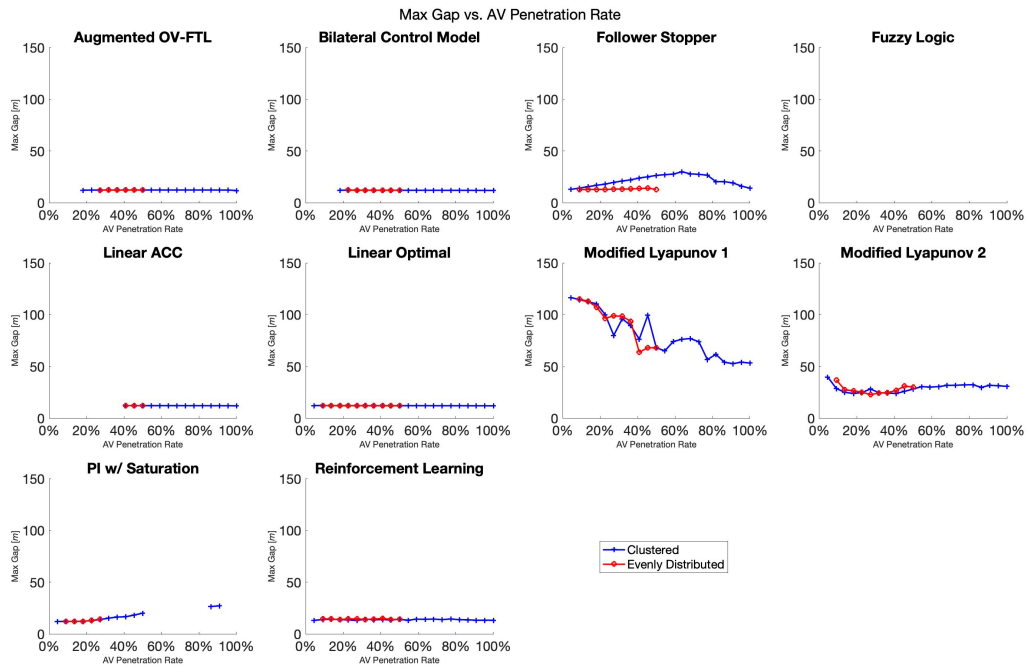

Figure 4.7: Maximum gap for AV controllers under different penetration rates and different distributions.

- The FUZ is the only controller that is not able to meet stability based on the set criterion but it is able to ensure that the traffic moves on the ring without encountering any vehicular crashes.

- RL controller shows the most consistent traffic improvement under all circumstances for all four metrics. It shows more than 40 percent VMT improvement while maintaining good fuel saving. MLYAU1 stabilizes the ring road with a trivial speed, where it almost stops all the vehicles in the system. For most of the AVs, the performance of the AVs are not much related to the way they are distributed among the traffic (except PI and BCM). No matter whether they are clustered (*i.e.,* platooned) or evenly distributed, performance of AVs is pretty much the same. However, this shall be treated with caveat. This might only be applicable when we treat control of AVs individually (*i.e.,* no cooperation/communication among them) as a recent study by Li *et al.*[44] mentions that the distribution of AVs may have a big impact when we consider the cooperation of multiple AVs.

- PI is one of the two controllers that shows some difference between two distributions. It is interesting to see that the performance of the PI is not as good as in the *clustered* case compared to being *evenly distributed*. When the PI is placed in the manner of

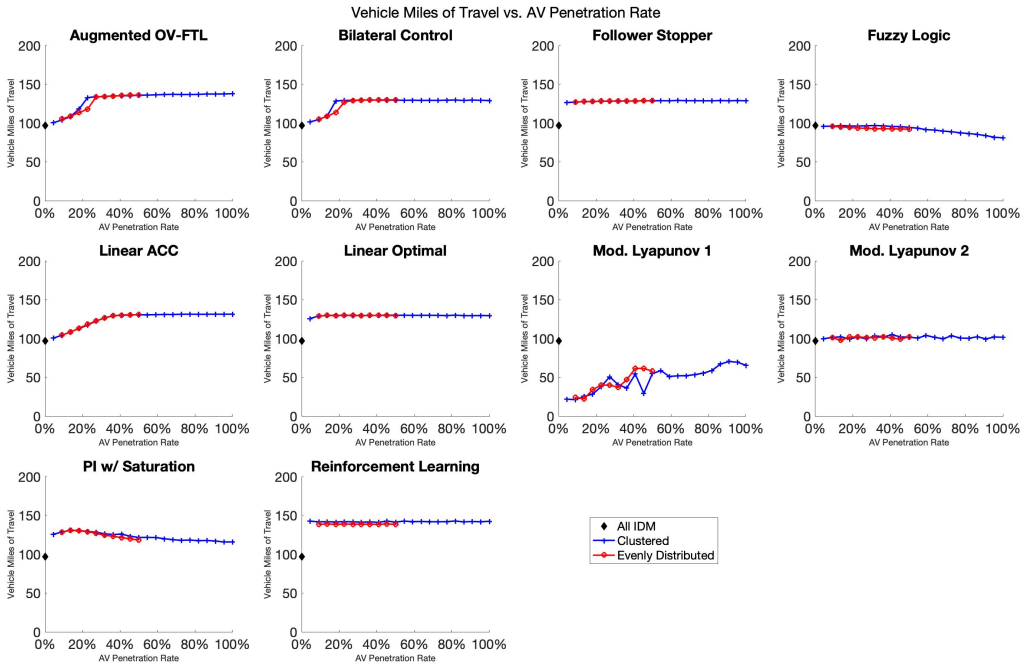

Figure 4.8: Vehicle Miles of Travel for AV controllers under different penetration rates and different distributions. The baseline VMT is 96.71.

scenario II, the performance of PI is degraded severely as multiple AVs are placed in the traffic.

- Another controller that shows quite different results for different distributions is BCM. The results of *time to stabilize* also show that it performs better under clustered scenario.

Compared to chapter 3, this chapter benchmarking controller numerically. Conditions shown in chapter 3 are conservative in the sense that they are under the assumption how human driving behavior is. Besides, the stability defined in chapter 3 is more restrictive than what we necessarily need. Other than converging to a unique equilibrium speed defined by the model, there are other possibilities of "stability" for traffic. For example, what we have seen for MLYPU1 is to slow down the traffic to a trivial steady state, although it is not desirable in reality. It is also interesting to notice that the learning based controller provides a quite different approach compared to other automated vehicle models. It firstly stops the traffic and then approaches the leading vehicle carefully to avoid inducing instability of the traffic. Another thing we learn from the simulation is that the more automated vehicles does not necessarily mean the traffic is better. The controller needs to be designed carefully so

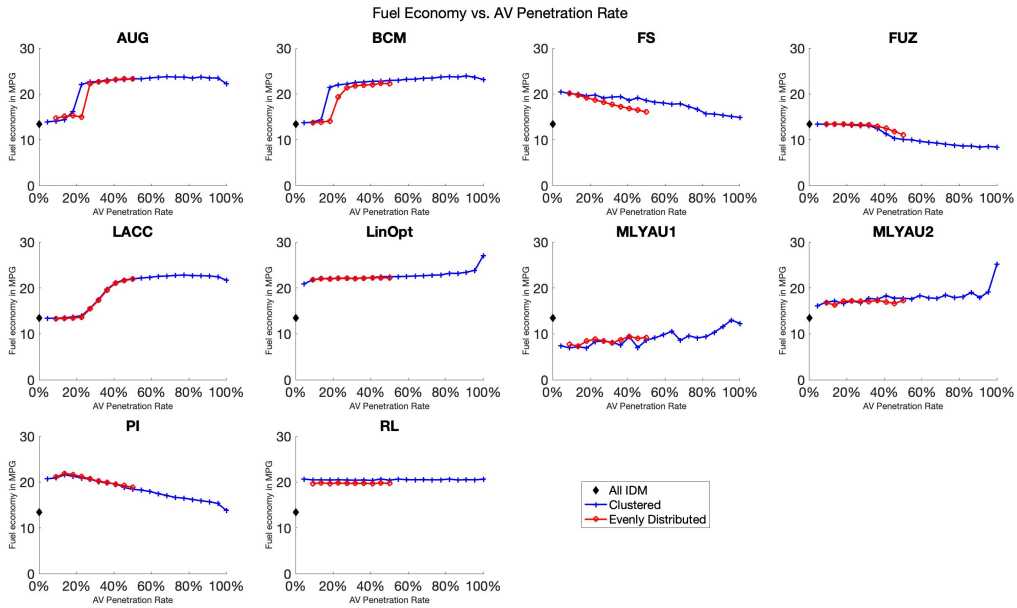

Figure 4.9: Fuel economy in MPG under different penetration rates and different distributions. The baseline fuel economy is 13.12 MPG.

that the impact to the traffic should not degrade as penetration rates increase and should ideally have a positive impact as penetration rate increases.

Chapter 5

Truck Longitudinal Dynamics and Control

In this chapter, we focus on design and implementation of longitudinal motion control for trucks. A model based longitudinal dynamics control is developed and implemented on a truck. The controller has a hierarchical structure, composed of an upper controller and a lower controller. The function of the lower controller is, for a given desired acceleration, to compute and execute commands for the engine and the service brake system. The performance of the controller relies on the accuracy of the parameters. Because the parameters may not be readily available, an adaptive parameter estimator is developed to adjust the parameters for the lower controller in real-time as new measurements are acquired. The upper controller is mainly composed of two control modes: cruise control and car following control. Depending on the driving conditions, the controller switched to one of the modes accordingly. Cruise control (CC) is a controller that regulates the vehicle speed to a reference speed. It is appropriate to use when the traffic flow is smooth, and the leading vehicle ahead is quite far away. For a given target speed, a reference speed trajectory is planned with a reference speed generator, which computes a speed trajectory from the current speed to the target speed while satisfying acceleration constraints and acceleration jerk constraints. The car following control (also known as Adaptive cruise control (ACC)) is a control that regulates the relative distance and relative speed with respect to the preceding vehicle. The goal of the car following controller is to regulate the difference between the time-headway and a given desired time headway. The proposed controller is implemented in simulation and on real trucks. Practically, vehicle to vehicle communication is essential to achieve string stability when leading vehicle speed is varying. Thus, we also incorporate V2V communication to access leading vehicle speed directly to achieve good car following performance while the leading vehicle speed is varying. Simulation results and experiment results are shown at the end to demonstrate the effectiveness of our design.

5.1 Overview

Cruise control and adaptive cruise control are two of most widely available advanced driver assistance systems, which could increase riding comfort and conveniences and potentially enhance safety and energy efficiency. They are also two fundamental systems for full automated vehicles.

Cruise control are widely available on many modern vehicles. It is a system that regulates the speed of the vehicle to a pre-set speed. It could reduce driving fatigue and riding comfort for long drives. However, it is less useful when traffic density is high, because it does not actively respond to the leading vehicles.

Adaptive cruise control is a system that can automatically respond to a leading vehicle ahead. An ACC system can measure relative speed and relative distance to the leading vehicle with on-board sensors, like radar, lidar, or vision sensor; and use these measurements to execute throttle and brake command in order to achieve steady car following behind the leading vehicle. Since the introduction of the first generation to the market about two decades ago, many researches with regard to their impacts on transportation and environment have been done, and much efforts have been placed to improve the performance in terms of safety, traffic efficiency, and energy economy. Some of the perspectives will be discussed below. Reviews of the development of ACC can be found in [108][31].

Spacing policy which governs the separation between the leading vehicle and the subject vehicle is critical for model-based ACC design. A variety of gap policies are available in the existing literature, where the constant distance-headway policy and constant time-headway policy are two of the most basic spacing policies. Constant distance-headway policy can maximally increase capacity of the highway because of the short following distance between vehicles. However, it is less desirable on public highways, since it requires extremely high precision control, and it is less theoretically more sensitive to speed variations of downstream vehicles. On the other hand, although maximum capacity of the time-headway policy would be limited because the desired following distance is proportional to driving speed, it is generally preferable since it is theoretically less sensitive to downstream traffic perturbation. It can be shown that controllers of constant-time headway policy with appropriate controller design could attenuate disturbance coming from downstream, while constant-distance headway could not [72]. Besides, time-headway policy is closer to human driving behavior, which would make it more acceptable for human drivers and passengers.

Sting stability is a critical property for car following controller. It characterizes whether a string of car following controller attenuates or amplifies disturbances upstream [88]. Considering both lags of system dynamics and sensor delays, ACC string stability may not be achievable [52] [72][109]. It has been shown that string stability is not achievable when desired time-headway is too short [72][109]. String stability can be achieved with appropriate controller design, for example, Liang *et al.* developed a LQR based control [46]. In this work, we formulate the string stability requirement as a robust control problem. String stability can be improved with vehicle to vehicle communication [60] [69]. In this work, we use also vehicle to vehicle communication to improve the car following control of the truck.

While majority of research and development focuses are on passenger cars and lots of the experiences can be carried over to trucks, inherent differences between trucks and passenger cars poses special opportunities and challenges for automated trucks [83] [2]. A few related works are summarized below. Yanakiev *et al.* [114] proposed adaptive methods for speed tracking and vehicle following controller design. In the vehicle following controller design, because of the nature of lower power-to-weight ratio, heavy duty vehicle needs to have larger car following space than passenger vehicles to maintain string stability. However, larger following space reduce the traffic throughput. To deal with this, wireless communication of leader vehicle speed to all the following vehicle in the platoon is proposed. With this extra information of platoon leader, follower vehicles in the platoon are able to follow with a shorter distance while maintain string stability. Lu *et al.* [50] developed a constant distance following for heavy duty truck with model based approach. Detailed physical model of a truck is used for controller design. In this work, we also consider model based approach for controller design.

One of main challenges of model based approach is that the performance of the controller is reliant on the physical parameters. Huang *et al.* [36] proposed an online estimator to estimate payload of a lightweight electric vehicle. Bae *et al.* [4] rearranged vehicle longitudinal dynamics and estimated vehicle parameters with measurements of vehicle speed, acceleration and road grade. In this work, we implement a similar approach which estimates lumped vehicle parameters which then are used for the lower controller.

Main contributions in this chapter include: (1) a parameter estimator is used to estimate parameters for lower controller, so that the controller is not reliant on unknown physical parameters; (2) an analytical string stable car-following control is designed considering model uncertainties; (3) a vehicle-to-vehicle communication is used to enhance the car following performance. The design is implemented and validated in the real world on trucks.

5.2 Longitudinal Vehicle Dynamics

Longitudinal vehicle dynamics is illustrated in figure 5.1. Let $F_x(t)$ be the traction force along the longitudinal direction; $F_{\text{aero}}(t)$ represent the aero drag force; and $F_r(t)$ represent total rolling resistance. Define $m \in \mathbb{R}$ be the vehicle mass and $g \in \mathbb{R}$ be the gravity constant. θ is the road grade and $V_x : [0, \infty) \to \mathbb{R}$ is vehicle longitudinal speed. Newtons second law, we can obtain following equation:

$$m\dot{V}_x(t) = F_x(t) - F_{\text{aero}}(t) - F_r(t) - mg\sin\theta(t), \tag{5.1}$$

The aero drag force $F_{\text{aero}}(t)$ is modeled as a function of the longitudinal vehicle speed:

$$F_{\text{aero}}(t) = \frac{1}{2}\rho_d C_d A_F (V_x(t) + V_{wind}(t))^2, \tag{5.2}$$

where $\rho_d \in \mathbb{R}$ denotes air density, $C_d \in \mathbb{R}$ denotes aero dynamics drag coefficient, $A_F \in \mathbb{R}$ is the effective frontal area, and $V_{wind} : [0, \infty) \to \mathbb{R}$ is the headwind speed. Let $F_r(t)$ represent

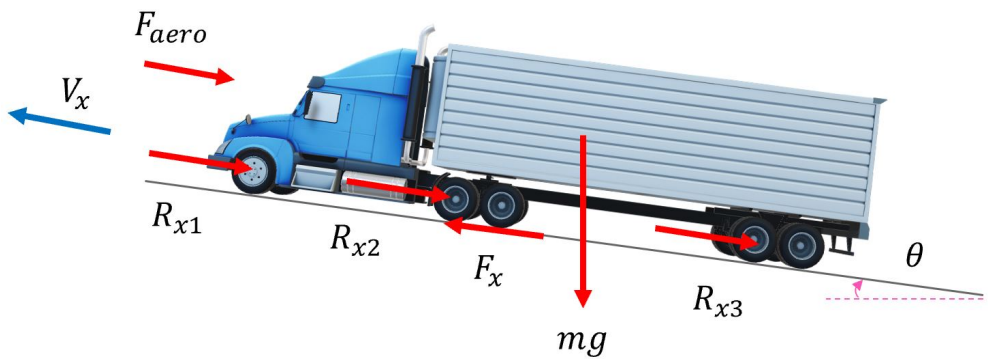

Figure 5.1: Longitudinal vehicle dynamics. $F_x(t)$ is the traction force along the longitudinal direction. $F_{\text{aero}}(t)$ represents the aero drag force. $R_{x1}(t)$, $R_{x2}(t)$, and $R_{x3}(t)$ are rolling resistances at wheels; for simplicity, only forces at three wheels are sketched here. m is vehicle mass and mg is gravity force. $\theta(t)$ is the slope angle and $V_x(t)$ is the vehicle speed along longitudinal direction.

overall effect of the rolling resistances, i.e. $F_r(t) = R_{x1}(t) + R_{x2}(t) + R_{x3}(t)$. The rolling resistances $R_{x1} : [0, \infty) \to \mathbb{R}$, $R_{x2} : [0, \infty) \to \mathbb{R}$, $R_{x3} : [0, \infty) \to \mathbb{R}$ are acting on each wheel an these forces are due to the distortions of the tires. The rolling resistance is proportional to the normal force at the tire. Therefore, total rolling resistance can be written as follow:

$$F_r(t) = C_r mg \cos\theta(t), \tag{5.3}$$

where $C_r \in \mathbb{R}$ is the rolling resistance coefficient, which is related to the property of the tire and the road condition. Ideally, if the traction force $F_x(t)$ can be controlled directly, the control of the vehicle sped and acceleration can be very easy and straight forward. However, in practice, the traction force can only be indirectly controlled by either applying appropriate engine torque, engine brake or the service brake. In order to execute appropriate engine torque command, engine brake command or service brake command, a model of powertrain is briefly reviewed.

Powertrain

A diagram of a typical automatic transmission powertrain is illustrated in figure 5.2. The

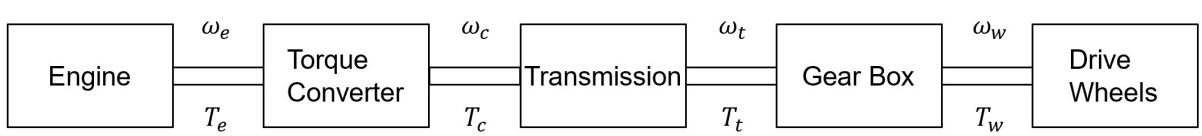

Figure 5.2: Powertrain configuration. A typical automatic transmission powertrain consists of an engine, a torque converter, a transmission, a gearbox, and a drive wheels.

main components considered here include: engine, torque converter, transmission, gearbox, and drive wheels, which will be introduced in sequence below. These components are linked mechanically by shafts. Their rotational speeds and their torques are $\omega_e : [0, \infty) \to \mathbb{R}$, $\omega_c : [0, \infty) \to \mathbb{R}$, $\omega_t : [0, \infty) \to \mathbb{R}$, $\omega_w : [0, \infty) \to \mathbb{R}$, $T_e : [0, \infty) \to \mathbb{R}$, $T_c : [0, \infty) \to \mathbb{R}$, $T_t : [0, \infty) \to \mathbb{R}$, and $T_w : [0, \infty) \to \mathbb{R}$, respectively. There are mainly three modes for trucks longitudinal controls.

Engine Driving

During acceleration, the engine generates power to pull the truck. Dynamics of an engine is sophisticated. Detailed engine model and intricate controller design [14] are needed to control engine torque. Fortunately, typically, there is a dedicated engine control system on vehicles, which allows us to execute torque command conveniently. Therefore, we can assume that the engine torque $T_e(t)$ can be controlled directly. The output shaft of the engine is connected to the input shaft of the torque converter. The torque converter is a component that allows speed mismatch between engine and the rest of the components in the powetrain. The input shaft and the output shaft of the torque converter are softly coupled with working fluid at lower vehicle speed to avoid engine being stalled, and they can be mechanically coupled at higher vehicle speed to increase fuel efficiency. At low speed, torques of input shaft and output shaft can be approximated as static functions of input shaft speed and output shaft speed; and at high speed, the torque converter is simply modeled as a shaft, where input torque $T_e(t)$ is equivalent to output torque $T_c(t)$ [1][41]. The control scenario in this work is mainly considered at higher speed. Therefore, we assume that the speed and torque of both the input shaft and the output shaft are the same:

$$\omega_e(t) = \omega_c(t), \tag{5.4}$$

$$T_e(t) = T_c(t). \tag{5.5}$$

The output shaft of the torque converter is linked to the transmission. The transmission is a component composed of several gears and gear trains to convert power from the engine side to the drive wheel side at different speeds. Larger gear ratio is used at lower vehicle speed to provide larger traction force at the drive wheels. At higher vehicle speed, lower gear ratio is used to match the engine speed and the vehicle speed. The gear ratios of the transmission are discrete at different gear numbers. Let $r_{\mathrm{G1},i} \in \mathbb{R}_{\geq 0}$ be the gear ratio at gear i. At gear i, the rotational speeds and the torque of the shaft on both ends of of the transmission are described as follows:

$$\omega_c(t) = \omega_t(t)/r_{\mathrm{G1},i}, \tag{5.6}$$

$$T_c(t) = T_t(t) r_{\mathrm{G1},i}. \tag{5.7}$$

The output shaft of the transmission is connected to the input shaft of the final gearbox with a fixed gear ratio $r_{\mathrm{G2}} \in \mathbb{R}_{>0}$. Assume the rotational inertia of the shaft between the transmission and the final gearbox is $I_t \in \mathbb{R}_{>0}$, the dynamic equation of the shaft can be written as follows:

$$I_t \dot{\omega}_t(t) = T_t(t) - r_{\mathrm{G2}} T_w(t). \tag{5.8}$$

The rotational speed of the shaft is proportional to the wheel speed ω_w:

$$r_{\mathrm{G2}}\omega_t(t) = \omega_w(t). \tag{5.9}$$

Finally, the wheel dynamics is modeled:

$$I_w\dot{\omega}_w(t) = T_w(t) - F_x(t)r_{\mathrm{eff}}, \tag{5.10}$$

where $I_w \in \mathbb{R}_{>0}$ denotes the moment of the inertia of the wheel, $r_{\mathrm{eff}} \in \mathbb{R}_{>0}$ denotes the effective wheel radius. Wheel traction force is a function of wheel slip ratio σ_x. Under normal driving, wheel slip ratio is small, wheel traction force is approximately linear with respect to wheel slip ratio:

$$F_x(t) = C_\sigma\sigma_x(t), \tag{5.11}$$

where $C_\sigma \in \mathbb{R}$ is called longitudinal tire stiffness parameters and wheel slip ratio σ_x is defined as:

$$\sigma_x(t) = \begin{cases} \frac{r_{\mathrm{eff}}\omega_w(t)-V_x(t)}{V_x(t)}, & V_x(t) > r_{\mathrm{eff}}\omega_w(t) \\ \frac{r_{\mathrm{eff}}\omega_w(t)-V_x(t)}{r_{\mathrm{eff}}\omega_w(t)}, & r_{\mathrm{eff}}\omega_w(t) \geq V_x(t) \end{cases}.$$

Engine Braking

In addition to acceleration, an engine can also generate moderate negative torque to decelerate the truck. When the engine braking is applied, similar formulation discussed above can be used to describe relation between the engine braking torque and the traction force. The engine braking torque can also be controlled directly by sending command to engine controller with $T_e(t) < 0$. When braking force is needed, using the engine braking appropriately can help save wear on service brakes. However, it is not able to fully stop the truck. Service brakes are still needed to stop the truck.

Service Brake System

Service brake system is another component that can apply braking force. It can generate more powerful braking force and can full stop trucks. Unlike engine braking, the service brake system is a component that can apply braking force directly at wheels. That is, during brake, the wheel torque is:

$$T_w(t) = T_{brake}(t),$$

where $T_{brake} : [0, \infty) \to \mathbb{R}$ is the service brake braking torque. However, in practice, T_{brake} is not able to controlled directly, because of the design of the brake system. Fortunately, the brake system of the truck we are using is calibrated so that we can control deceleration command directly. Therefore, we do not control T_{brake}, instead, we can control deceleration directly when service brakes are needed.

5.3 Hierarchical Controller Overview

A hierarchical controller is considered in this work. A diagram of the hierarchical controller is illustrated in figure 5.3. In the scheme of the hierarchical controller, there is an upper controller and a lower controller. For a given control object, the upper controller computes a desired acceleration command as an input to the lower controller. The lower controller is designed to interface with mechanical actuators in order to follow the desired acceleration or the desired speed from upper controller. The benefit of the hierarchical control is that the controller design of the controller can be simplified. Particularly, the design of the upper controller can focus only on the kinematics of the subject vehicle and/or the other vehicles without considering nonlinearity in the powertrain. In addition, the modularity allows us to replace upper controllers easily for different control purposes.

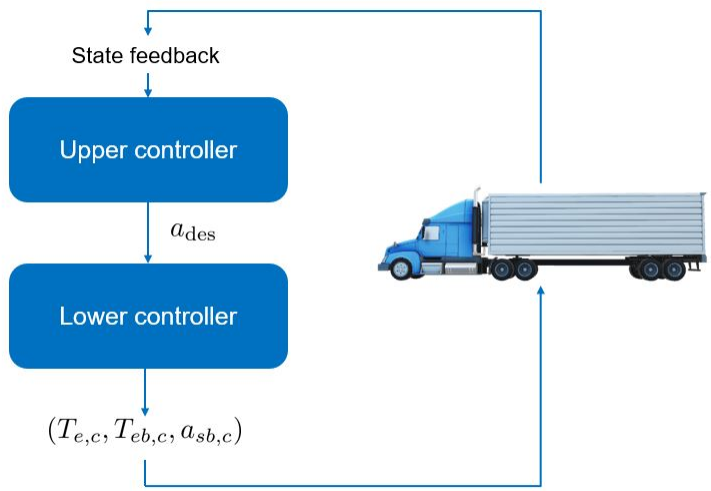

Figure 5.3: Schematic of hierarchical controller. The upper controller computes the desired acceleration a_{des} with state feedback. The lower controller computes the engine driving torque command $T_{e,c}$, the engine braking torque command $T_{eb,c}$ and the service braking command $a_{sb,c}$ for the desired acceleration.

In this work, acceleration control is considered. Given the desired acceleration, the lower controller determines the engine driving torque value, the engine braking torque value, and the service brake value to achieve the desired acceleration. To control these components to attain desired acceleration, a lower controller is derived based on physical principle of components in the powertrain.

5.4 Lower Controller

The lower controller is a controller that executes engine driving torque command $T_{e,c}$, engine braking torque command $T_{eb,c}$, and service brake command $a_{sb,c}$ in order to control the truck

to track the desired acceleration from the upper controller. A model based lower controller is developed, which is composed of formulations derived based on the longitudinal vehicle dynamics model and the powertrain model shown above.

We first derive the formulation for engine driving torque command. We assume wheel slip ratio is small, $\sigma_x << 1$, which is generally true under normal driving condition. Based on (5.1)-(5.10), acceleration of the vehicle for given engine torque can be computed:

$$\dot{V}_x(t) = \frac{r_{\text{eff}} r_{\text{G1},i} r_{\text{G2}} T_e(t) - r_{\text{eff}}^2 r_{\text{G1},i}^2 r_{\text{G2}}^2 F_{\text{aero}}(t) - r_{\text{eff}}^2 r_{\text{G1},i}^2 r_{\text{G2}}^2 F_r(t) - r_{\text{eff}}^2 r_{\text{G1},i}^2 r_{\text{G2}}^2 mg \sin\theta(t)}{m r_{\text{eff}}^2 r_{\text{G1},i}^2 r_{\text{G2}}^2 + I_t r_{\text{G1},i}^2 + I_w r_{\text{G1},i}^2 r_{\text{G2}}^2}. \tag{5.12}$$

We can use this to derive the engine torque command for desired acceleration. Let engine torque command $T_{e,c}$ be

$$\begin{aligned} T_{e,c}(t) :=& \frac{m r_{\text{eff}}^2 r_{\text{G1},i}^2 r_{\text{G2}}^2 + I_t r_{\text{G1},i}^2 + I_w r_{\text{G1},i}^2 r_{\text{G2}}^2}{r_{\text{eff}} r_{G_1,i} r_{\text{G2}}} a_{\text{des}(t)} + r_{\text{eff}} r_{\text{G1},i} r_{\text{G2}} F_{\text{aero}}(t) \\ &+ r_{\text{eff}} r_{\text{G1},i} r_{\text{G2}} F_r(t) + r_{\text{eff}} r_{\text{G1},i} r_{\text{G2}} mg \sin\theta(t). \end{aligned} \tag{5.13}$$

Let $T_e(t) = T_{e,c}(t)$, acceleration of the vehicle (5.12) then becomes

$$\dot{V}_x(t) = a_{\text{des}}(t).$$

Therefore, for a desired a_{des}, we can use (5.13) to compute the corresponding engine torque command. When the desired acceleration is positive, then the engine driving mode is activated while the other commands are off. On the other hand, if the desired acceleration is negative, the engine would switch to engine brake mode, which would decelerate the truck. The engine braking torque can also be computed using (5.13). The engine brake can only provide mild braking force. When greater braking force is needed, the service brake system is needed. For the service brake command, as mentioned above, thanks to the embedded controller for the service brake system, we can control desired deceleration command $a_{sb,c}$ directly. By aggregating the commands for the engine and the service brake system, we can formally write the lower controller as follows:

$$(T_{e,c}(t), T_{eb,c}(t), a_{sb,c}(t)) = \begin{cases} (f_e^{(i)}(a_{\text{des}}(t), V_x(t), \theta(t)), 0, 0) & \text{if } a_{\text{des}}(t) > 0 \\ (0, f_e^{(i)}(a_{\text{des}}(t), V_x(t), \theta(t)), 0) & \text{if } 0 \geq a_{\text{des}}(t) > a_{eb,max} \\ (0, f_e^{(i)}(a_{eb,max}, V_x(t), \theta(t)), a_{\text{des}}(t) - a_{eb,max}) & \text{if } a_{eb,max} \geq a_{\text{des}}(t) \end{cases}, \tag{5.14}$$

where $e_{eb,max}$ is the maximum acceleration that can be achieved with engine brake only, which can be determined based on experiments. $f_e^{(i)}$ is derived based on (5.13) for transmission gear number i. We neglect wind speed and assume that the road grade is small ($\theta << 1 \rightarrow \cos\theta \approx 1$). Thus,

$$\begin{aligned} F_{\text{aero}}(t) &\approx \frac{1}{2} \rho_d C_d A_f r_{\text{eff}} r_{\text{G1},i} r_{\text{G2}} V_x(t)^2, \\ F_r &\approx mgC_r, \end{aligned}$$

and $f_e^{(i)}$ is:

$$\begin{aligned} f_e^{(i)}(a_{\text{des}}(t), V_x(t), \theta(t)) &= \frac{(m r_{\text{eff}}^2 r_{\text{G1},i}^2 r_{\text{G2}}^2 + I_t {r_{\text{G1},i}}^2 + I_w {r_{\text{G1},i}}^2 r_{\text{G2}}^2)}{r_{\text{eff}} r_{\text{G1},i} r_{\text{G2}}} a_{\text{des}}(t) \\ &+ \frac{1}{2}\rho_d C_d A_f r_{\text{eff}} r_{\text{G1},i} r_{\text{G2}} V_x(t)^2 + mgC_r r_{\text{eff}} r_{\text{G1},i} r_{\text{G2}} + mg\sin\theta(t) r_{\text{eff}} r_{\text{G1},i} r_{\text{G2}}. \end{aligned} \tag{5.15}$$

The implementation of the model based lower controller design requires accurate parameters, for example, rotational shaft inertia, drag coefficient, etc. These parameters may be attained based on design specification. However, because of engineering tolerance, the physical parameters of each component may not be guaranteed. These parameters are generally unknown. To deal with unknown parameters, we present an approach reformulating (5.12) as a parametric model with fewer unknown parameters and estimating these unknown parameters using real world driving data.

5.4.1 Parametric Model

Suppose vehicle mass is large and the mass term dominates the denominator of (5.12). Let $a(t) := \dot{V}_x(t)$. We can reformulate it (5.12) as follows:

$$T_e(t) = \beta_1 r_{\text{eff}} r_{\text{G1},i} r_{\text{G2}}(a(t) + g\sin\theta(t)) + \beta_2 r_{\text{eff}} r_{\text{G1},i} r_{\text{G2}} V_x(t)^2 + \beta_3 r_{\text{eff}} r_{\text{G1},i} r_{\text{G2}}, \tag{5.16}$$

where

$$\begin{aligned} \beta_1 &\approx m, \\ \beta_2 &= \frac{1}{2}\rho_d C_d A_f, \\ \beta_3 &= mgC_r. \end{aligned}$$

In (5.16), generally unknown parameters are collectively represented by β_1, β_2, and β_3, which we want to estimate using field test data. The other parameters are either given or can be measured easily. Wheel radiusr_{eff} can be measured directly. Suppose the measurement of the engine speed, the transmission shaft speed and the wheel speed are available. Estimation of gear ratios r_{G1} and r_{G2} can be done with (5.6) and (5.9). We assume T_e, a, θ, and V_x are variables that can be measured with on-board sensors and recorded with a on-board computer. With field test data, we can fit the model by solving a least square error minimization problem:

$$[\hat{\beta}_1, \hat{\beta}_2, \hat{\beta}_3]^T = \arg\min_{\beta} \|X\beta - Y\|_2^2.$$

$X \in \mathbb{R}^{N\times 3}$ and $Y \in \mathbb{R}^N$ are matrices that aggregates the N driving data points according to the model (5.16) such that each row of X is

$$X = [(a(t) + g\sin\theta(t)) r_{\text{eff}} r_{\text{G1},i} r_{\text{G2}}, \quad V_x(t)^2 r_{\text{eff}} r_{\text{G1},i} r_{\text{G2}}, \quad r_{\text{eff}} r_{\text{G1},i} r_{\text{G2}}],$$

and each entry of Y is $T_e(t)$.

With estimated parameters $\hat{\beta}_1, \hat{\beta}_2, \hat{\beta}_3$, we can reformulate $f_e^{(i)}$ for lower level controller as follows:

$$f_e^{(i)}(a_{\text{des}}(t), V_x(t)) = \hat{\beta}_1 r_{\text{eff}} r_{\text{G1},i} r_{\text{G2}}(a_{\text{des}}(t) + g\sin\theta(t)) + \hat{\beta}_2 r_{\text{eff}} r_{\text{G1},i} r_{\text{G2}} V_x(t)^2 + \hat{\beta}_3 r_{\text{eff}} r_{\text{G1},i} r_{\text{G2}}.$$

5.4.2 Lower Controller with Adaptive Parameter Estimator

The above offline approach is sufficient for models with time invariant parameters. However, in practice, vehicle parameters may change from time to time. For example, the weight may change every time because different payload is being carried; the aero drag coefficient may change because of the weather; and the friction may change because of the mechanical wear. The controller performance is expected to be improved if the parameters can be fine tuned in real time with new measurements. An adaptive parameter estimator is used to update parameters for the lower controller. Let $\beta_1^{(i)} = \beta_1 r_{\text{eff}} r_{\text{G1},i} r_{\text{G2}}$, $\beta_2^{(i)} = \beta_2 r_{\text{eff}} r_{\text{G1},i} r_{\text{G2}}$, and $\beta_3^{(i)} = \beta_3 r_{\text{eff}} r_{\text{G1},i} r_{\text{G2}}$. We can rewrite (5.16) as follows:

$$Z = \phi^T \Theta^{(i)},$$

where $Z = T_e$, $\Theta^{(i)} = [\beta_1^{(i)}, \beta_2^{(i)}, \beta_3^{(i)}]^T$, $\phi = [a + g\sin\theta, V_x^2, 1]^T$. Let $\hat{\Theta}^{(i)}(:= [\hat{\beta}_1^{(i)}, \hat{\beta}_2^{(i)}, \hat{\beta}_3^{(i)}]^T)$ represent the estimation of the $\Theta^{(i)}$. A general discrete adaptive parameter estimator is used to estimate unknown parameters online [38, Chapter 4]:

$$\begin{aligned} \hat{\Theta}[k+1] &= \hat{\Theta}[k] + \alpha\epsilon[k]\phi[k], \\ \epsilon[k] &= \frac{Z[k] - \phi[k]^T\hat{\Theta}[k]}{c + \phi[k]^T\phi[k]}, \end{aligned} \tag{5.17}$$

where $k \in \mathbb{Z}_{\geq 0}$ is a discrete time step; $\alpha \in \mathbb{R}$, $c \in \mathbb{R}$ are parameters. The controller $f_e^{(i)}$ can then be rewrite as:

$$f_e^{(i)}(a_{\text{des}}(t), V_x(t), \theta(t)) = \hat{\beta}_1^{(i)}(a_{\text{des}} + g\sin\theta(t)) + \hat{\beta}_2^{(i)} V_x(t)^2 + \hat{\beta}_3^{(i)}. \tag{5.18}$$

5.4.2.1 Adaptive Lower Controller without Road Grade Measurement

So far, we have assumed the measurement of $\theta(t)$ is available. However, road grade measurement may not be available on all vehicles. Suppose the measurement of $\theta(t)$ is not unavailable, we can see $g\sin\theta(t)$ term of the model (5.12) as a slow varying disturbance and rewrite the model in a way that the $g\sin\theta(t)$ term is absorbed into the third term of the parametric model. More precisely, the model (5.12) is reformulated as follows:

$$T_e(t) = \gamma_1^{(i)} a(t) + \gamma_2^{(i)} V_x(t)^2 + \gamma_3^{(i)}, \tag{5.19}$$

where

$$\gamma_1^{(i)} = \frac{(mr_{\text{eff}}^2 r_{\text{G1},i}^2 r_{\text{G2}}^2 + I_t r_{\text{G1},i}^2 + I_w r_{\text{G1},i}^2 r_{\text{G2}}^2)}{r_{\text{eff}} r_{\text{G1},i} r_{\text{G2}}},$$
$$\gamma_2^{(i)} = \frac{1}{2}\rho_d C_d A_f r_{\text{eff}} r_{\text{G1},i} r_{\text{G2}},$$
$$\gamma_3^{(i)} = (mgC_r + mg\sin\theta) r_{\text{eff}} r_{\text{G1},i} r_{\text{G2}}.$$

We can also use the same adaptive law (5.17) shown in the section 5.4.2 to estimate $\gamma_1^{(i)}$, $\gamma_2^{(i)}$, and $\gamma_3^{(i)}$ with $\phi = [a, V_x^2, 1]^T$ and $\hat{\Theta}^{(i)} = [\hat{\gamma}_1^{(i)}, \hat{\gamma}_2^{(i)}, \hat{\gamma}_3^{(i)}]^T$. Presumably, the $\gamma_3^{(i)}$ term should be able to adapt to the change of the road grade. The lower controller with $\hat{\gamma}_1^{(i)}$, $\hat{\gamma}_2^{(i)}$, and $\hat{\gamma}_3^{(i)}$ is:

$$f_e^{(i)}(a_{\text{des}}(t), V_x(t)) = \hat{\gamma}_1^{(i)} a_{\text{des}}(t) + \hat{\gamma}_2^{(i)} V_x(t)^2 + \hat{\gamma}_3^{(i)}. \tag{5.20}$$

5.4.3 Simulation Validation

To validate the controller, we build the controller in the Simulink and test the performances with TruckSim, a high fidelity truck dynamics simulation software. For the purpose of validating the lower controller with parameter estimator, a speed tracking control is selected for the upper controller, where the desired acceleration is computed as following formula:

$$a_{\text{des}}(t) = K(v_{ref} - V_x(t)), \tag{5.21}$$

where $K \in \mathbb{R}_{>0}$ is the control parameter and $v_{ref} \in \mathbb{R}_{>0}$ is the reference speed.

The lower controller we are testing is the adaptive lower controller without road grade measurement. Particularly, adaptive law (5.17) is implemented to estimate parameters of the parametric model (5.19), and the estimated parameters are used with (5.20) and (5.14) to compute the engine commands and service brake commands. To benchmark the performance, the lower controller based on physical models (5.15) is also implemented and tested. We first test the lower controller based on physical models (5.15) with $v_{ref} = 20$ $[m/s]$ and $k = 1$ for the upper controller (5.21). Figure 5.4 shows the results of the physical model based lower controller. The lower controller with correct parameters of the truck models enables the speed of the truck eventually track the reference speed. In practice, correct parameters may not be available. To simulate this, we artificially distort the parameters used in the controller and repeat the test. The simulation results is shown in figure 5.5. The speed of the truck cannot track the reference speed, because of the mismatched parameters. The results emphasize how sensitive the controller is to the parameters and the need to deal with it. We then tested the proposed adaptive lower controller. The adaptive lower controller does not need physical parameters and should be able to find the suitable parameters that matches the vehicle dynamics. The testing result is shown in figure 5.6. The controller enables the truck successfully tracking the reference speed and its performance is as well as the physical based model with correct parameters.

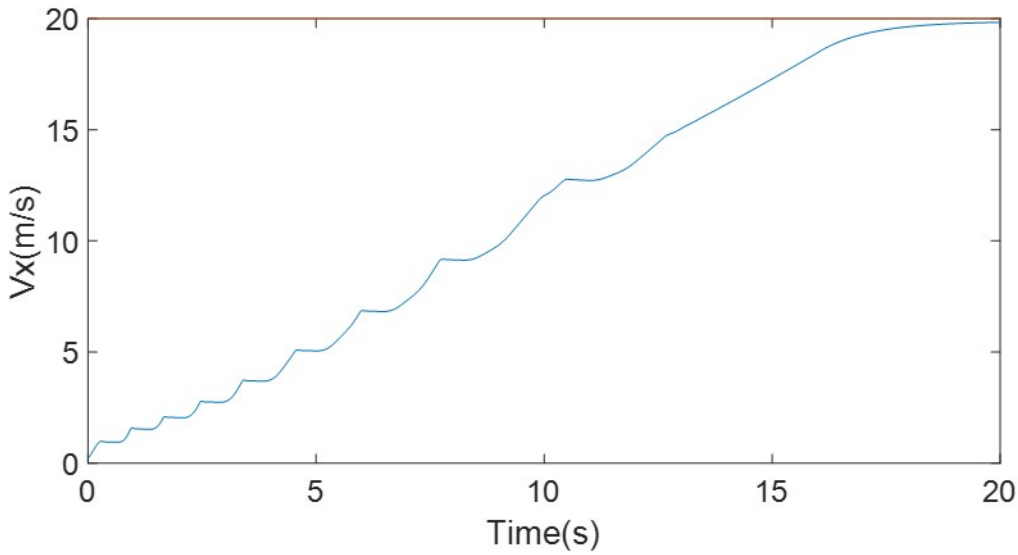

Figure 5.4: Speed profiles of the truck. The lower controller is the physical model based with correct parameters. The lower controller successfully enables the speed of the truck eventually track the reference speed.

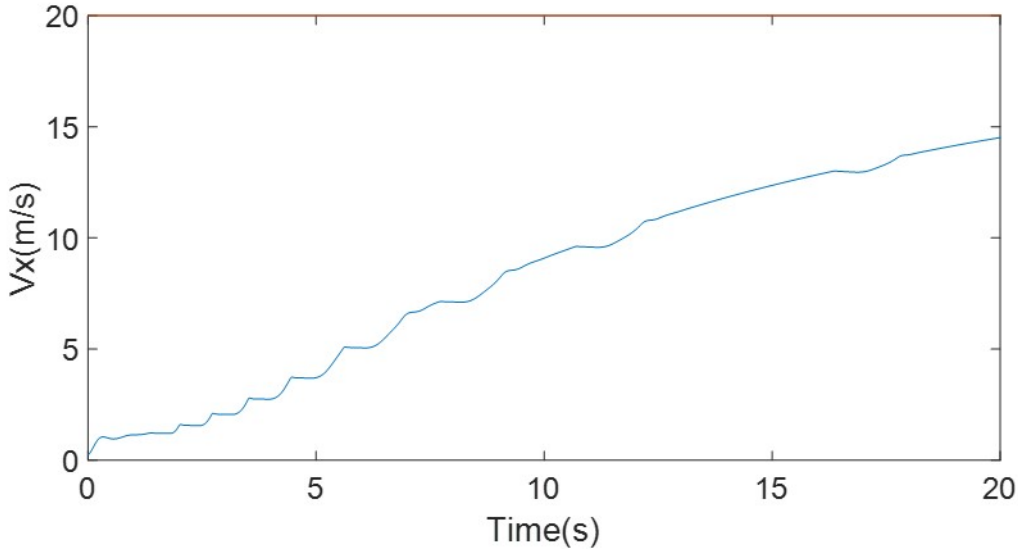

Figure 5.5: Speed profiles of the truck. The lower controller is the physical model with mismatched parameters and without adaptive parameter estimator. The speed of the truck cannot successfully track the reference speed.

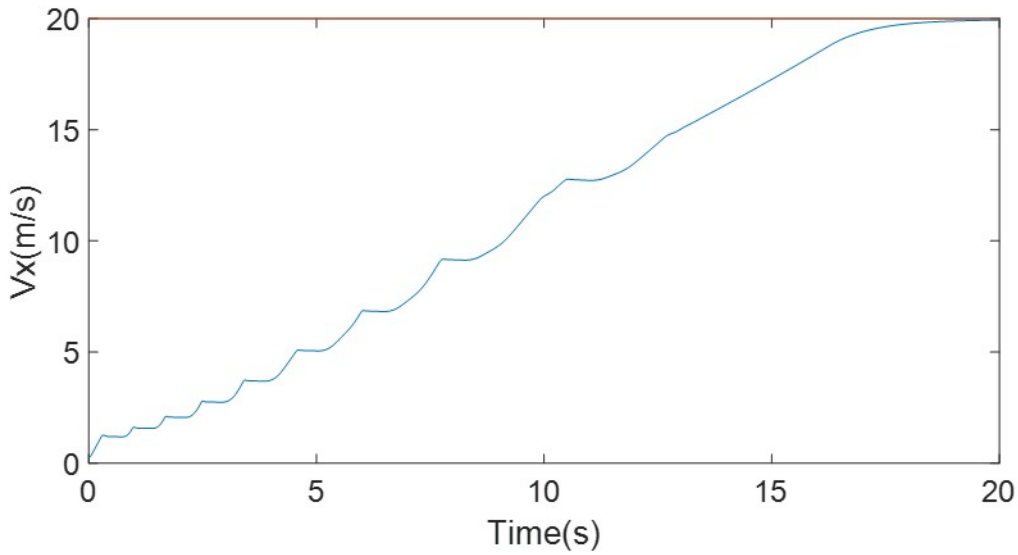

Figure 5.6: Speed profiles of the truck. The lower controller is the adaptive lower controller. The speed of the truck successfully follows the reference speed.

5.4.4 Experimental Validation

The cruise control with adaptive parameter estimator is implemented on the real truck and validated. The lower controller is implemented with a parameter estimator using measurements of the engine torque, the vehicle acceleration and the vehicle speed. In practice, if the truck does not have accelerometer, finite difference of the speed measurement can be used as substitute of the acceleration measurement. The initial condition of the estimator is fitted beforehand offline using data previously collected. Two different set speeds were being tested. Figure 5.7 shows the results of the tests. At both the high-speed ($28m/s$) and the low-speed ($20m/s$) tests, the controller with adaptive parameter estimator performs reasonably well. Real speeds converge to the reference speeds in the end with very small speed errors in both cases.

5.5 Longitudinal Motion Control

5.5.1 Cruise Control

The object of the cruise control is to control the subject vehicle to follow a given reference speed. A proportional gain controller is implemented for speed tracking control:

$$a_{\text{des}}(t) = K(v_{ref}(t) - V_x(t)),$$

$K \in \mathbb{R}$ is a controller parameter, and $v_{ref}(t) \in \mathbb{R}$ is a reference speed trajectory. The reference speed trajectory is a smooth speed transition trajectory from the current speed to

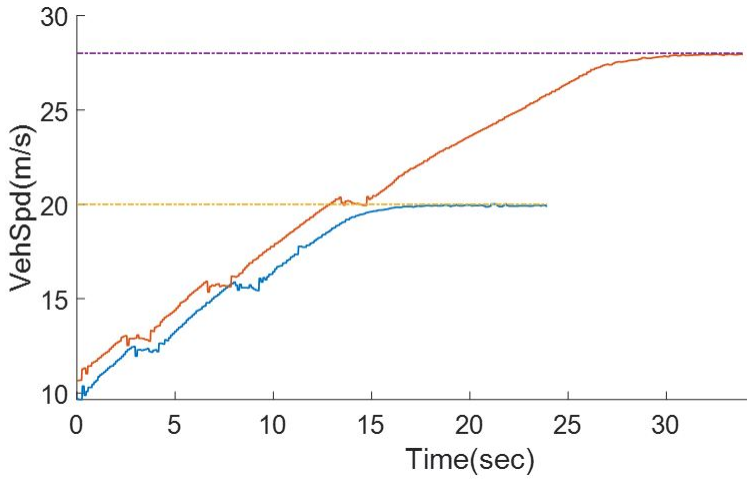

Figure 5.7: Speed profiles of the truck. Two reference speed are tested: $28m/s$ and $20m/s$. The dotted lines represent the reference speed. The two solid curves represent the corresponding speed responses of the truck.

a target speed. The generation of the speed trajectory in the section 5.5.1.1.

5.5.1.1 Speed Planner

To have smooth speed transition from current speed to a target speed, we can also use speed trajectory planner to shape speed response by generating a speed trajectory for cruise controller to follow. The speed trajectory can be planned based on some criterion, for example, physical limitations or comfort of passengers. The simplest speed trajectory is continuous speed with bounded acceleration. However, in this case acceleration of the vehicle is not continuous in time, which is not desirable in practice. We want to find the fastest speed trajectory from current speed to target speed with continuous and bounded acceleration, while vehicle acceleration and acceleration jerk are both bounded. The problem of the trajectory generation can be formulated as follows:

$$
\begin{aligned}
T^* = \min_{a(t),J(t)} \; & T \\
s.t. \quad & \dot{v}(t) = a(t), \forall t \in [t_0, T] \\
& \dot{a}(t) = J(t), \forall t \in [t_0, T] \\
& a_{min} \leq a(t) \leq a_{max}, \forall t \in [t_0, T] \\
& J_{min} \leq J(t) \leq J_{max}, \forall t \in [t_0, T] \\
& v(t_0) = v_0, v(T) = v_T, \\
& a(t_0) = 0, a(T) = 0.
\end{aligned}
$$

where $J_{max} \in \mathbb{R}_{>0}$, and $J_{min} \in \mathbb{R}_{<0}$ are acceleration jerk bounds; $a_{max} \in \mathbb{R}_{>0}$, and $a_{min} \in \mathbb{R}_{>0}$ are acceleration bounds. $v_0 \in \mathbb{R}_{>0}$ the initial speed and $v_T \in \mathbb{R}_{>0}$ is a target speed. Once the

optimal acceleration trajectory is solved, the optimal speed trajectory can be computed by integration. The closed form solution for this problem can be solved heuristically. Suppose $v_T > v_0$, in order to minimize the time it takes to accelerate from current speed to the target speed, one needs to accelerate as much as possible while satisfying acceleration jerk bounds. Therefore, we would expect at the beginning of the acceleration profile and at the end of the acceleration profile time derivative of the acceleration would be J_{max} and J_{min} respectively. Following this line of thought, it can be shown that the optimal solution is:

- If $\frac{1}{2}a_{max}^2(\frac{J_{min}-J_{max}}{J_{min}J_{max}}) \geq v_T - v_0$, the acceleration profile would need to decrease before reaching the maximum acceleration; otherwise, the acceleration would not be 0, when the speed reaches the target speed. The optimal solution would be $T^* = \frac{\bar{a}}{J_{max}} - \frac{\bar{a}}{J_{min}}$, where $\bar{a} \in \mathbb{R}_{\geq 0}$ is the peak of the acceleration profile satisfying follows:
$$\frac{1}{2}\bar{a}^2(\frac{1}{J_{max}} - \frac{1}{J_{min}}) = v_T - v_0.$$
The corresponding optimal acceleration profile is:
$$a^*(t) = \begin{cases} J_{max}t & \text{if } t \in [0, \frac{\bar{a}}{J_{max}}) \\ \bar{a} + J_{min}(t - \frac{\bar{a}}{J_{max}}) & \text{if } t \in [\frac{\bar{a}}{J_{max}}, T^*) \\ 0 & \text{otherwise} \end{cases}.$$

- On the other hand, if the difference between v_T and v_0 is larger, the acceleration profile would be able to reach the acceleration upper bound. The optimal solution is $T^* = \frac{a_{max}}{J_{max}} - \frac{a_{max}}{J_{min}} + \frac{v_T - v_0}{a_{max}} - \frac{1}{2}a_{max}(\frac{1}{J_{max}} - \frac{1}{J_{min}})$. The corresponding acceleration trajectory is:
$$a^*(t) = \begin{cases} J_{max}t & \text{if } t \in [0, \frac{a_{max}}{J_{max}}) \\ a_{max} & \text{if } t \in [\frac{a_{max}}{J_{max}}, \frac{a_{max}}{J_{max}} + \frac{v_T - v_0}{a_{max}} - \frac{1}{2}a_{max}(\frac{1}{J_{max}} - \frac{1}{J_{min}})) \\ a_{max} + J_{min}(t - T^* + \frac{a_{max}}{J_{min}}) & \text{if } t \in [T^* - \frac{a_{max}}{J_{min}}, T^*) \\ 0 & \text{otherwise} \end{cases}.$$

Similarly, the closed form acceleration profile when target speed is lower than current speed ($v_T < v_0$) can also be derived:

- If $\frac{1}{2}a_{min}^2(\frac{J_{min}-J_{max}}{J_{min}J_{max}}) \geq |v_T - v_0|$, then the solution is $T^* = \frac{\bar{a}}{J_{min}} - \frac{\bar{a}}{J_{max}}$, where $\bar{a} \in \mathbb{R}_{\leq 0}$ now represents the peak deceleration the deceleration profile would reach, which satisfies follows:
$$\frac{1}{2}\bar{a}^2(\frac{1}{J_{max}} - \frac{1}{J_{min}}) = |v_T - v_0|.$$
The corresponding acceleration profile is:
$$a^*(t) = \begin{cases} J_{min}t & \text{if } t \in [0, \frac{\bar{a}}{J_{min}}) \\ \bar{a} + J_{max}(t - \frac{\bar{a}}{J_{min}}) & \text{if } t \in [\frac{\bar{a}}{J_{min}}, T^*) \\ 0 & \text{otherwise} \end{cases}.$$

- Otherwise, the solution is $T^* = \frac{a_{min}}{J_{min}} - \frac{a_{min}}{J_{max}} + \frac{v_T - v_0}{a_{min}} - \frac{1}{2}a_{min}(\frac{1}{J_{min}} - \frac{1}{J_{max}})$. The corresponding acceleration trajectory is:

$$a^*(t) = \begin{cases} J_{min}t & \text{if } t \in [0, \frac{a_{min}}{J_{min}}) \\ a_{min} & \text{if } t \in [\frac{a_{min}}{J_{min}}, \frac{a_{min}}{J_{min}} + \frac{v_T - v_0}{a_{min}} - \frac{1}{2}a_{min}(\frac{1}{J_{min}} - \frac{1}{J_{max}})) \\ a_{min} + J_{max}(t - T^* - \frac{a_{min}}{J_{max}}) & \text{if } t \in [T^* + \frac{a_{min}}{J_{max}}, T^*) \\ 0 & \text{otherwise} \end{cases}.$$

The closed form solution can be used online to compute a speed trajectory for a given target speed for speed tracking.

5.5.1.2 Experimental Validation

The cruise control is implemented on a truck and tested. Figure 5.8 shows an example that the target speed is above the initial speed of the vehicle. Figure 5.9 shows another experiments that the target speed is lower than the initial speed of the vehicle. These results show that the cruise control and the speed planner we implemented could make the truck speed transition from the current speed to a target speed smoothly.

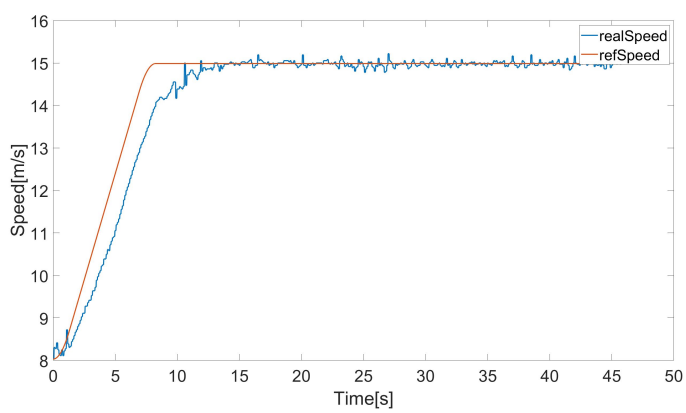

Figure 5.8: Cruise control experiment on a heavy duty vehicle-speed up. Initial speed is around $8[m/s]$ and the target speed is $15[m/s]$. The red curve is the reference speed and the blue curve is the truck speed.

5.5.2 Adaptive Cruise Control

Adaptive Cruise Control (ACC) is a controller that can control the relative distance to follow a desired following distance and regulate the relative speed to a leading vehicle stably. For different purposes, different spacing policies are proposed to determine the desired following

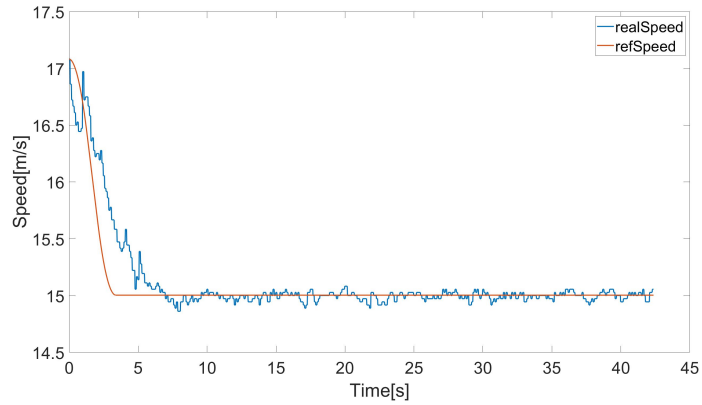

Figure 5.9: Cruise control experiment on a heavy duty vehicle-slow down. Initial speed is around $17[m/s]$ and the target speed is $15[m/s]$. The red curve is the reference speed and the blue curve is the truck speed.

distance [108]. In this work, a time-headway based spacing policy is adopted. The time-headway spacing policy picks the following distance linearly proportional to driving speed. Formally speaking, for a time-headway $h \in \mathbb{R}_{>0}$ and the vehicle driving speed is at $v_i(t) \in \mathbb{R}$ (i is used to denote the subject vehicle, later we will use $i-1$ to denote the preceding vehicle, similar to notations used in previous chapters), the desired following distance $d_{des}(t) \in \mathbb{R}$ would be:

$$d_{des}(t) = h\ v_i(t).$$

As one can see, with the time-gap policy, the desired following distance increases with driving speed. Not only this improves the response damping and stability, but also yields a more human-like car-following.

As mentioned, the primary goal of the car following controller is to regulate the following distance gap towards desired gap. Here, we design a output feedback controller to regulate the difference. Let $x_{i-1}(t), x_i(t) \in \mathbb{R}$ be the rear end position of the preceding vehicle and the position of the subject vehicle, respectively; and $L_i \in \mathbb{R}$ be the length of the subject vehicle. The bumper-to-bumper distance is $x_{i-1}(t) - x_i(t) - L_i$. The gap error $e_{x,i}(t) \in \mathbb{R}$ is the difference between the time-headway distance and the bumper-to-bumper distance:

$$e_{x,i}(t) = x_{i-1}(t) - x_i(t) - L_i - hv_i(t).$$

We would like to design a controller that output acceleration command for a gap error as the input. A block diagram of the closed-loop system is shown in the figure 5.10, where we use C to denote controller, G to denote closed-loop dynamics of the vehicle dynamics and the lower controller (section 5.4), the block of $1/s^2$ is used to denote a double integrator in frequency domain, and $H(s)$ is defined as follows: $H(s) := hs + 1$. Ideally, the transfer function G should be $G = 1$, which means the response of the vehicle dynamics is perfect.

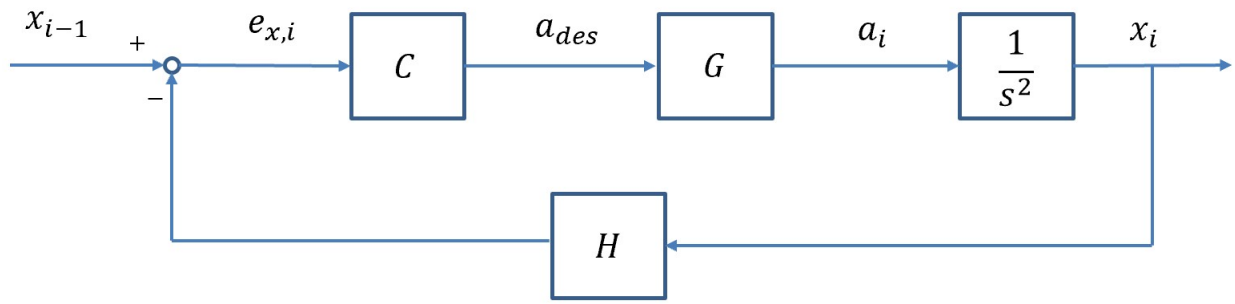

Figure 5.10: Block diagram of the car following control system

However, in reality, the response of vehicle powertrain is limited. By observing engine response data, we found that the engine torque to a vehicle acceleration response can be approximated by a first order transfer function. For controller design purpose, we then approximate response from a_{des} to a_i as

$$G(s) = \frac{1}{\tau s + 1},$$

where $\tau \in \mathbb{R}_{>0}$ is modeled as a uncertain parameter. The designed controller should be able to deal with this this in addition to other requirements state below.

We pick the controller $C(s)$ in the following structure and the parameters of the controller is what we need to design so that the system is stable and robust to model uncertainties and disturbances.

$$C(s) = \frac{k_1 s + k_2}{s^2 + d_1 s + d_0}.$$

Parameters k_1, k_2, d_1, and d_0 are what need to be determined. We have a few objectives for the selection of parameters:

- Closed-loop system is stable;
- The controller should be robust to uncertainty of the vehicle dynamics. We consider uncertain G with varying $\tau \in [\tau_{min}, \tau_{max}]$. Thus, the controller should keep the closed-loop system stable for all G with $\tau \in [\tau_{min}, \tau_{max}]$. To incorporate the parameter uncertainty in G, we use $\tilde{G}$ to represent the model with disturbance at the parameter τ:

  $$\tilde{G}(s) = \frac{1}{(\bar{\tau} + \Delta\tau)s + 1},$$

  where $\bar{\tau} = \frac{\tau_{min}+\tau_{max}}{2}$ and $\Delta\tau \in [-(\tau_{max} - \tau_{min})/2, (\tau_{max} - \tau_{min})/2]$, and the corresponding block diagram of the $\tilde{G}$ with $\Delta\tau$ is depicted in figure 5.11;

- Closed-loop transfer function should satisfy string stability condition:

$$\|T_{x_{i-1}x_i}\|_{\mathcal{H}_\infty} \leq 1.$$

$T_{x_{i-1}x_i}$ denotes the transfer matrix from x_{i-1} to x_i. For a transfer matrix T, $\mathcal{H}_\infty$ norm of T is defined as $\|T\|_{\mathcal{H}_\infty} := \sup_\omega \sigma_{max}(T(j\omega))$, where $\sigma_{max}(T(j\omega)$ is the maximum singular value of $T(j\omega)$. This performance requirement is a desirable property so that the disturbance arising from leading vehicle's speed variation would not propagate and amplify to the following vehicles.

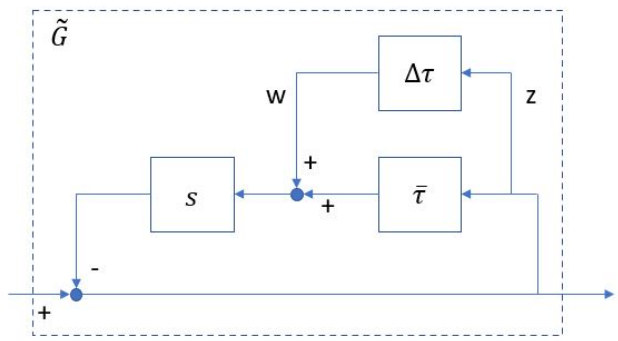

Figure 5.11: Representation of the vehicle dynamics model $\tilde{G}$ with a perturbed parameter to the nominal plant.

The model with uncertainty and the control design problem can be expressed pictorially as shown in figure 5.12. We want to find a controller C such that the model is stable for all stable transfer function Δ and $\|\Delta\|_{\mathcal{H}_\infty} < 1$, and in the mean while, we want the response from x_{i-1} to x_i satisfying $\|T_{x_{i-1}x_i}\|_{\mathcal{H}_\infty} \leq 1$. Δ is corresponding to the uncertainty of τ; more specifically, in our problem, we pick $\Delta \in [-1, 1]$ and $\Delta\tau = W_1\Delta$, with $W_1 = (\tau_{max} - \tau_{min})/2$. P is a transfer matrix with each entry corresponding to a pair of input and output. Let M represent the closed-loop system of C and P, that is, M represents the transfer matrix from w and x_{i-1} to z and x_i:

$$M = \begin{bmatrix} M_{wz}, & M_{x_{i-1}z} \\ M_{x_{i-1}z}, & M_{x_{i-1}x_i} \end{bmatrix}.$$

The transfer matrix stability can be attained straightforwardly design the controller C when the disturbance is neglected. When the disturbance plays a role, we can use necessary and sufficient condition for stability to derive the controller. Recall small gain theorem:

Theorem 5.5.1. *(small gain theorem) Suppose M_1 and M_2 are two stable transfer matrix and they are interconnected such that the output of M_1 is input of M_2, and output of M_2 is input of M_1. $\|M_1\|_{\mathcal{H}_\infty} \leq 1$. The interconnected system is stable if and only if $\|M_2\|_{\mathcal{H}_\infty} < 1$.*

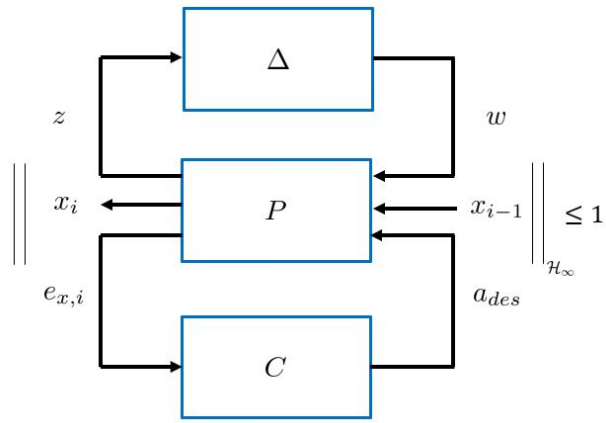

Figure 5.12: Pictorial representation of the control objective. The objective of the controller C is to have the closed-loop system stable under the disturbance of Δ, while H_∞ norm from x_{i-1} to x_i is less or equal than 1.

By small gain theorem, we know that the interconnected system of figure 5.12 with disturbance Δ (Δ is a stable transfer function and $\|\Delta\|_{\mathcal{H}_\infty} \leq 1$) is stable if and only if we can find a controller C such that $\|M\|_{\mathcal{H}_\infty} < 1$. The performance requirement of $\|T_{x_{i-1}x_i}\|_{\mathcal{H}_\infty} \leq 1$ can also be formulated as a robust control problem with another disturbance term Δ_1, where Δ_1 is also stable and $\|\Delta_1\|_{\mathcal{H}_\infty} < 1$. The closed-loop system block diagram with Δ_1 is illustrated in figure 5.13. We can again apply small gain theorem, if the system interconnected with Δ_1 is stable, then the string stability condition would be satisfied, and vice versa.

Furthermore, we can combine both disturbance block Δ and Δ_1 into a structured disturbance. The block diagram of the problem with structured disturbance is depicted in figure 5.14. Let $R = [w, x_{i-1}]^T$, and $Y = [z, x_i]^T$. The disturbance block is now in the diagonal form $\bar{\Delta} = diag(\Delta, \Delta_1)$. For structure disturbance, less conservative constraint on the M is needed to attain robust stability, since extra constraint is imposed on the disturbance block. Recall structured disturbance theorem:

Theorem 5.5.2. *(structured disturbance small gain theorem) Suppose disturbance transfer matrix $\bar{\Delta}$ is stable and $\bar{\Delta}$ is taken the form of $\mathbf{\Delta} = \{diag[\delta_1, \delta_2, \ldots, \delta_n] | \delta_i \in \mathbb{C}, \forall i \in \{1, \ldots, n\}\}$. M is stable. Interconnection of M and $\bar{\Delta}$ is stable for all $\bar{\delta} \in \mathbf{\Delta}$ with $\|\bar{\Delta}\|_{\mathcal{H}_\infty} < 1$ if and only if $\sup_\omega \mu_{\mathbf{\Delta}}(M(j\omega)) \leq 1$.*

The variable $\mu_{\mathbf{\Delta}}(M)$ is the structured singular value of a complex matrix M with respect to a class of disturbance matrix $\mathbf{\Delta}$:

$$\mu_{\mathbf{\Delta}}(M) := \begin{cases} 0, & \text{if } det(I - M\Delta) \neq 0 \\ \frac{1}{\inf\{\sigma_{\max}(\Delta) | det(I - M\Delta) = 0, \Delta \in \mathbf{\Delta}\}}, & \text{otherwise} \end{cases}.$$

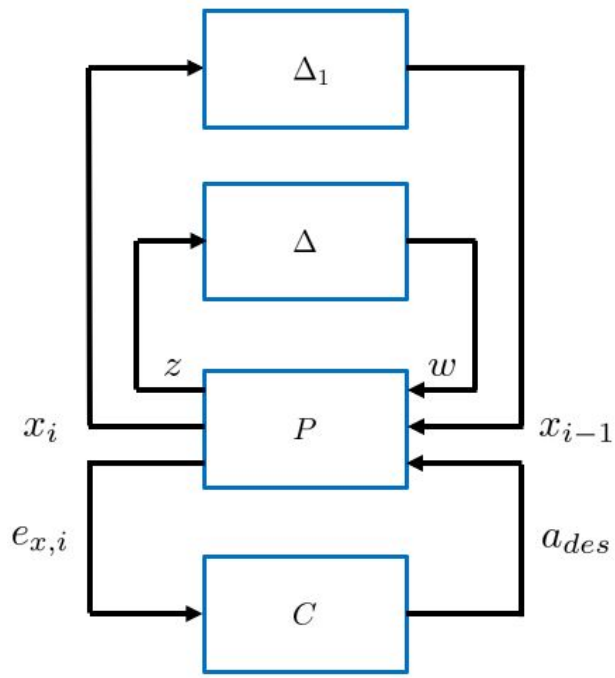

Figure 5.13: Illustration of formulating performance requirement as stability problem with Δ_1. The requirement that $\|T_{x_{i-1}x_i}\|_{\mathcal{H}_\infty} \leq 1$ can be reformulated as stability problem by connecting x_i and x_{i-1} with a stable Δ_1. The requirement can be satisfied if the closed-loop system is stable.

The problem is then finding a controller C such that $\sup_\omega \mu_{\bar{\Delta}}(M(j\omega)) \leq 1$. The problem could be solve as a optimization problem [119].

$$\min_C \inf_{D \in \mathcal{D}} \|D(s)M(P,C)D^{-1}(s)\|_{\mathcal{H}_\infty}.$$

If the optimal value < 1 can be attained, then the robust stability and performance requirement can be guaranteed. A numerical solver is used to synthesize the controller.

5.5.2.1 Simulation Validation

The controller is firstly validated in the simulation using TruckSim and Simulink. Two scenarios are tested. In both scenarios, a subject vehicle is controlled to follow a leading truck. In the first testing scenario, the subject vehicle is controlled to follow a given time-headway while the leading vehicle is following a given time-varying speed profile. Simulation results are shown in figure 5.15. The results show that the time-gap of the controlled vehicle can be kept around the desired time gap while matching the leading vehicle speed closely. In principle, keeping the time-gap constant while keeping subject vehicle speed matches varying leading vehicle speed is not feasible, because variation of the subject vehicle would

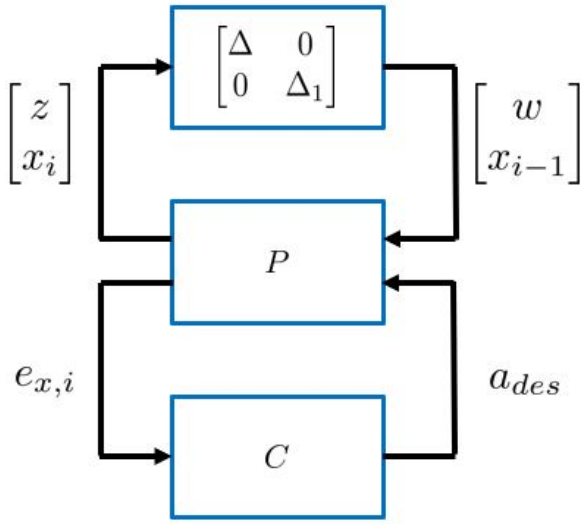

Figure 5.14: Representation of a model with structured disturbances.

have counter effect on the numerator term (distance gap) and denominator term (speed) of the time-gap. For example, suppose leading vehicle speed is increasing and the subject vehicle manages to match its speed to leading vehicle speed exactly, the relative distance would remain constant, but the time gap would be decreasing because subject vehicle speed is increasing. Therefore, to keep the time-gap around a desired time-gap, subject vehicle speed cannot match its speed exactly to the leading vehicle speed. We can observe this phenomenon in the simulation results. For example, between 25 and 30 seconds when the leading vehicle speed is decreasing, the subject vehicle's speed is kept slightly higher than the leading vehicle speed so that the distance gap would decrease, and the corresponding time-gap would be kept around the desired time-gap.

In the second scenario, the leading vehicle is driving at a constant speed, while the desired time-gap varies. The desired time-gap varied from one second to two seconds and came back to one second within 20 seconds. Figure 5.16 shows that real time-headway response is following the desired time headway reasonably well. For the first 10 seconds, the desired time gap increases. For the same described in the first scenario, to track the desired time gap, the subject vehicle needs to decrease its speed to increase the real time-gap. Between 10 and 20 seconds, the desired time gap decreases, the subject vehicle increases its speed to close the gap.

5.5.2.2 Experimental Validation

Following the success in the simulation, the controller is then implemented on a heavy duty vehicle. Two sets of representative results are shown in figure 5.17 and figure 5.18. In figure 5.17, one can see that the leading vehicle is almost driving at constant speed, but gradually

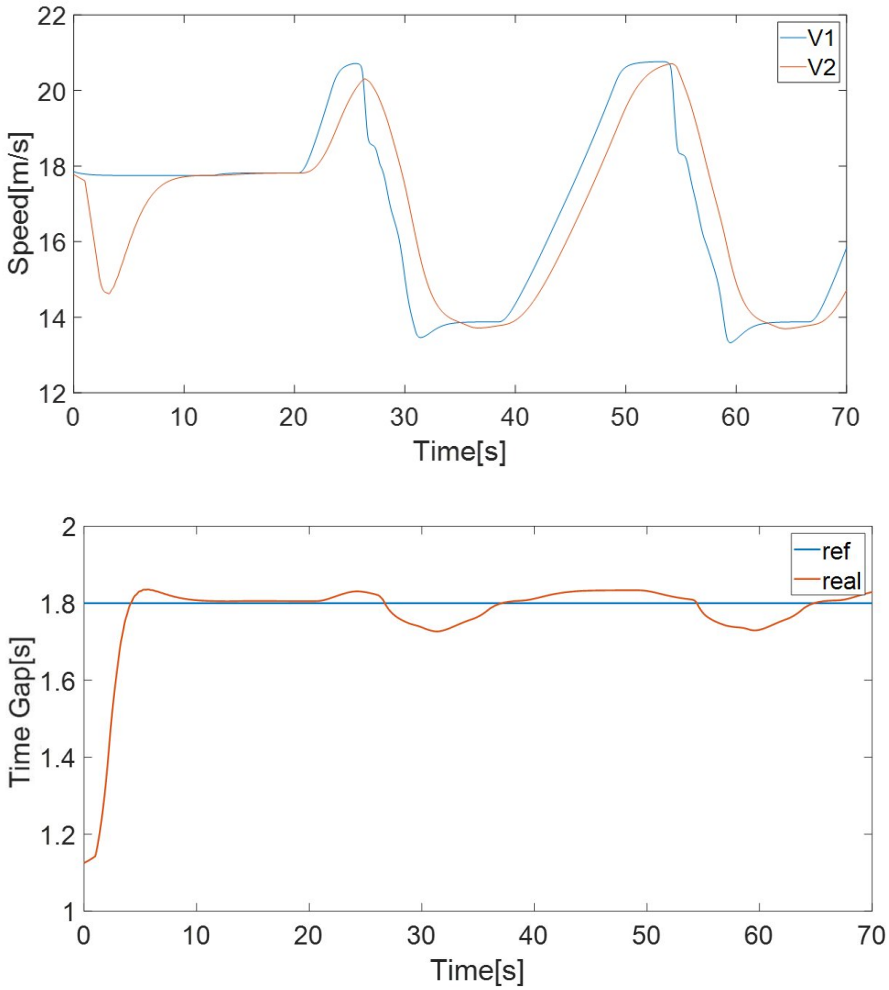

Figure 5.15: Simulation results in TruckSim with fixed reference time-gap and varying speed profile. The top figure shows the speed profiles of both vehicles, where $V1$ denotes the speed of the leading vehicle and $V2$ denotes the speed of the subject vehicle. The bottom figure shows the reference time gap (blue) and the real time gap (red).

speeding up at around 78 seconds. At the same time, the subject vehicle is following the leading vehicle speed reasonably well; the time gap is gradually controlled to the desired time gap. In the second test (figure 5.18), the leading vehicle is firstly driving at a constant speed, followed by gradual deceleration. The speed response and time gap response of the subject vehicle shows that the controller controlled the vehicle matching the leading vehicle speed very well while keeping the time gap bounded around the desired time gap. In both scenarios, the controller is able to regulate the time-gap close to the reference time-gap in the range of 0.05 seconds.

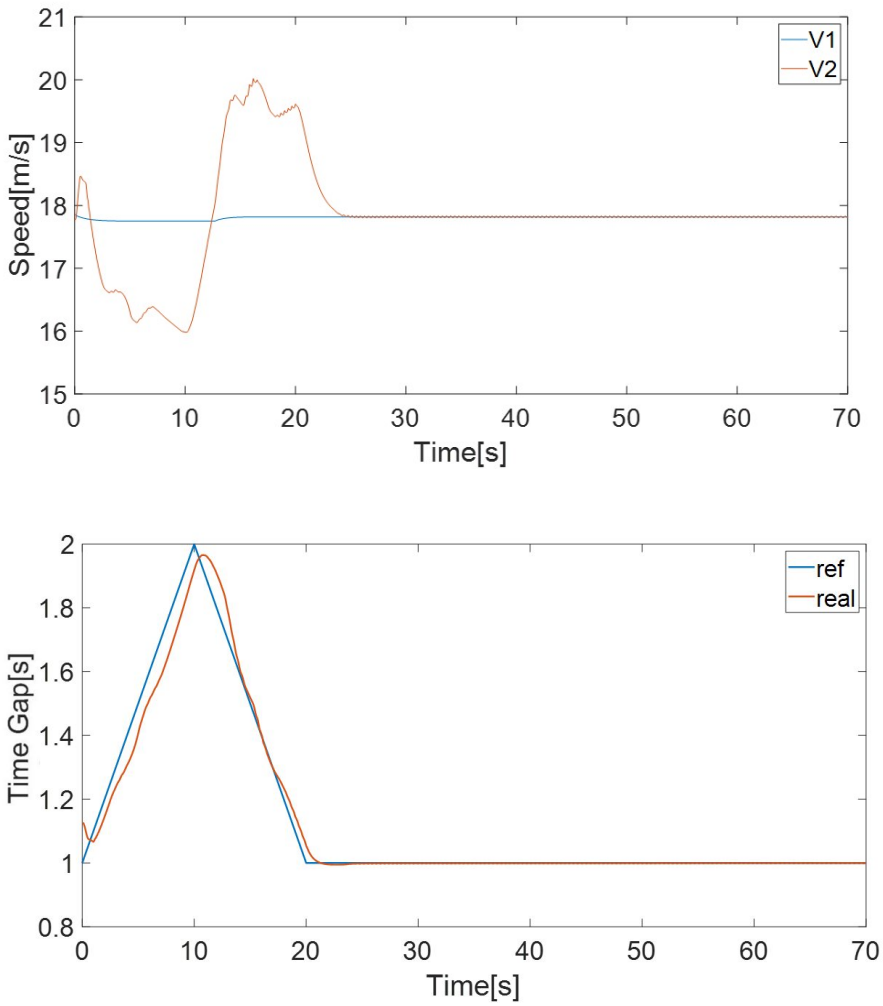

Figure 5.16: Simulation results in TruckSim with fixed leading vehicle speed and varying reference time-headway. The top figure shows the speed profiles of both vehicles, where $V1$ denotes the speed of the leading vehicle and $V2$ denotes the speed of the subject vehicle. The bottom figure shows the reference gap(blue) and the real time gap (red).

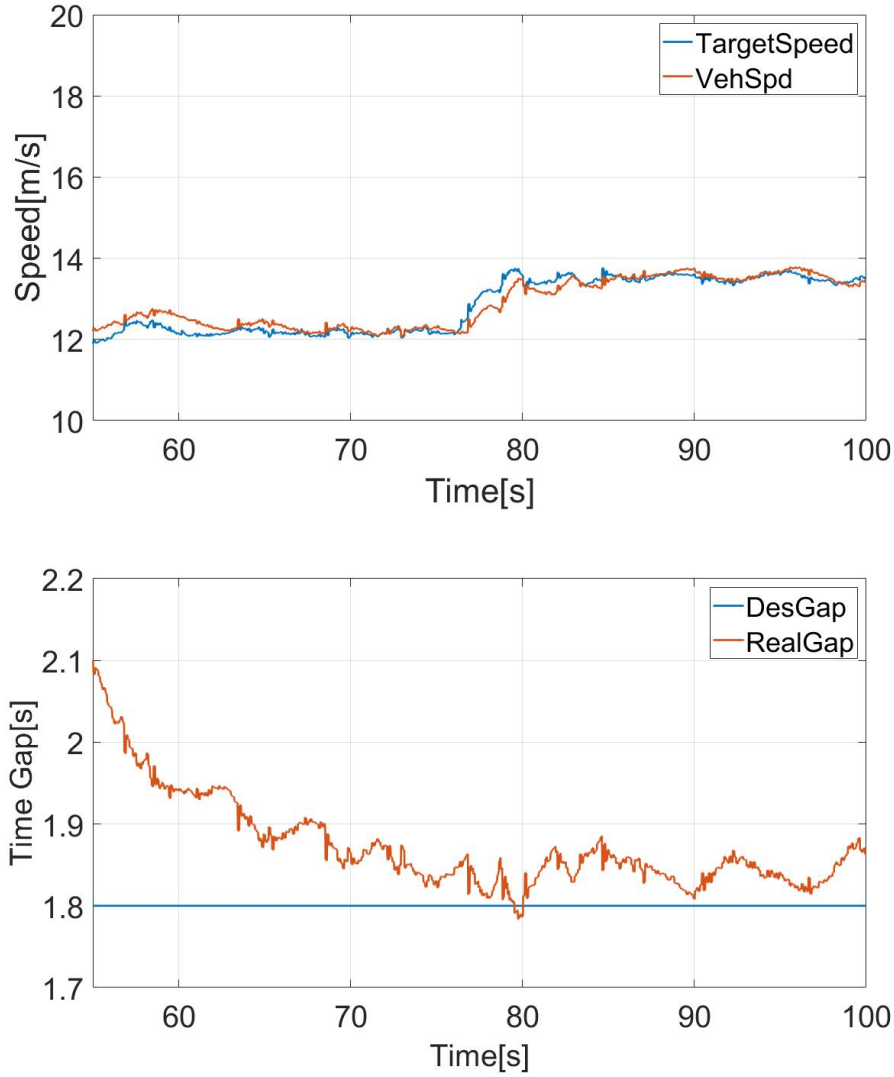

Figure 5.17: Experimental results on a heavy duty truck. The initial time gap is about 2.1 seconds. The controller gradually regulates the time gap to a desired target time-gap and keeps the error around 0.05 seconds. Spikes in the measurements are due to sensor noise.

5.5.3 Adaptive Cruise Control with V2V communication

One of main challenge we are facing when using radar to detect the leading vehicle speed and distance is that the measurement is error prone and too noisy due to vibration of the vehicle. This causes the controller system less stable when the leading vehicle speed varies.

In order to improve the performance of the system so that it can be able to handle the situations when the leading vehicle speed is varying, we incorporate vehicle to vehicle communication between the leading vehicle and the subject vehicle so that the subject vehicle

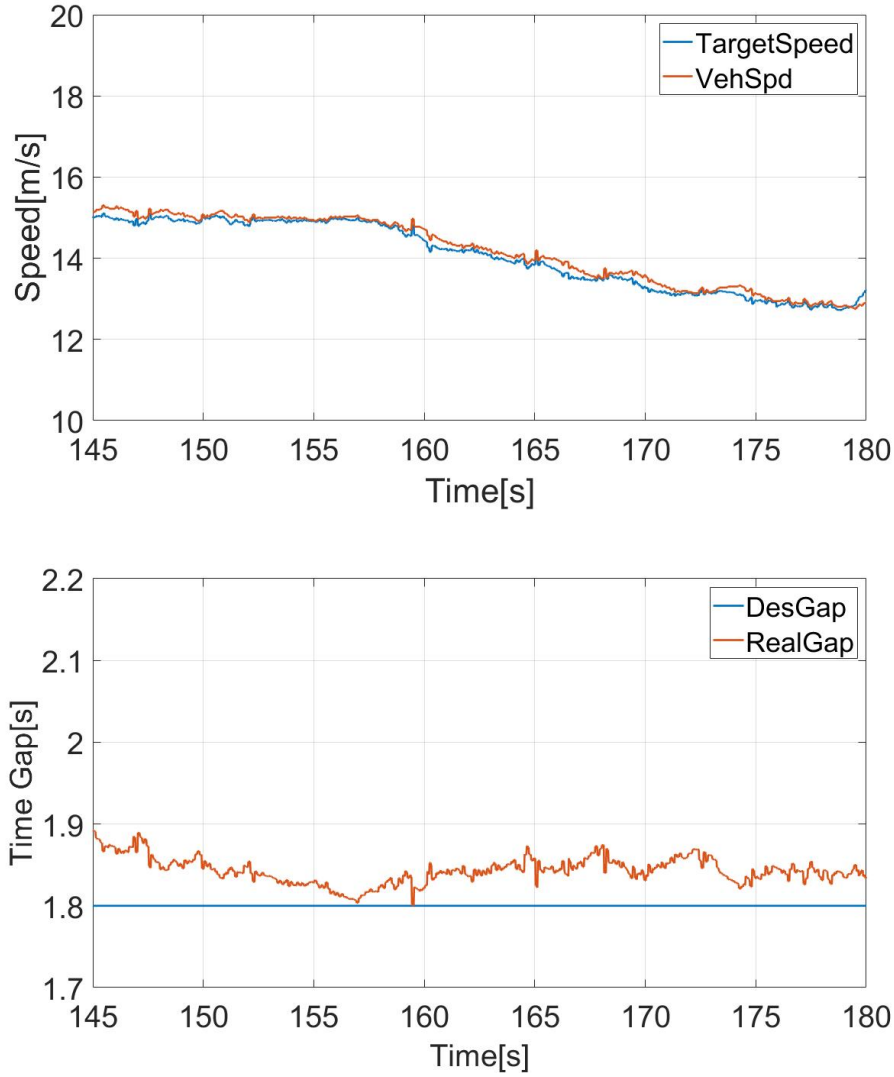

Figure 5.18: Experimental results on a heavy duty truck. While the leading vehicle is gradually reducing its speed (after 155 seconds), the controller regulates the time gap around a desired target time-gap and keeps the error around 0.05 seconds. Spikes in the measurements are due to sensor noise.

can use the leading vehicle speed directly.

To incorporate V2V signal, we replace the speed measurement from the radar by the reading of the leading vehicle via vehicle to vehicle communication. To be more specific, we first decompose the controller above into two parts $C(s) = C_1(s) + C_2(s)$, where $C_1(s) = k_1 s/C_D(s)$, and $C_2(s) = k_2/C_D(s)$. Let the output of the controller $C_1(s)$ and $C_2(s)$ be u_1 and u_2. The output $u(t)$ of $C(s)$ would be $u(t) = u_1(t)+u_2(t)$. Let V_{i-1}, V_i, and A_i be the Laplace transform of v_{i-1}, v_i, and a_i, respectively. Recall that the input to the controller $C(s)$ is

$x_{i-1}(t)-x_i(t)-L_i-hv_i(t)$. The output $u_1(t)$ would then be $u_1(t) = k_1(V_{i-1}-V_i-hA_i)/C_D(s)$, which is explicitly dependent on leading vehicle speed v_{i-1}. In the case when we rely on on-board sensor only, the measurement $v_{i-1}(t)$ would be from the radar. With the vehicle to vehicle communication, we use the signal of $v_{i-1}(t)$ from the leading vehicle directly.

5.5.3.1 Experimental validation

We validate the controller with both leading truck and the controlled truck equipped with vehicle to vehicle communication devices. The leading truck would transmit the speed measurement to the following truck and the following truck would use the received speed signal for control. Resultant speed profiles and time gaps are shown in the figure 5.19, respectively. During this experiment, the following truck is trying to control the time-headway at 1.8s, while the leading vehicle varies its speed between $14\,\mathrm{m\,s^{-1}}$ and $19\,\mathrm{m\,s^{-1}}$. The speed profiles show that the following vehicle is capable of following the leading vehicle speed closely. Although the time-gap is not as close to the desired time-gap as we have seen above, the error is still within a reasonable range. This could be improved with further calibrations of the model and fine tuning of the controller.

5.6 Summary

In this chapter, a model-based longitudinal controller for a heavy-duty vehicle is developed. The controller is composed of a lower controller and an upper controller, where the lower controller is for executing engine command and service brake command for a given desired acceleration command from the upper controller. To deal with parameter uncertainty, a parameter estimator is integrated with the lower controller to estimate unknown parameters in real time. We validate the design in simulation experiments and real-world experiments. Some results are shown.

For the upper level controller, two main functions are developed: speed tracking and car following. For speed tracking, to avoid overshoot, a smooth speed trajectory is generated. Experimental results show that speed tracking performance is reasonably well. For the car following controller, a controller design considering the robustness with respect to model uncertainty and the requirement for string stability is developed. The controller design problem can be formulated as a robust control problem and it is solved numerically. In practice, due to the limitation of the on-board sensors and actuators, car following controllers cannot deal with the situations well when the leading vehicle speed is varying more aggressively. To deal with this, a vehicle-to-vehicle communication is used to enable the following vehicle to access leading vehicle speed directly. The integration enables the subject vehicle to follow the leading vehicle steadily while the leading vehicle's speed is varying. Our controllers are tested in the real world. Some results are shown to demonstrate the performance of our controllers.

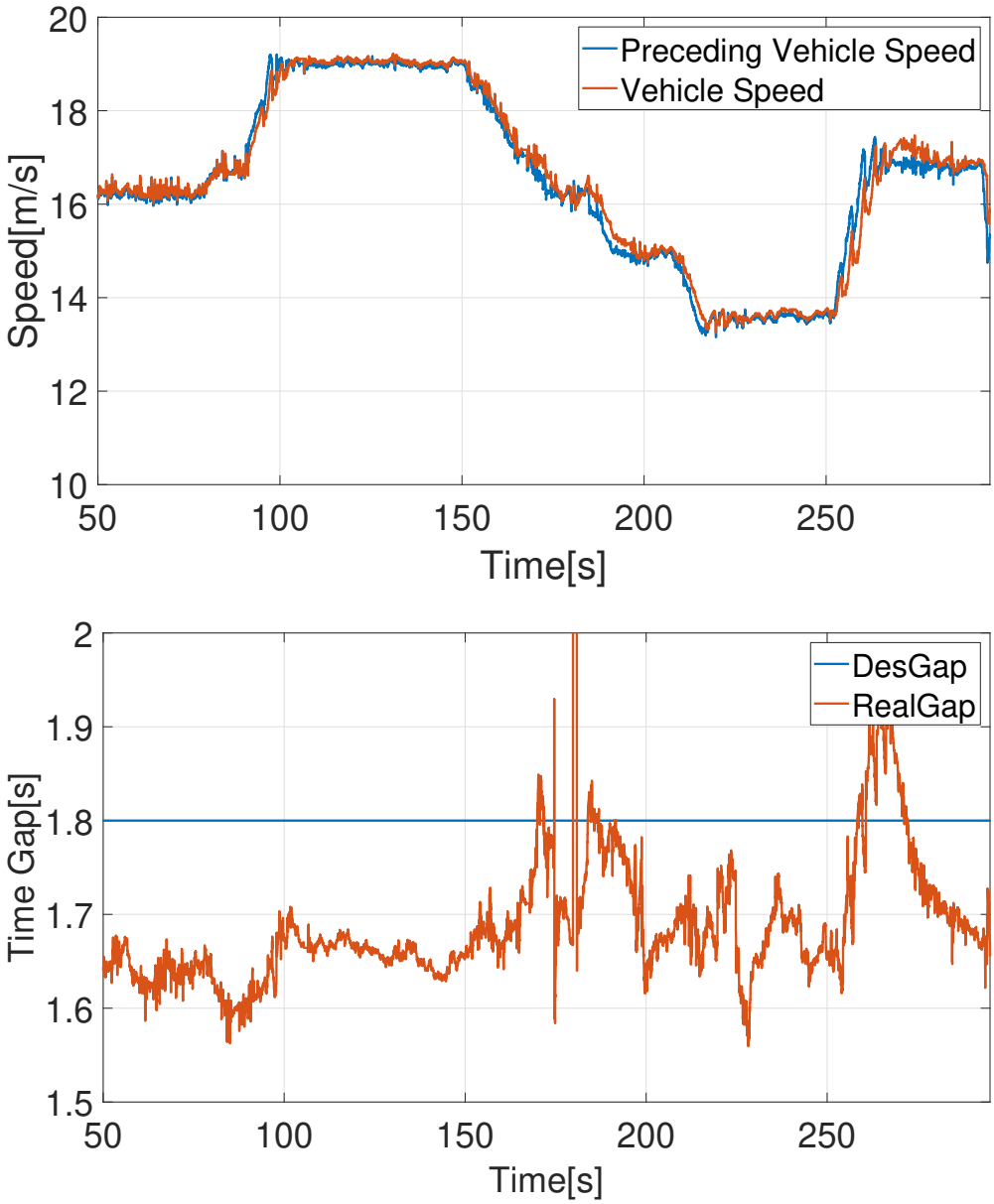

Figure 5.19: Experimental results of car following controller with V2V communication. Top: Speed profiles of the leading vehicle and the following vehicle. Blue curve is the leading vehicle speed and red curve is the subject vehicle speed. Bottom: Desired time gap (blue line) and real time gap (red curve).

Chapter 6

Concluding Remarks

Although vehicles in the transportation system will mainly operate by human drivers for years to come, with the rise of the automated vehicles in recent years, it can be expected the dynamics of the automated controls would gradually play more important roles in the transportation system in the future. With the help of advanced sensors, actuators, and powerful computers, automated vehicles could have more accurate perception, more precise control, and more reliable decision than average human drivers, which could make the transportation system safer, more efficient, and more energy economic. It will still need a lot of effort for researchers and engineers to make the imagination become true. The work of this dissertation is a small piece for that. Particularly, in this dissertation, we study highway traffic jams and propose solutions with control of automated vehicles. Highway traffic jams can be caused by driving behaviors of participants in the traffic. Controls of automated vehicles should be designed such that their behaviors would not trigger congestion.

One of the major causes of highway traffic jams is accumulated conflicts between traffic flow. Especially at the merging section, accumulated disturbances induced by conflicts between traffic from two directions can have a negative impact on traffic flow. Coordination among vehicles is essential for reducing conflicts between vehicles in the traffic. In chapter 2, we have seen how coordination among vehicles from two directions at the highway merging section can effectively improve the throughput and reduce travel delay.

Phantom traffic jams are traffic jams that are related to driving behaviors. It is because that human driving behaviors tend to propagate and amplify the speed perturbations from downstream to upstream. We can study the propagation of perturbation using a ring road. As we have seen in chapter 3 and chapter 4, undesirable driving dynamics would cause stop-and-go waves on the ring road. Thus, it is important to design controllers properly not only in order to reduce the negative impact on the traffic and even improve the overall traffic. In chapter 3, theoretical analysis is presented. We prove conditions of car following models for stability of the ring road of identical/heterogeneous traffic. Provable sufficient condition for traffic stability is used to design a controller that can be used to dissipate disturbance in the traffic. Although the controller designed in chapter 3 is provable, it is relatively conservative. In practice, the sufficient condition is not necessary to derive a controller that

could make the traffic stable. Many different approaches of controller designs have been proposed in the literature. However, those controllers are not thoroughly investigated under different scenarios. In chapter 4, we benchmark 10 AV controllers including linear controller, heuristic based controller, and learning based controller. Performance evaluations of the 10 AV controllers are done under different penetration rates and different distributions among the traffic. The evaluation metrics include the time to dissipate stop-and-go waves, maximum headway, VMT, and fuel economy.

Since trucks contribute to congestion relative larger than light duty vehicles and it is expected that the VMT is going to be growing faster than light duty vehicles, truck automation has its critical role in the transportation system. In the chapter 5, we develop and implement an automated control for trucks. In addition to parameter uncertainties and actuator perturbations, the controller also takes into account the sufficient condition of the traffic stability - string stability. In practice, V2V communication is needed to achieve string stability. We use V2V communication to access the leading vehicle speed and demonstrate good car following performance. Simulation and real-world experiments are shown to validate our controller design.

Coordination and awareness of traffic conditions would be critical factors for automated vehicles to successfully mitigate traffic congestion by reducing conflicts and responding properly to attenuate perturbation. Wireless communication would be a possible solution for vehicles to coordinate directly with other vehicles at the same time compensate for the limitations of the on-board sensor. Hence, wireless communications would be essential to enable full capability of the automated vehicles. While the main focus of this dissertation is on traffic jam mitigation with vehicle automation, automated vehicles would definitely have potential to benefit future transportation systems in different ways; it is essential to consider broader perspectives in the future development of automated vehicles.

Bibliography

[1] Hadi Adibi Asl, Nasser Lashgarian Azad, and John McPhee. "Modeling Torque Converter Characteristics in Automatic Drivelines: Lock-up Clutch and Engine Braking Simulation". In: *Proceedings of the ASME 2012 International Design Engineering Technical Conferences and Computers and Information in Engineering Conference*. Vol. 6. Aug. 2012, pp. 359–367. URL: https://doi.org/10.1115/DETC2012-70222.

[2] Assad Alam et al. "Heavy-duty vehicle platooning for sustainable freight transportation: A cooperative method to enhance safety and efficiency". In: *IEEE Control Systems* 35.6 (2015), pp. 34–56.

[3] A. Alam et al. "Heavy-Duty Vehicle Platooning for Sustainable Freight Transportation: A Cooperative Method to Enhance Safety and Efficiency". In: *IEEE Control Systems Magazine* 35.6 (2015), pp. 34–56. DOI: 10.1109/MCS.2015.2471046.

[4] H. S. BAE. "Road Grade and Vehicle Parameter Estimation for Longitudinal Control Using GPS". In: *Proceedings of the IEEE Conference on Intelligent Transportation Systems, Oakland, CA, 2001* (2001), pp. 166–171. URL: https://ci.nii.ac.jp/naid/10013329204/en/.

[5] Masako Bando et al. "Dynamical model of traffic congestion and numerical simulation". In: *Physical review E* 51.2 (1995), p. 1035.

[6] Masako Bando et al. "Phenomenological study of dynamical model of traffic flow". In: *Journal de Physique I* 5.11 (1995), pp. 1389–1399.

[7] Masako Bando et al. "Structure stability of congestion in traffic dynamics". In: *Japan Journal of Industrial and Applied Mathematics* 11.2 (1994), p. 203.

[8] Robert L. Bertini and Shazia Malik. "Observed Dynamic Traffic Features on Freeway Section with Merges and Diverges". In: *Transportation Research Record* 1867.1 (2004), pp. 25–35. DOI: 10.3141/1867-04. eprint: https://doi.org/10.3141/1867-04. URL: https://doi.org/10.3141/1867-04.

[9] B. Besselink and K. H. Johansson. "String Stability and a Delay-Based Spacing Policy for Vehicle Platoons Subject to Disturbances". In: *IEEE Transactions on Automatic Control* 62.9 (2017), pp. 4376–4391. DOI: 10.1109/TAC.2017.2682421.

[10] D. Bevly et al. "Lane Change and Merge Maneuvers for Connected and Automated Vehicles: A Survey". In: *IEEE Transactions on Intelligent Vehicles* 1.1 (2016), pp. 105–120. DOI: 10.1109/TIV.2015.2503342.

[11] R. K. Bhadani et al. "Dissipation of Emergent Traffic Waves in Stop-and-Go Traffic Using a Supervisory Controller". In: *2018 IEEE Conference on Decision and Control (CDC)*. 2018, pp. 3628–3633.

[12] Rahul Bhadani et al. "Real-time distance estimation and filtering of vehicle headways for smoothing of traffic waves". In: *Proceedings of the 10th ACM/IEEE International Conference on Cyber-Physical Systems*. 2019, pp. 280–290.

[13] Mark Brackstone and Mike McDonald. "Car-following: a historical review". In: *Transportation Research Part F: Traffic Psychology and Behaviour* 2.4 (Dec. 1999), pp. 181–196. ISSN: 13698478. DOI: 10.1016/S1369-8478(00)00005-X. URL: https://linkinghub.elsevier.com/retrieve/pii/S136984780000005X.

[14] D. Cho and J. K. Hedrick. "Automotive Powertrain Modeling for Control". In: *Journal of Dynamic Systems, Measurement, and Control* 111.4 (Dec. 1989), pp. 568–576. ISSN: 0022-0434. DOI: 10.1115/1.3153093. eprint: https://asmedigitalcollection.asme.org/dynamicsystems/article-pdf/111/4/568/5546085/568_1.pdf. URL: https://doi.org/10.1115/1.3153093.

[15] Fang-Chieh Chou et al. "Modeling Vehicle-Following Dynamics of Heavy Trucks Under Automatic Speed Control Based on Experimental Data". In: *Transportation Research Board 97th Annual Meeting*. Washington DC, United States, 2018.

[16] D. Corona and B. De Schutter. "Adaptive Cruise Control for a SMART Car: A Comparison Benchmark for MPC-PWA Control Methods". In: *IEEE Transactions on Control Systems Technology* 16.2 (2008), pp. 365–372.

[17] Shumo Cui et al. "Stabilizing traffic flow via a single autonomous vehicle: Possibilities and limitations". In: *2017 IEEE Intelligent Vehicles Symposium (IV)*. IEEE, 2017, pp. 1336–1341.

[18] L. C. Davis. "Effect of adaptive cruise control systems on traffic flow". In: *Phys. Rev. E* 69 (6 June 2004), p. 066110. DOI: 10.1103/PhysRevE.69.066110. URL: https://link.aps.org/doi/10.1103/PhysRevE.69.066110.

[19] L.C. Davis. "Effect of adaptive cruise control systems on mixed traffic flow near an on-ramp". In: *Physica A: Statistical Mechanics and its Applications* 379.1 (2007), pp. 274–290. ISSN: 0378-4371. URL: https://www.sciencedirect.com/science/article/pii/S0378437106013690.

[20] Maria Laura Delle Monache et al. "Feedback control algorithms for the dissipation of traffic waves with autonomous vehicles". In: *Computational Intelligence and Optimization Methods for Control Engineering*. Springer, 2019, pp. 1–20. URL: https://hal.inria.fr/hal-01930724.

[21] Ernst Dickmanns. "Vision for ground vehicles: History and prospects". In: *International Journal of Vehicle Autonomous Systems* 1 (Jan. 2002), pp. 1–44. DOI: 10.1504/IJVAS.2002.001804.

[22] Yan Duan et al. *Benchmarking Deep Reinforcement Learning for Continuous Control*. 2016. arXiv: 1604.06778 [cs.LG].

[23] Cristofer Englund et al. "Future Applications of VANETs". In: *Vehicular ad hoc Networks: Standards, Solutions, and Research*. Ed. by Claudia Campolo, Antonella Molinaro, and Riccardo Scopigno. Cham: Springer International Publishing, 2015, pp. 525–544. ISBN: 978-3-319-15497-8. DOI: 10.1007/978-3-319-15497-8_18. URL: https://doi.org/10.1007/978-3-319-15497-8_18.

[24] Shuo Feng et al. "String stability for vehicular platoon control: Definitions and analysis methods". In: *Annual Reviews in Control* 47 (2019), pp. 81–97. ISSN: 1367-5788.

[25] R.E. Fenton and R.J. Mayhan. "Automated highway studies at the Ohio State University-an overview". In: *IEEE Transactions on Vehicular Technology* 40.1 (1991), pp. 100–113. DOI: 10.1109/25.69978.

[26] R. Firoozi et al. "Safe Adaptive Cruise Control with Road Grade Preview and **V**2**V** Communication". In: *2019 American Control Conference (ACC)*. 2019, pp. 4448–4453.

[27] Gene F. Franklin, J. David Powell, and Abbas Emami-Naeini. *Feedback Control of Dynamic Systems*. Pearson, 2006.

[28] Jin I. Ge and Gábor Orosz. "Dynamics of connected vehicle systems with delayed acceleration feedback". In: *Transportation Research Part C: Emerging Technologies* 46 (2014), pp. 46–64. ISSN: 0968090X. DOI: 10.1016/j.trc.2014.04.014. URL: http://dx.doi.org/10.1016/j.trc.2014.04.014.

[29] Tuomas Haarnoja et al. "Soft Actor-Critic: Off-Policy Maximum Entropy Deep Reinforcement Learning with a Stochastic Actor". In: *Proceedings of the 35th International Conference on Machine Learning*. Stockholm, Sweden, 2018. arXiv: 1801.01290. URL: http://arxiv.org/abs/1801.01290.

[30] R'mani Haulcy et al. "A Fuzzy-based Approach to Dampen Emergent Traffic Waves". In: *2020 American Control Conference (ACC) (to be appeared)*. IEEE. 2020.

[31] Yinglong He et al. "Adaptive Cruise Control Strategies Implemented on Experimental Vehicles: A Review". In: *IFAC-PapersOnLine* 52.5 (2019). 9th IFAC Symposium on Advances in Automotive Control AAC 2019, pp. 21–27. ISSN: 2405-8963. DOI: https://doi.org/10.1016/j.ifacol.2019.09.004. URL: https://www.sciencedirect.com/science/article/pii/S2405896319306238.

[32] A. Hegyi, Bart De Schutter, and J. Hellendoorn. "Optimal coordination of variable speed limits to suppress shock waves". In: *IEEE Transactions on Intelligent Transportation Systems* 6.1 (2005), pp. 102–112. DOI: 10.1109/TITS.2004.842408.

[33] Robert Herman et al. "Traffic Dynamics: Analysis of Stability in Car Following". In: *Operations Research* 7.1 (1959), pp. 86–106. DOI: 10.1287/opre.7.1.86. eprint: https://doi.org/10.1287/opre.7.1.86. URL: https://doi.org/10.1287/opre.7.1.86.

[34] Berthold K. P. Horn. "Suppressing traffic flow instabilities". In: *16th International IEEE Conference on Intelligent Transportation Systems (ITSC 2013)*. Oct. 2013, pp. 13–20. DOI: 10.1109/ITSC.2013.6728204.

[35] Berthold K. P. Horn and Liang Wang. "Wave Equation of Suppressed Traffic Flow Instabilities". In: *IEEE Transactions on Intelligent Transportation Systems* 99 (2017), pp. 1–10.

[36] Xiaoyu Huang and Junmin Wang. "Longitudinal Motion Based Lightweight Vehicle Payload Parameter Real-Time Estimations". In: *Journal of Dynamic Systems, Measurement, and Control* 135.1 (Nov. 2012). 011013. ISSN: 0022-0434. DOI: 10.1115/1.4007554. eprint: https://asmedigitalcollection.asme.org/dynamicsystems/article-pdf/135/1/011013/6114461/ds-135-1-011013.pdf. URL: https://doi.org/10.1115/1.4007554.

[37] Cambridge Systematics Inc. *Traffic Congestion and Reliability: Trends and Advanced Strategies for Congestion Mitigation*. Federal Highway Administration, 2005. URL: https://rosap.ntl.bts.gov/view/dot/20656.

[38] Petros Ioannou and Baris Fidan. *Adaptive control tutorial*. Advances in design and control. Society for Industrial and Applied Mathematics, 2006. URL: http://gen.lib.rus.ec/book/index.php?md5=deb3369ad71b0d7a0cfb801808da6291.

[39] Hassan K. Khalil and Jessy W. Grizzle. *Nonlinear systems*. Vol. 3. Prentice hall Upper Saddle River, NJ, 2002.

[40] E. Kometani and T. Sasaki. "Dynamic behavior of traffic with a nonlinear spacing-speed relationship". In: *Proceedings of the Symposium on Theory of Traffic Flow*. Research Laboratories, General Motors: New York: Elsevier, 1959, pp. 105–119.

[41] Allan J. Kotwicki. "Dynamic Models for Torque Converter Equipped Vehicles". In: *SAE Technical Paper*. SAE International, Feb. 1982. DOI: 10.4271/820393. URL: https://doi.org/10.4271/820393.

[42] A. R. Kreidieh, C. Wu, and A. M. Bayen. "Dissipating stop-and-go waves in closed and open networks via deep reinforcement learning". In: *2018 21st International Conference on Intelligent Transportation Systems (ITSC)*. 2018, pp. 1475–1480. DOI: 10.1109/ITSC.2018.8569485.

[43] Abdul Rahman Kreidieh, Cathy Wu, and Alexandre M. Bayen. "Dissipating stop-and-go waves in closed and open networks via deep reinforcement learning". In: *IEEE Conference on Intelligent Transportation Systems, Proceedings, ITSC* 2018-November (2018), pp. 1475–1480. DOI: 10.1109/ITSC.2018.8569485.

[44] Keqiang Li, Jiawei Wang, and Yang Zheng. *Cooperative Formation of Autonomous Vehicles in Mixed Traffic Flow: Beyond Platooning*. 2020. arXiv: 2009.04254 [eess.SY].

[45] Yunxin (Jeff) Li. "An Overview of the DSRC/WAVE Technology". In: *Quality, Reliability, Security and Robustness in Heterogeneous Networks*. Ed. by Xi Zhang and Daji Qiao. Berlin, Heidelberg: Springer Berlin Heidelberg, 2012, pp. 544–558. ISBN: 978-3-642-29222-4.

[46] Chi-Ying Liang and Huei Peng. "Optimal adaptive cruise control with guaranteed string stability". In: *Vehicle System Dynamics* 32.4-5 (1999), pp. 313–330.

[47] Eric Liang et al. "RLlib: Abstractions for Distributed Reinforcement Learning". In: *International Conference on Machine Learning (ICML)*. 2018.

[48] Hao Liu et al. "Impact of cooperative adaptive cruise control on multilane freeway merge capacity". In: *Journal of Intelligent Transportation Systems* 22.3 (2018), pp. 263–275. DOI: 10.1080/15472450.2018.1438275. eprint: https://doi.org/10.1080/15472450.2018.1438275. URL: https://doi.org/10.1080/15472450.2018.1438275.

[49] Pablo Alvarez Lopez et al. "Microscopic Traffic Simulation using SUMO". In: *The 21st IEEE International Conference on Intelligent Transportation Systems*. IEEE, 2018. URL: https://elib.dlr.de/124092/.

[50] Xiao-Yun Lu and J. Karl Hedrick. "Heavy-duty vehicle modelling and longitudinal control". In: *Vehicle System Dynamics* 43.9 (2005), pp. 653–669.

[51] Xiao-Yun Lu and J. Karl Hedrick. "Longitudinal control algorithm for automated vehicle merging". In: *International Journal of Control* 76.2 (2003), pp. 193–202. URL: https://doi.org/10.1080/0020717031000079418.

[52] Xiao-Yun Lu and J. Karl Hedrick. "Practical string stability for longitudinal control of automated vehicles". In: *Vehicle System Dynamics* 41 (2004), pp. 577–586.

[53] Xiao-Yun Lu et al. "An Enhanced Microscopic Traffic Simulation Model for Application to Connected Automated Vehicles". In: *Transportation Research Board 96th Annual Meeting*. Washington DC, United States, 2017.

[54] Xiao-Yun Lu et al. "Implementation of Longitudinal Control Algorithm for Vehicle Merging". In: *Proceeding of AVEC 2000-5th Int'l Symposium on Advanced Vehicle Control*. 2000.

[55] Xiao-Yun Lu et al. "Novel Freeway Traffic Control with Variable Speed Limit and Coordinated Ramp Metering". In: *Transportation Research Record* 2229.1 (2011), pp. 55–65. DOI: 10.3141/2229-07. URL: https://doi.org/10.3141/2229-07.

[56] Silvia Magdici and Matthias Althoff. "Adaptive Cruise Control with Safety Guarantees for Autonomous Vehicles". In: *IFAC-PapersOnLine* 50.1 (2017). 20th IFAC World Congress, pp. 5774–5781. ISSN: 2405-8963. DOI: https://doi.org/10.1016/j.ifacol.2017.08.418. URL: http://www.sciencedirect.com/science/article/pii/S2405896317307681.

[57] A. A. Malikopoulos et al. "Optimal Control for Speed Harmonization of Automated Vehicles". In: *IEEE Transactions on Intelligent Transportation Systems* 20.7 (2019), pp. 2405–2417. DOI: 10.1109/TITS.2018.2865561.

[58] J. A. Marshall, M. E. Broucke, and B. A. Francis. "Formations of vehicles in cyclic pursuit". In: *IEEE Transactions on Automatic Control* 49.11 (Nov. 2004), pp. 1963–1974.

[59] Vicente Milanés and Steven E. Shladover. "Modeling cooperative and autonomous adaptive cruise control dynamic responses using experimental data". In: *Transportation Research Part C: Emerging Technologies* 48 (2014), pp. 285–300.

[60] Vicente Milanés et al. "Cooperative Adaptive Cruise Control in Real Traffic Situations". In: *IEEE Transactions on Intelligent Transportation Systems* 15.1 (Feb. 2014), pp. 296–305. ISSN: 1558-0016. DOI: 10.1109/TITS.2013.2278494.

[61] V. Milanes et al. "Automated On-Ramp Merging System for Congested Traffic Situations". In: *IEEE Transactions on Intelligent Transportation Systems* 12.2 (2011), pp. 500–508. DOI: 10.1109/TITS.2010.2096812.

[62] G. F. Newell. "A simplified car-following theory: A lower order model". In: *Transportation Research Part B: Methodological* 36.3 (2002), pp. 195–205. ISSN: 01912615. DOI: 10.1016/S0191-2615(00)00044-8.

[63] Gábor Orosz, R. Eddie Wilson, and Gabor Stefan. "Traffic jams: Dynamics and control". In: *Philosophical Transactions of the Royal Society A: Mathematical, Physical and Engineering Sciences* 368.1928 (2010), pp. 4455–4479. ISSN: 1364503X. DOI: 10.1098/rsta.2010.0205.

[64] Gábor Orosz, Jeff Moehlis, and Francesco Bullo. "Delayed car-following dynamics for human and robotic drivers". In: *ASME 2011 International Design Engineering Technical Conferences and Computers and Information in Engineering Conference*. American Society of Mechanical Engineers, 2011, pp. 529–538.

[65] Hyungjun Park, Chiranjivi Sarma Bhamidipati, and Brian Lee Smith. "Development and Evaluation of Enhanced IntelliDrive-Enabled Lane Changing Advisory Algorithm to Address Freeway Merge Conflict". In: *Transportation Research Record* 2243.1 (2011), pp. 146–157. DOI: 10.3141/2243-17. eprint: https://doi.org/10.3141/2243-17. URL: https://doi.org/10.3141/2243-17.

[66] Andres A. Peters, Richard H. Middleton, and Oliver Mason. "Cyclic interconnection for formation control of 1-D vehicle strings". In: *European Journal of Control* 27 (2016), pp. 36–44. ISSN: 0947-3580. DOI: https://doi.org/10.1016/j.ejcon.2015.12.002. URL: http://www.sciencedirect.com/science/article/pii/S0947358015001302.

[67] L. A. Pipes. "An Operational Analysis of Traffic Dynamics". In: *Journal of Applied Physics* 24 (1953), pp. 274–281.

[68] Jeroen Ploeg. "Analysis and Design of Controller of Cooperative Adaptive Cruise Control". PhD thesis. Eindhoven University of Technology, 2014.

[69] Jeroen Ploeg, Nathan Van De Wouw, and Henk Nijmeijer. "Lp string stability of cascaded systems: Application to vehicle platooning". In: *IEEE Transactions on Control Systems Technology* 22.2 (2013), pp. 786–793.

[70] R. Pueboobpaphan, F. Liu, and B. van Arem. "The impacts of a communication based merging assistant on traffic flows of manual and equipped vehicles at an on-ramp using traffic flow simulation". In: *13th International IEEE Conference on Intelligent Transportation Systems*. 2010, pp. 1468–1473. DOI: 10.1109/ITSC.2010.5625245.

[71] Qing Xu and R. Sengupta. "Simulation, analysis, and comparison of ACC and CACC in highway merging control". In: *IEEE IV2003 Intelligent Vehicles Symposium. Proceedings (Cat. No.03TH8683)*. 2003, pp. 237–242. DOI: 10.1109/IVS.2003.1212915.

[72] Rajesh Rajamani. *Vehicle dynamics and control*. Springer Science & Business Media, 2011.

[73] Hani Ramezani et al. "Micro-Simulation of Truck Platooning with Cooperative Adaptive Cruise Control: Model Development and a Case Study". In: *Transportation Research Record* 2672.19 (2018), pp. 55–65. DOI: 10.1177/0361198118793257. eprint: https://doi.org/10.1177/0361198118793257. URL: https://doi.org/10.1177/0361198118793257.

[74] A. Reuschel. "Fahrzeugbewegungen in der Kolonne". In: *Österreichisches Ingenieur-Archiv* 4.3-4 (1950), pp. 193–215.

[75] J. A. Rogge and D. Aeyels. "Vehicle Platoons Through Ring Coupling". In: *IEEE Transactions on Automatic Control* 53.6 (July 2008), pp. 1370–1377.

[76] Riccardo Scarinci and Benjamin Heydecker. "Control Concepts for Facilitating Motorway On-ramp Merging Using Intelligent Vehicles". In: *Transport Reviews* 34.6 (2014), pp. 775–797. DOI: 10.1080/01441647.2014.983210. eprint: https://doi.org/10.1080/01441647.2014.983210. URL: https://doi.org/10.1080/01441647.2014.983210.

[77] David Schrank, Bill Eisele, and Tim Lomax. *2019 urban mobility report*. Texas A&M Transportation Institute, 2019.

[78] John Schulman et al. "Proximal Policy Optimization Algorithms". In: *arXiv* (2017), pp. 1–12. arXiv: 1707.06347. URL: http://arxiv.org/abs/1707.06347.

[79] Elaine Shaw and J. Karl Hedrick. "String stability analysis for heterogeneous vehicle strings". In: *American Control Conference, 2007. ACC'07*. IEEE, 2007, pp. 3118–3125.

[80] S. Sheikholeslam and C. A. Desoer. "Longitudinal Control of a Platoon of Vehicles". In: *1990 American Control Conference*. 1990, pp. 291–296.

[81] Steven Shladover. "Roadway automation technology – research needs". In: *Transportation Research Record* (1283 1990), pp. 158–167. URL: http://onlinepubs.trb.org/Onlinepubs/trr/1990/1283/1283-015.pdf.

[82] Steven E. Shladover. "Connected and automated vehicle systems: Introduction and overview". In: *Journal of Intelligent Transportation Systems* 22.3 (2018), pp. 190–200. DOI: 10.1080/15472450.2017.1336053. eprint: https://doi.org/10.1080/15472450.2017.1336053. URL: https://doi.org/10.1080/15472450.2017.1336053.

[83] Peter Slowik and Ben Sharpe. "Automation in the long haul: Challenges and opportunities of autonomous heavy-duty trucking in the United States". In: *The International Council on Clean Transportation* (2018).

[84] Raphael E. Stern et al. "Dissipation of stop-and-go waves via control of autonomous vehicles: Field experiments". In: *Transportation Research Part C: Emerging Technologies* 89.February (2018), pp. 205–221. ISSN: 0968090X. DOI: 10.1016/j.trc.2018.02.005. arXiv: 1705.01693. URL: https://doi.org/10.1016/j.trc.2018.02.005.

[85] Yuki Sugiyama et al. "Traffic jams without bottlenecks experimental evidence for the physical mechanism of the formation of a jam". In: *New journal of physics* 10.3 (2008), p. 033001.

[86] Richard S. Sutton and Andrew G. Barto. *Introduction to Reinforcement Learning*. 1st. Cambridge, MA, USA: MIT Press, 1998. ISBN: 0262193981.

[87] D. V. A. H. G. Swaroop. "String Stability of Interconnected Systems: An Application to Platooning in Automated Highway Systems". PhD thesis. University of California, Berkeley, 1994.

[88] D. Swaroop and J. Karl Hedrick. "String stability of interconnected systems". In: *IEEE transactions on automatic control* 41.3 (1996), pp. 349–357.

[89] Shin Ichi Tadaki et al. "Phase transition in traffic jam experiment on a circuit". In: *New Journal of Physics* 15 (2013). ISSN: 13672630. DOI: 10.1088/1367-2630/15/10/103034.

[90] Martin Treiber, A Hennecke, and Dirk Helbing. "Congested traffic states in empirical observations and microscopic simulations". In: *Physical review. E, Statistical physics, plasmas, fluids, and related interdisciplinary topics* 62 (Sept. 2000), pp. 1805–24.

[91] Martin Treiber and Arne Kesting. "Traffic Flow Dynamics". In: (2013). DOI: 10.1007/978-3-642-32460-4. URL: http://link.springer.com/10.1007/978-3-642-32460-4.

[92] S. Tsugawa, T. Saito, and A. Hosaka. "Super smart vehicle system: AVCS related systems for the future". In: *Proceedings of the Intelligent Vehicles '92 Symposium*. 1992, pp. 132–137. DOI: 10.1109/IVS.1992.252245.

[93] Valerio Turri et al. "A model predictive controller for non-cooperative eco-platooning". In: *American Control Conference (ACC), 2017*. IEEE, 2017, pp. 2309–2314.

[94] *US Energy Information Administration*. https://www.eia.gov/dnav/pet/hist/LeafHandler.ashx?n=pet&s=wgfupus2&f=4. Accessed: 2021-03-27.

[95] B. van Arem, C. J. G. van Driel, and R. Visser. "The Impact of Cooperative Adaptive Cruise Control on Traffic-Flow Characteristics". In: *IEEE Transactions on Intelligent Transportation Systems* 7.4 (2006), pp. 429–436. DOI: 10.1109/TITS.2006.884615.

[96] Jiawei Wang et al. "Leading cruise control in mixed traffic flow". In: *arXiv* (2020). arXiv: 2007.11753.

[97] J. Wang et al. "Controllability Analysis and Optimal Control of Mixed Traffic Flow With Human-Driven and Autonomous Vehicles". In: *IEEE Transactions on Intelligent Transportation Systems* (2020), pp. 1–15. DOI: 10.1109/TITS.2020.3002965.

[98] L. Wang and B. K. P. Horn. "On the Chain Stability of Bilateral Control Model". In: *IEEE Transactions on Automatic Control* 65.8 (2020), pp. 3397–3408. DOI: 10.1109/TAC.2019.2945877.

[99] J.A. Ward. "Heterogeneity, lane-changing and instability in traffic: a mathematical approach". PhD thesis. University of Bristol, 2009.

[100] Willem van Willigen et al. "Safety in the Face of Uncertainty: Critical Headway Estimation in Cooperative Adaptive Cruise Control". In: *International Journal of Intelligent Transportation Systems Research* 13 (2015), pp. 95–106.

[101] R.E. Wilson and J.A. Ward. "Car-following models: fifty years of linear stability analysis – a mathematical perspective". In: *Transportation Planning and Technology* 34.1 (2011), pp. 3–18. DOI: 10.1080/03081060.2011.530826. eprint: https://doi.org/10.1080/03081060.2011.530826. URL: https://doi.org/10.1080/03081060.2011.530826.

[102] C. Wu, A. M. Bayen, and A. Mehta. "Stabilizing Traffic with Autonomous Vehicles". In: *2018 IEEE International Conference on Robotics and Automation (ICRA)*. May 2018, pp. 6012–6018. DOI: 10.1109/ICRA.2018.8460567.

[103] Cathy Wu et al. "Emergent Behaviors in Mixed-Autonomy Traffic". In: *Proceedings of the 1st Annual Conference on Robot Learning*. Ed. by Sergey Levine, Vincent Vanhoucke, and Ken Goldberg. Vol. 78. Proceedings of Machine Learning Research. PMLR, Nov. 2017, pp. 398–407.

[104] Cathy Wu et al. "Flow: A Modular Learning Framework for Autonomy in Traffic". In: (2019). arXiv: 1710.05465 [cs.AI].

[105] Cathy Wu et al. "Flow: Architecture and Benchmarking for Reinforcement Learning in Traffic Control". In: (2017), pp. 1–16. arXiv: 1710.05465. URL: http://arxiv.org/abs/1710.05465.

[106] C. Wu et al. "Framework for control and deep reinforcement learning in traffic". In: *2017 IEEE 20th International Conference on Intelligent Transportation Systems (ITSC)*. Oct. 2017, pp. 1–8. DOI: 10.1109/ITSC.2017.8317694.

[107] Fangyu Wu et al. "Tracking vehicle trajectories and fuel rates in phantom traffic jams: Methodology and data". In: *Transportation Research Part C: Emerging Technologies* 99.July 2017 (2019), pp. 82–109. ISSN: 0968090X. DOI: 10.1016/j.trc.2018.12.012. URL: https://doi.org/10.1016/j.trc.2018.12.012.

[108] Lingyun Xiao and Feng Gao. "A comprehensive review of the development of adaptive cruise control systems". In: *Vehicle System Dynamics* 48.10 (2010), pp. 1167–1192. DOI: 10.1080/00423110903365910. eprint: https://doi.org/10.1080/00423110903365910. URL: https://doi.org/10.1080/00423110903365910.

[109] Lingyun Xiao and Feng Gao. "Practical string stability of platoon of adaptive cruise control vehicles". In: *IEEE Transactions on intelligent transportation systems* 12.4 (2011), pp. 1184–1194.

[110] Xiao-Yun Lu and K. J. Hedrick. "Longitudinal control algorithm for automated vehicle merging". In: *Proceedings of the 39th IEEE Conference on Decision and Control (Cat. No.00CH37187)*. Vol. 1. 2000, 450–455 vol.1. DOI: 10.1109/CDC.2000.912805.

[111] D. Xie, X. Zhao, and Z. He. "Heterogeneous Traffic Mixing Regular and Connected Vehicles: Modeling and Stabilization". In: *IEEE Transactions on Intelligent Transportation Systems* 20.6 (2019), pp. 2060–2071. DOI: 10.1109/TITS.2018.2857465.

[112] B. Xu et al. "Cooperative Method of Traffic Signal Optimization and Speed Control of Connected Vehicles at Isolated Intersections". In: *IEEE Transactions on Intelligent Transportation Systems* 20.4 (2019), pp. 1390–1403. DOI: 10.1109/TITS.2018.2849029.

[113] D. Yanakiev and I. Kanellakopoulos. "Nonlinear spacing policies for automated heavy-duty vehicles". In: *IEEE Transactions on Vehicular Technology* 47.4 (1998), pp. 1365–1377.

[114] Diana Yanakiev and Ioannis Kanellakopoulos. "Speed tracking and vehicle follower control design for heavy-duty vehicles". In: *Vehicle System Dynamics* 25.4 (1996), pp. 251–276.

[115] Hwasoo Yeo et al. "Oversaturated Freeway Flow Algorithm for Use in Next Generation Simulation". In: *Transportation Research Record* 2088.1 (2008), pp. 68–79. DOI: 10.3141/2088-08. eprint: https://doi.org/10.3141/2088-08. URL: https://doi.org/10.3141/2088-08.

[116] Hanwen Yi and Thomas E. Mulinazzi. "Urban Freeway On-Ramps: Invasive Influences on Main-Line Operations". In: *Transportation Research Record* 2023.1 (2007), pp. 112–119. DOI: 10.3141/2023-12. eprint: https://doi.org/10.3141/2023-12. URL: https://doi.org/10.3141/2023-12.

[117] Liuhui Zhao, Andreas Malikopoulos, and Jackeline Rios-Torres. "Optimal Control of Connected and Automated Vehicles at Roundabouts: An Investigation in a Mixed-Traffic Environment". In: *IFAC-PapersOnLine* 51.9 (2018). 15th IFAC Symposium on Control in Transportation Systems CTS 2018, pp. 73–78. ISSN: 2405-8963. DOI: https://doi.org/10.1016/j.ifacol.2018.07.013. URL: http://www.sciencedirect.com/science/article/pii/S2405896318307365.

[118] Y. Zheng, J. Wang, and K. Li. "Smoothing Traffic Flow via Control of Autonomous Vehicles". In: *IEEE Internet of Things Journal* 7.5 (2020), pp. 3882–3896. DOI: 10.1109/JIOT.2020.2966506.

[119] Kemin Zhou. "H Infinity Control". In: *Wiley Encyclopedia of Electrical and Electronics Engineering*. Wiley Online Library, 1999. ISBN: 9780471346081. DOI: https://doi.org/10.1002/047134608X.W1015. URL: https://onlinelibrary.wiley.com/doi/abs/10.1002/047134608X.W1015.